Juliana Albertoni de Miranda

Dynamics of Brazil Current dipoles: barotropic instabilities and flow-western boundary interactions

Corrected copy

Presented as partial fulfillment of the requirements for the degree of Doctor of Philosophy in Oceanography at Oceanographic Institute of University of São Paulo, with emphasis in Physical Oceanography.

Adviser:
Prof. Dr. Ilson Carlos Almeida da Silveira
University of São Paulo
Co-adviser:
Prof. Dr. Glenn Richard Flierl
Massachusetts Institute of Technology

São Paulo
2013

UNIVERSIDADE DE SÃO PAULO
INSTITUTO OCEANOGRÁFICO

Dynamics of Brazil Current dipoles: barotropic instabilities and flow-western boundary interactions

Corrected copy

Juliana Albertoni de Miranda

Presented as partial fulfillment of the requirements for the degree of Doctor of Philosophy in Oceanography at Oceanographic Institute of University of São Paulo, with emphasis in Physical Oceanography.

Evaluated in _____ /_____ /_____

Prof. Dr.	Grade
Prof. Dr.	Grade
Prof. Dr.	Grade
Prof. Dr.	Grade
Prof. Dr.	Grade

"If A is a success in life, then A equals x plus y plus z. Work is x; y is play; and z is keeping your mouth shut."

Albert Einstein

Contents

Agradecimentos

É um pouco difícil escrever esta parte, já que em 5 anos de doutorado muita coisa aconteceu, e muitas pessoas fizeram parte da minha vida nesse período. Mas enfim, tentarei expor meus agradecimentos e, como sempre, de forma suscinta, já que não sou de falar muito. Evitei citar nomes, mas existem muitas pessoas importantes, que me apoiaram muito.

Primeiramente, a família, que vem sempre em primeiro lugar. Meus pais e querida irmã sempre me apoiaram e meus avós, alguns tios e primos sempre vibraram muito pelo meu ingresso no doutorado. Aqui é claro que incluo o meu querido companheiro, melhor amigo, marido e "tampa da minha panela" (como diz a minha avó) Rafael, e toda a família dele, que também sempre nos deram muita força.

Obrigada ao meu orientador (Ilson) por tudo. Neste período tivemos fases e fases, altos e baixos, coisas que deram certo e coisas que deram errado, como qualquer típico doutorado. Mas tudo valeu. Graças ao apoio dele, pude morar um ano e meio em Massachusetts, nos EUA (para o estágio sanduíche), e lá tive uma fase maravilhosa da minha vida. Tive muitas experiências boas e lições de vida que guardarei pra sempre. O Rafa viveu isso comigo e sabe o que estou falando. Enfim, agradeço pela orientação e pelas lições que levarei pra sempre.

Agradeço também ao meu co-orientador (Glenn) por me receber como aluna nos EUA. Pude comprovar que ele é um cientista de altíssimo nível, e muitas vezes era difícil de acompanhar. Vi que ele é uma pessoa simples e humilde, e o admiro muito.

Aos amigos do IO, tanto o pessoal antigo quanto o mais recente. Adoro as pessoas de lá, sempre me senti muito bem recebida e acho que isso se deve às pessoas boas que habitam aquele lugar. O IO sempre foi minha segunda casa, e sempre sentirei saudades da época boa que vivi lá, e que completa 10 anos este ano.

Aos amigos dos EUA, com quem tive ótimos momentos, e com quem compartilhei o fato de estar tão longe de casa. Estes amigos serão eternos para mim, mesmo estando longe. Não posso deixar de comentar sobre os amigos do IEAPM. Lá recebi muita força e apoio na reta final, e graças a eles, pude ter tempo de me dedicar ao doutorado e conciliá-lo com o trabalho.

Ao doutorado em si. Muitos altos e baixos, vontade de desistir, mudanças de rumo. Mas ele saiu. Estou feliz e aliviada por ter conseguido finalizar um projeto que, pra mim, foi bem grande. Aprendi muito, tanto sobre oceanografia física (principalmente teórica) quanto sobre aspectos da vida em geral.

Finalmente agradeço ao Conselho Nacional de Desenvolvimento Científico e Tecnológico (CNPq) e à Coordenação de Aperfeiçoamento de Pessoal de Nível Superior (CAPES) pelo apoio financeiro durante o transcurso do doutorado, tanto no Brasil, como no período de estágio no exterior.

Abstract

This dissertation examines the nature of jet-boundary interactions and the role of barotropic instabilities in the Brazil Current system while still attached to the western boundary. The motivation was due to the frequent observation of bipolar features associated to the Brazil Current flow south of Cape Frio (RJ) and off Santos Bight (22° - 28° S). Such observations were mainly obtained from sea surface temperature images, and also from few "*in situ*" hydrographic and direct velocity measurements data. Therefore, our main focus is on the formation of bipolar features associated with the flow, and the main hypothesis is that barotropic instability is responsible for the generation of such dipoles along the western boundary current jet, while it has to deal with topographic variations along its path poleward. We address the system dynamics from a semi-theoretical perspective, and also through the application of numerical modeling on a process study approach. So it includes semi-theoretical studies of jet-lateral boundary interactions in idealized configurations relevant to the Brazil Current system off Cape Frio, considering the quasi-geostrophic theory as an appropriate approximation of the system we want to investigate. Additionally, numerical modeling is used through the construction of idealized scenarios where we simplify the physics in order to isolate the dynamical process of interest. All the dynamical analyzes were initialized from synoptic hydrographic data set which comprised the Brazil Current system off Cape Frio region. We validated the quasi-geostrophic theory we assumed and obtained the kinematics characteristics of the jet. In the dynamical analyses, we started the investigation from the simplest framework applied here, where we evaluate a piecewise constant potential vorticity field in a quasi-geostrophic contour dynamics model. It dealt with a meridionally-oriented jet flowing southward along a straight western boundary. Next, in a second model, we added more complexity in the system,

idealizing western boundary coastline scenarios considering a quasi-continuous potential vorticity field in a quasi-geostrophic numerical model. Finally, in a third model, we constructed a more complex scenario for the Brazil Current jet that incorporated real topography and stratification of the water column in a primitive equation numerical model.

Among our main finds, we verified that purely barotropic instability is able to generate vortex dipoles. Moreover, variations in the western boundary can indeed trigger perturbations in the jet and dipoles form. Therefore, sites with abrupt change in bathymetry and coastline orientation are preferred to the formation of the BC vortical dipoles. Vortex streets and instability trains can also develop downstream of such locations as consequence of perturbing a potentially batropically unstable jet. Hence, the horizontal shear is key to the generation of vortex dipoles. A weak shear does not allow these features to form, instead, frontal eddies are possibly generated, with the predominance of anticyclones. Although the three different model strategies applied here differ in dynamical configurations and approximations, they still kept nearly the same regime for the Brazil Current vortex-dipole formation. Topographic variations such as those associated with the change of coastline orientation near Cape Frio (23°S) account for those vortex dipoles and streets be dominantly observed within the Santos Bight.

Keywords: Brazil Current, dipoles, quasi-geostrophy, barotropic instability, western boundary.

Resumo

A presente tese examina a natureza das interações entre jato e contorno e o papel de instabilidades barotrópicas no sistema Corrente do Brasil (CB) quando este ainda se encontra fluindo junto à margem continental oeste. A motivação se deu através da frequente observação de feições bipolares associadas ao escoamento da CB ao sul de Cabo Frio (RJ) e ao largo da Bacia de Santos (entre 22° e 28° S). Tais observações se devem principalmente a imagens termais de temperatura da superfície do mar, a algumas raras observações "*in situ*" através de dados hidrográficos e medições diretas de velocidade. Assim, o principal foco é na formação de feições bipolares associadas ao fluxo médio, sendo a principal hipótese a de que instabilidade barotrópica é responsável pela formação destes dipolos ao longo da corrente quando esta tem que lidar com variações da topografia. Este estudo tenta abordar os problemas em uma perspectiva semi-teórica, e também através de modelagem numérica em uma abordagem de estudos de processo. Assim, inclui estudos semi-teóricos em configurações idealizadas relevantes para o sistema Corrente do Brasil ao largo de Cabo Frio, considerando a teoria quase-geostrófica como a aproximação apropriada para a dinâmica do sistema que queremos avaliar. Adicionalmente, a modelagem numérica é usada através da construção de cenários idealizados onde simplificamos a física a fim de isolar os processos que queremos investigar. Toda a análise dinâmica partiu de um conjunto de dados que compreendeu o sistema Corrente do Brasil ao largo de Cabo Frio. Validamos a teoria quase-geostrófica que estamos considerando e obtivemos as características cinemáticas do jato. Nas análises dinâmicas, começamos a investigação do problema partindo do cenário mais simples utilizado aqui, onde consideramos um campo de vorticidade potencial discretizado em camadas horizontais em um modelo quase-geostrófico de dinâmica de contornos. O modelo incorporou a presença de

uma linha de costa retilínea orientada meridionalmente no contorno oeste. Posteriormente, incluímos mais complexidade no sistema, idealizando diferentes cenários de linha de costa e considerando um campo de vorticidade potencial quase-contínuo em um modelo numérico quase-geostrófico. Finalmente, construímos um cenário ainda mais complexo para a Corrente do Brasil, o qual incorporou a topografia real da região e a estratificação da coluna de água em um modelo numérico de equações primitivas.

Dentre as principais conclusões, pudemos comprovar que instabilidade barotrópica pode promover a formação de dipolos. Além disso, variações no contorno podem consequentemente ser gatilhos para gerar perturbações no jato e dipolos se formam. Assim, locais de mudança abrupta de batimetria e orientação de linha de costa são preferidos para a formação de dipolos vorticais. Rua de vórtices e trens de instabilidade também podem se desenvolver à juzante de tais locais como consequência de se perturbar um jato potencialmente barotropicamente instável. Consequentemente, um cisalhamento horizontal é chave para a geração de dipolos vorticais. Um cisalhamento relativamente fraco não permite a formação de tais feições, e em vez disso, vórtices frontais são possivelmente gerados, com a predominância de anticiclones. Apesar de as três diferentes estratégias aplicadas aqui diferirem em termos de configurações dinâmicas e aproximações, estas ainda mantiveram aproximadamente o mesmo regime para a formação de dipolos. Variações na topografia tais como aquelas associadas com mudanças de orientação de costa próximo a Cabo Frio (23°S) contam com o fato de dipolos vorticais e rua de vórtices serem frequentemente observados dentro da Bacia de Santos.

Palavras-chave: Corrente do Brasil, dipolos, quase-geostrofia, instabilidade barotrópica, contorno oeste.

List of Figures

List of Tables

Chapter 1

Introduction

This thesis is an effort to extend our understanding of the role of topography and barotropic instabilities in the dynamics of western boundary current (WBC) jets while attached to the continental margin. It was motivated by the Brazil Current system scenario, where the geostrophic current deals with topographic variations and, additionally, presents an intense mesoscale activity, such as meanders, eddies and bipolar features. Here, we try to address our theoretical ideas about topography-mean flow-eddy interactions, idealizing scenarios in accordance to the actual system through the use of analytical and numerical modeling, and isolating the physical process we are interested in. The main focus is the investigation of dipoles formation.

1.1 Background and Motivation

1.1.1 The Brazil Current context

WBCs are confined geostrophic jets that flow attached along the western continental margins of the oceans. Regarding the oceanic large scale wind-driven circulation, WBCs are seen as the return of the Sverdrup transport integrated for the ocean basin interior, inside the subtropical gyre regions. The dominance of time-dependent eddies over the mean flow implies that the characteristics of the current vary strongly in time [*Cessi & Ierley*, 1993].

In the South Atlantic, a complex system of WBCs takes place (Figure 1.1). The upper layer is composed by the Brazil Current (BC) jet that flows poleward along the Brazil-

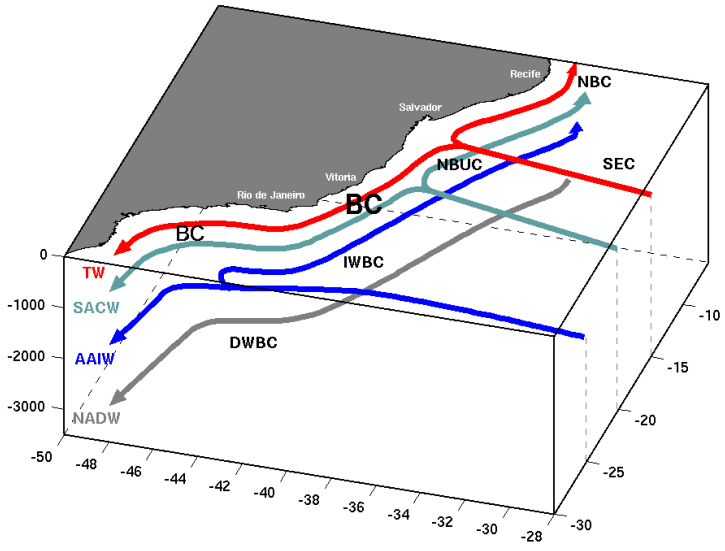

Figure 1.1: Representation of the large scale circulation pattern present along the Brazilian continental margin, southwestern Atlantic, in which the western boundary current system is indicated. Based on *Stramma & England* [1999].

ian continental margin. Bellow, the Intermediate Western Boundary Current (IWBC) and the North Brazil Undercurrent (NBUC) flow equatorward. Such system is mostly induced by the large scale wind-driven circulation and it is resultant from the bifurcation of the southernmost branch of the South Equatorial Current (sSEC) at several vertical levels.

Considering the above system at surface, BC originates at the sSEC bifurcation, between 14.5°S and 16°S, according to the near-surface large-scale climatological flow patterns [*Stramma*, 1991; *Stramma & England*, 1999; *Rodrigues et al.*, 2007]. At this area, BC is a shallow flow of about 100 m deep, transporting Tropical Water (TW), and it is characterized by a eddy-dominated flow still organizing itself as a jet, as recently pointed out by *Soutelino et al.* [2011].

About 20°S, BC is incremented by the flow coming from the sSEC bifurcation at intermediate depths, correspondent to the thermocline layer. In this region, the South Atlantic Central Water (SACW) is carried at a depth range of 150 m to 500 m, which makes the BC to become deeper. Therefore, downstream of it, within the 20°-26°S latitude range, the BC flow is stronger and better organized along the western boundary. Nevertheless, BC is associated to an intense mesoscale activity, presenting frequent me-

anders and eddies that may detach from the jet [*Signorini*, 1978; *Garfield*, 1990; *Silveira et al.*, 2000; *Calado*, 2001; *Silveira et al.*, 2004].

Around 26°-28°S, according to *Böebel et al.* [1999], the sSEC bifurcates in deeper levels (500 m to 1200 m), which corresponds to the Antarctic Intermediate Water (AIW) layer [*Stramma & England*, 1999]. Then, BC flow is even more robust and characterized by a poleward jet flowing between 0 m and 1200 m. The BC flows until it encounters the Malvinas Current, around 38°S [*Olson et al.*, 1988]. Such as its analogous Florida Current in the northern hemisphere, the BC presents a rich mesoscale activity, frequently reported in the literature [*Mascarenhas et al.*, 1971; *Signorini*, 1978; *Silveira et al.*, 2000, 2004], characterized by the formation of meanders and eddies along its track.

Regarding the equatorward flow originated from the sSEC bifurcation, the IWBC is originated within the AIW vertical domain, in 26°-28°S, and flows under the BC flow. Up north, IWBC flow receives the contribution of sSEC bifurcation within SACW vertical domain, in 20°S, and becomes NBUC [*Stramma & England*, 1999]. Up to this area, NBUC flow has a vertical extension of about 800 m and flows northward right below BC. North of 15°S, the bifurcation increments NBUC flow with a surface flow, originating the North Brazil Current [*Silveira et al.*, 1994]. *Silveira et al.* [2000] presented a good review of the upper ocean WBC system off the Brazilian coast, characterizing transports, velocities, water masses composition, vertical extension, occurrence of meanders and eddies. Going downward in the water column, below the described system of WBCs, the wind-driven circulation vanishes and the thermohaline general circulation takes place, composing the deep ocean motion.

Given the large scale wind-driven circulation patterns present at the southwestern Atlantic, one can see that the vertical structure of the system of WBCs in the upper ocean is composed basically by 2 layers of opposing flows, which suggests the existence of a very baroclinic system. Some studies, such as *Silveira et al.* [2008], propose that geophysical instabilities due to the vertical shear are responsible for the growth of some of the recurrent mesoscale features present along the BC flow. Such intense mesoscale activity is present since its origin until the BC-Malvinas confluence region. In between this locations (Figure 1.2), the so called southeastern Brazilian coast presents a more robust BC that very often meanders and form eddies. In general, these

meanders and eddies present a diameter of about 100 km, having the same scale of the BC horizontal extension. In this scenario, it becomes important to point out to the topographic characteristics of the region, which is very peculiar and it is probably associated with the intense mesoscale activity cited above. As we can note in Figure 1.2, Cape São Tomé and Cape Frio are locations where the continental margin presents considerable variations. In that figure, the 200 m and 1000 m isobaths are indicated with gray contours, and it is approximately the location of the continental shelf break and slope regions, respectively. North of Cape Frio, the continental shelf is narrower, the slope is very steep, and the continental margin presents a north-south orientation. South of Cape Frio, its direction suddenly changes, firstly becoming dominantly west-east, and afterward presenting a northeast-southwest direction. In this region, the continental shelf is wider and the slope smoother. Such characteristics bring several consequences to the WBC system that takes place in the region. In theory, the geostrophic current tends to flow along a constant isobath, conserving potential vorticity. Variations in the topography may cause deviations in the stretching vorticity and, consequently, in the relative vorticity. Therefore, deviation of the mean steady state flow may occur as a tentative of the geostrophic jet in conserve potential vorticity. *Silveira et al.* [2000] suggested this explanation to the BC meandering off southeast Brazil. Such mesoscale activity will be better described and discussed in section 1.1.2. Nevertheless it is important to keep in mind the topographic configuration in this region.

1.1.2 The Brazil Current mesoscale activity and dipoles

Evidence of finite amplitude cyclonic and anticyclonic meanders in the BC system has been widely reported in the literature, as mentioned by several authors, such as *Signorini* [1978], *Garfield* [1990], *Silveira et al.* [2000], *Calado et al.* [2006], *Silveira et al.* [2008], to cite just a few (and other works cited therein). First observations and descriptions were reported by the classical studies of *Mascarenhas et al.* [1971] and *Signorini* [1978]. Those studies focused on the description of the BC frontal meanders that are frequently observed off Cape Frio and Cape São Tomé, southeastern Brazilian coast (22°-23°S, Figure 1.2). Those meanders very often close in eddies that pinch off from the BC and shed into the subtropical gyre or are reabsorbed by BC flow [*Silveira et al.*, 2008]. Figure 1.3

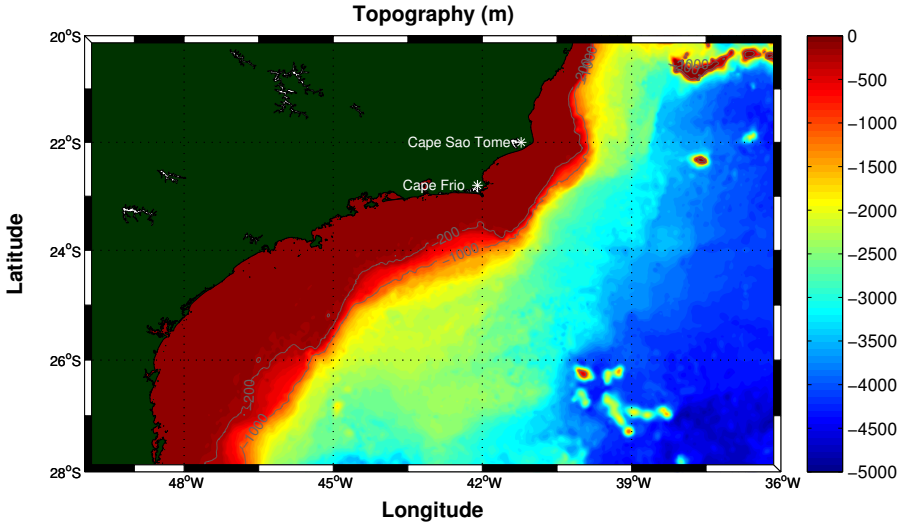

Figure 1.2: Representation of topography at southeast Brazilian continental margin (centered in Cape Frio). The 200 m and 1000 m isobaths are indicated as gray contours. Cape Frio and Cape São Tomé locations are pointed by * symbol.

illustrates the anticyclonic eddy off Cape Frio described in *Signorini* [1978] through a map of dynamical topography derived from hydrographic data. Figure 1.4, presented by *Silveira et al.* [2008], shows a sea surface temperature image exemplifying the recurrent Cape São Tomé cyclonic meander pinching off from the BC. The authors, through current-meter mooring data analyses, applied an instability model which pointed to baroclinic instability as the mechanism responsible for the meander growth in Cape Frio-Cape São Tomé region. *Mano et al.* [2009] focused on the investigation of energy transfer between the BC-IWBC system and in the formation of the Cape Frio eddies. They found out that, due to the vertical shear, baroclinic instability drains energy from the mean flow of the IWBC at a first moment, and the perturbation signal propagates upward, ending up in energy drain from the BC. This process allow the cyclonic eddies to grow through the energy transfer between the mean flow and the perturbations. The interesting point in this study is the evidence that the energy transfer to the perturbations starts at intermediate depths, which corresponds to the IWBC layer.

Southwestward-propagating, slowly growing meanders were described by *Campos et al.* [1995] and *Campos et al.* [1996] through the observation of a meandering pattern composed by strong cyclonic and anticyclonic frontal eddies south of Cape Frio. *Campos et al.* [2000] suggested that the change in the coastline orientation induces such meandering. A close analogy is seen in the western North Atlantic where the Gulf Stream

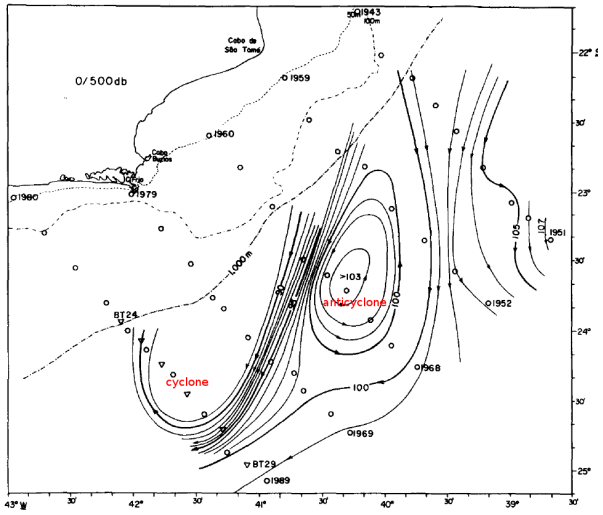

Figure 1.3: Anticyclonic eddy represented through dynamical topography (in dynamical cm) relatively to 500 dbar, centered in 40.2°W. A cyclonic meander is also present, centered in 41.6°W. From: *Signorini* [1978].

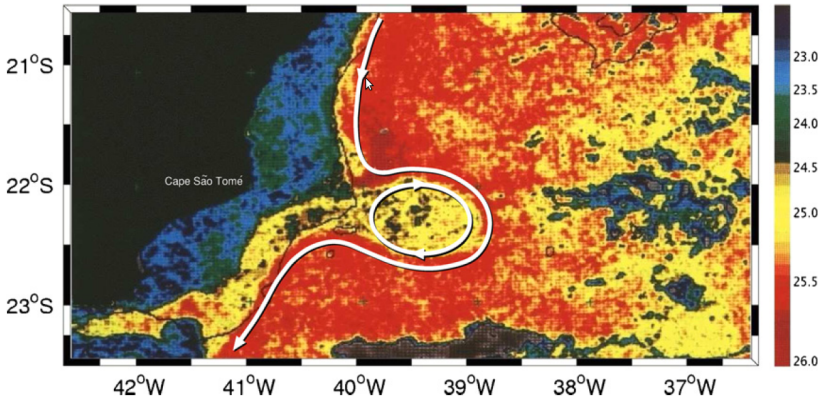

Figure 1.4: An AVHRR image from 20 March 1995 exemplifying the recurrent Cape São Tomé cyclonic meander pinching off from the Brazil Current. The bluish-yellow colors are associated with the cooler- and fresher-Coastal Water (CW) on the shelf and the reddish colors mark the presence of the warmer- and saltier-Tropical Water (TW). From: *Silveira et al.* [2008].

leaves the edge of the continental shelf near Cape Hatteras and large instabilities begin to develop a short distance downstream [*Fofonoff*, 1981]. These instabilities form a sequence of cold core and warm core rings that occasionally detach from the current main axis. *Pratt et al.* [1991] used a contour dynamics idealized model and could show that the Gulf Stream warm rings, known as "warm outbreaks", are the consequence of barotropic instabilities in a propagating Rossby wave. *Silveira et al.* [2000] discussed that the sequence of opposing signal meanders off Brazil consists of vortex pairs connected to the BC main axis, and have horizontal length scale smaller than the cyclones off Cape Frio (e.g. smaller than 100 km). Yet, they compare such phenomenon with the "warm outbreaks" present in the Gulf Stream, and speculated that the phenomenon is a barotropically unstable topographic Rossby wave. Figure 1.5 illustrates, through a sea-surface temperature satellite image, a sequence of cyclonic and anticyclonic meanders along the Brazilian continental margin. This sequence of opposing signal meanders suggests the existence of non-paired bipolar features connected to the BC flow. In Figure 1.6, it is more evident the presence of a non-paired dipole, which was described by *Campos et al.* [1996] off southeast Brazil (upper panel). In the lower panel, a paired bipolar feature is indicated, where two eddies of opposing signs are connected to the current main axis, and it was presented by *Velhote* [1998]. The figure also indicates a frontal cyclonic meander upstream. Despite not discussed by *Signorini* [1978], in Figure 1.3 a cyclonic meander is associated with the anticyclonic eddy discussed by the author, which characterizes a bipolar feature captured by the dataset.

Description of those dipoles along the southeast Brazilian coast and studies focusing on the dynamics of this phenomenon are very limited, although they are frequent observed through sea-surface temperature satellite images. Here we present 3 snapshots of satellite sea-surface temperature (SST) maps that seem to have captured bipolar features along the southeastern Brazilian continental margin in different times. The SST data was obtained from the *Group for High-Resolution Sea Surface Temperature* (SST) (`https://www.ghrsst.org/`). Over the SST images we plotted the correspondent geostrophic velocities maps computed from sea-surface height, obtained from altimeter data. The ready-to-use gridded velocity data was extracted from the AVISO database - *Archiving, Validation and Interpretation of Satellite Oceanographic data*

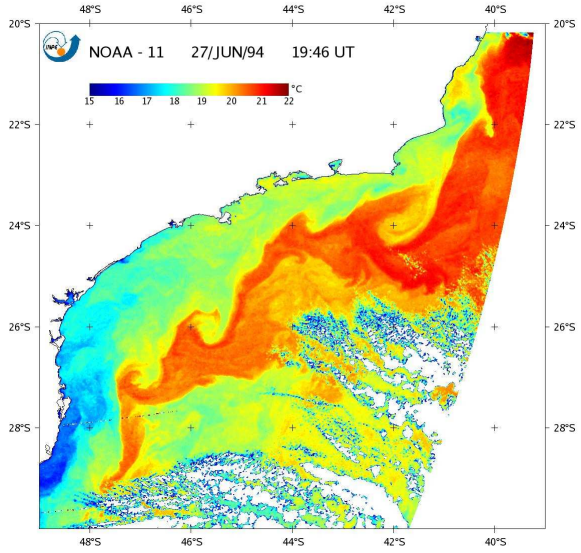

Figure 1.5: An AVHRR image from 27 June 1994, illustrating the southwestward propagating meanders associated to the BC flow. The bluish-green colors are associated with the cooler- and fresher-Coastal Water on the shelf and the reddish colors mark the presence of the warmer- and saltier-Tropical Water. From: *Mattos* [2006].

(`http://www.aviso.oceanobs.com/en/`). Figure 1.7 (left panel) shows a snapshot from April 21, 2003. The BC signature can be noticed by the warm waters (reddish colors), while the continental shelf cold waters are signed by the bluish colors. Figure 1.7 (right panel) shows a snapshot for April 25, 2008. In this one, it is possible to see a sequence of opposing signs meanders and eddies along the BC axis. The meandering pattern in centered along the continental shelf break (represented in the figures by the 200 m isobath). Figure 1.8 shows a snapshot for September 5, 2011. In this last one, we could not obtain the correspondent geostrophic velocity data information. However, it is still possible to note the signature of a mushroom-like feature.

Additionally to the above evidences, *Pereira* [2009], in his master thesis, described a bipolar feature captured by a hydrographic cruise conducted between 22-29 of September, 2003. The cruise was part of the Project "Dinâmica do Ecossistema da Plataforma da Região Oeste do Atlântico Sul", the DEPROAS Project. It was the last of a series of five synoptic cruises conducted off southeast Brazil, within the parallels 23°-26°S and meridians 45°-41°W. The dipole signature was captured both in the referenced geostrophic velocities and in direct-measured velocities. Figure 1.9 illustrates the directely-observed velocity horizontal field over the streamfunction field obtained

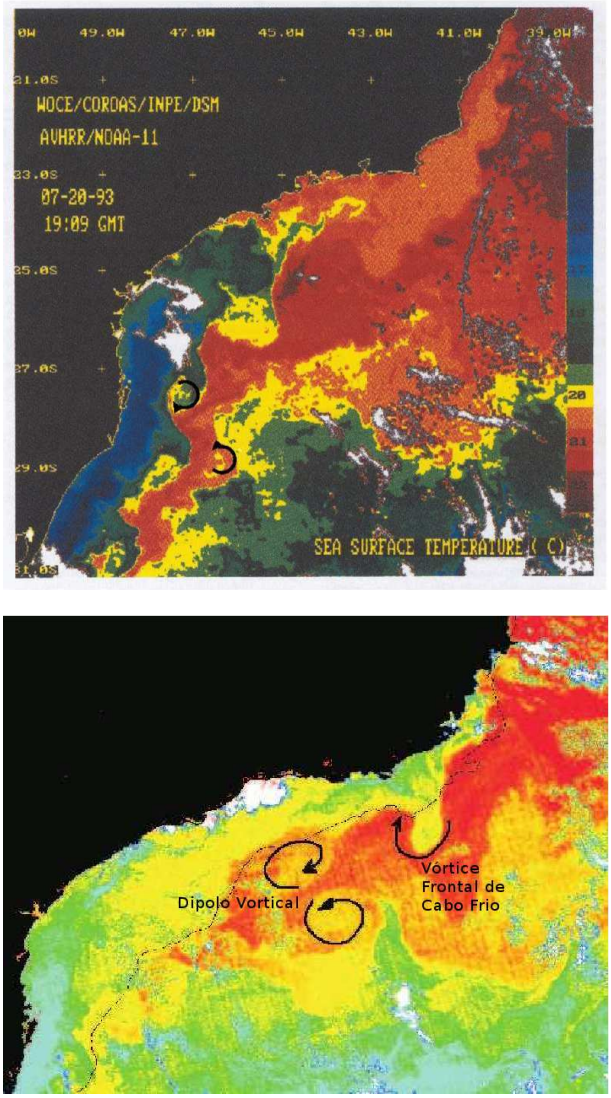

Figure 1.6: Evidences of bipolar structures. Upper panel: AVHRR image presented by *Campos et al.* [1996]. Lower panel: AVHRR image presented by *Velhote* [1998]. For the present study, we edited the figures in order to highlight the bipolar feature. The arrows indicate the direction of rotation of each vortex.

by the author in 20 m depth (upper panel) and 100 m depth (lower panel). In both maps, the bipolar signature is evident. Trying to go inward the dynamics of the captured feature, and still using the same cruise dataset, the author applied a barotropic instability model under the $1^1/_2$-layers approximation and could see some incipient dynamical characteristics. The first one was the evidence of the weakness of the BC flow after passing by the bipolar structure. A second characteristic pointed by the author was that relative vorticity and stretching vorticity compete for the system dynamics. This indicates that the feature under investigation belongs to typical mesoscale dynamics. Third, the streamfunction fields associated to the cyclone and to the anticyclone act in a way to amplify the potential vorticity structures associated reciprocally to those fields. This is a general form to define an instability process and, consequently, he concluded the dipole was under a barotropic growth process. Moreover, the cyclone induces downstream movement on the anticyclone and vice-versa.

Looking for additional evidences of the presence of the September 2003 dipole, we called upon again the AVISO data and plotted the geostrophic velocities for the same period of the DEPROAS V cruise. Figure 1.10 illustrates a snapshot of September 29, 2003, which is within the period the cruise was carried out. It is general consensus altimeter data is not so reliable in continental shelf and slope regions as it is in the deep ocean, but the velocity vectors seem to indicate the presence of two eddies of opposing vorticity right off Cape Frio. The eddies are not so intense or evident as they were in Figure 1.9, and we can also see the BC flow is continuous south of Cape Frio. The jet was following the 200 m isobath upstream (around 22°-24°S), and south of this latitude the current headed straight southwestward, separating from the 200 m isobath and developing a meandering pattern of opposing signs eddies.

1.1.3 Western Boundary Current dynamical studies

We revise next several idealized dynamical studies about WBC processes that investigated the role of barotropic instability, topography and coastline orientation on the formation of vortex-dipoles.

According to *Rodríguez-Marroyo & Viúdez* [2009], oceanic vortex dipoles are basically two closely packed regions of opposite sign vertical vorticity. Dipoles are stable

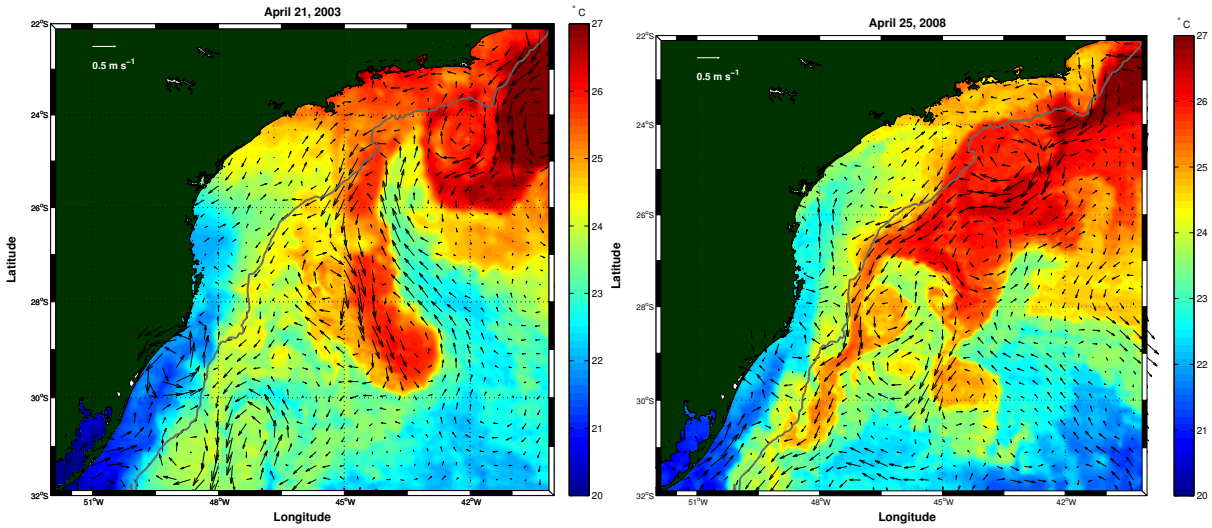

Figure 1.7: Sea-surface temperature snapshot from GHRSST. The arrows indicate the surface geostrophic velocity from AVISO for the same day. Left panel: April 21, 2003; right panel: April 25, 2008. The gray contour represents the 200 m isobath. Temperature in °C.

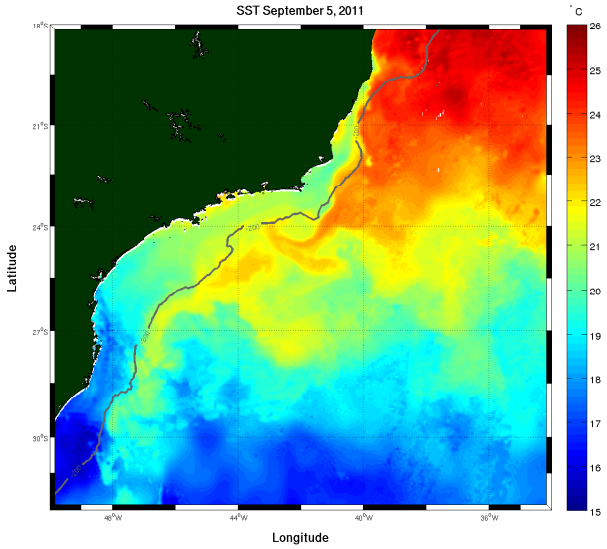

Figure 1.8: Sea-surface temperature snapshot from GHRSST: September 5, 2011. The gray contour represents the 200 m isobath. Temperature in °C.

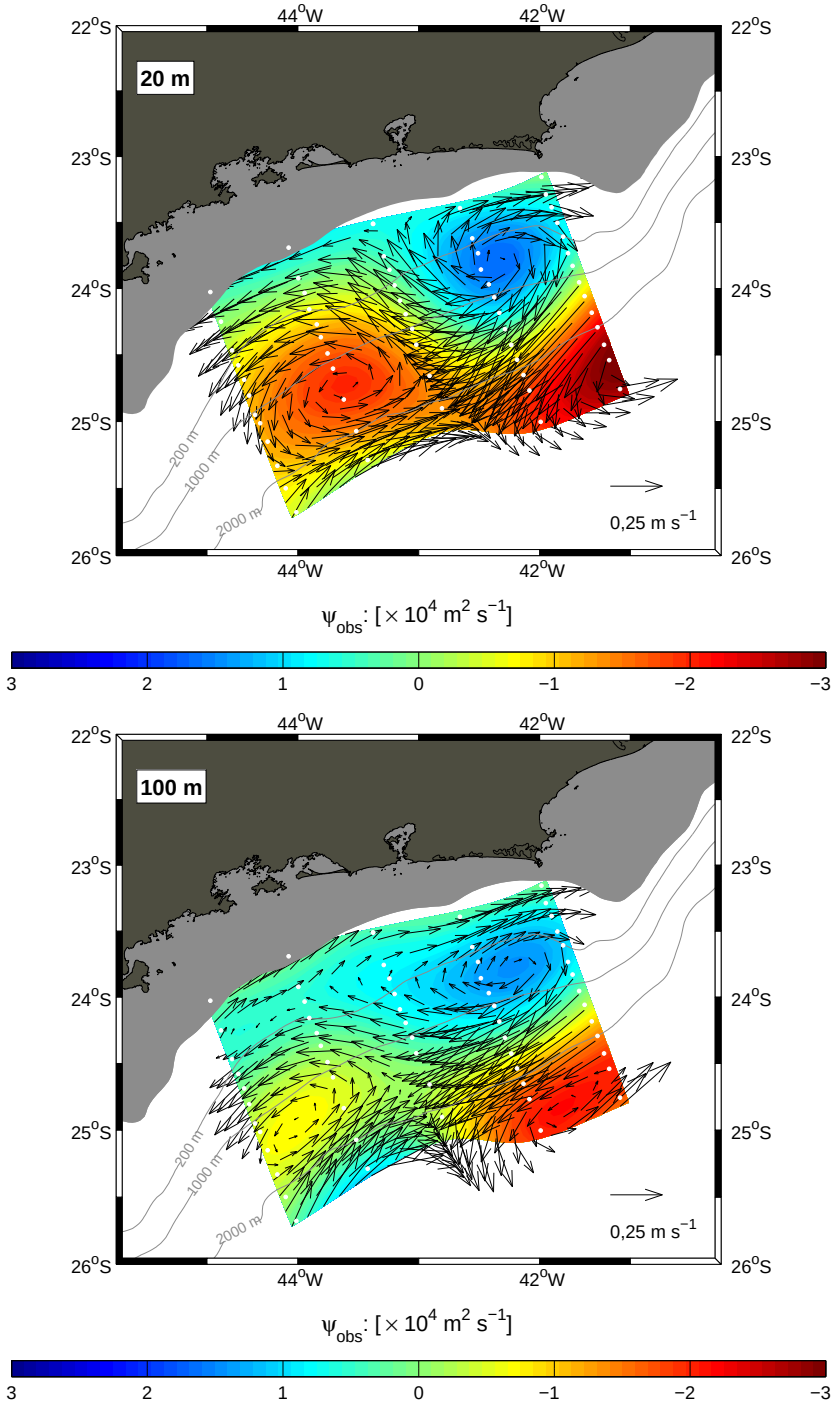

Figure 1.9: Streamfunction horizontal field over velocity vectors obtained from the velocity direct measurements of DEPROAS V cruise (September 22-29, 2003). Upper panel corresponds to 20 m depth, lower panel corresponds to 100 m depth. The white dots indicate the location of the 61 hydrographic stations of DEPROAS V cruise. From *Pereira* [2009].

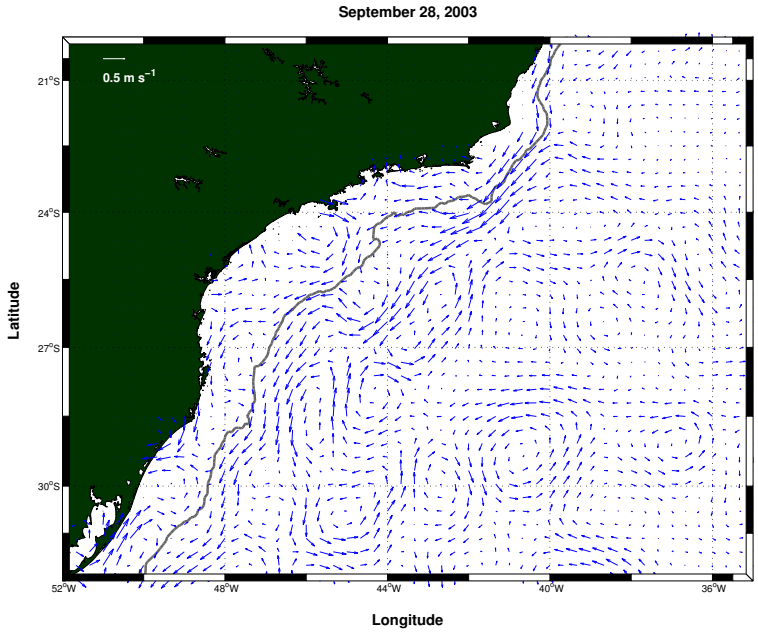

Figure 1.10: Sea-surface geostrophic velocity from AVISO in September 28, 2003 (DEPROAS V cruise period).The gray contour represents the 200 m isobath.

coherent vortex structures frequently found in the oceans and atmosphere, especially at the mesoscale and submesoscale. The processes responsible for the formation of such structures may vary. If we consider that the BC vortex dipoles are immersed in a barotropic topographic Rossby wave (such as the Gulf Stream warm outbreaks), barotropic instability might be the mechanism responsible for the formation of such features. This was pointed out by the study of *Pereira* [2009]. The kinematic scenario favorable to the occurrence of barotropic instability in a jet is basically the existence of horizontal shear. According to the linear instability theory, the necessary but not sufficient conditions for barotropic instability is the potential vorticity gradient to change signal at least once in the cross-jet direction. In a f plane approximation, this is known as the Rayleigh condition. For the β plane case, it is called Kuo criterion.

Leal Silva [2000] explained the evolution of dipoles in a model of converging WBCs off a western boundary. The author used a contour dynamics model in a $1^1/_2$-layers configuration and determined that the perturbations prescribed in the central front create regions of potential vorticity anomaly immersed in regions of larger or smaller potential vorticity, but of opposing signals. This scenario induced a circular motion that produced eddies. The phase difference among the vortex structures can stimulate an amplification of those eddies, which start interacting with each other, and conse-

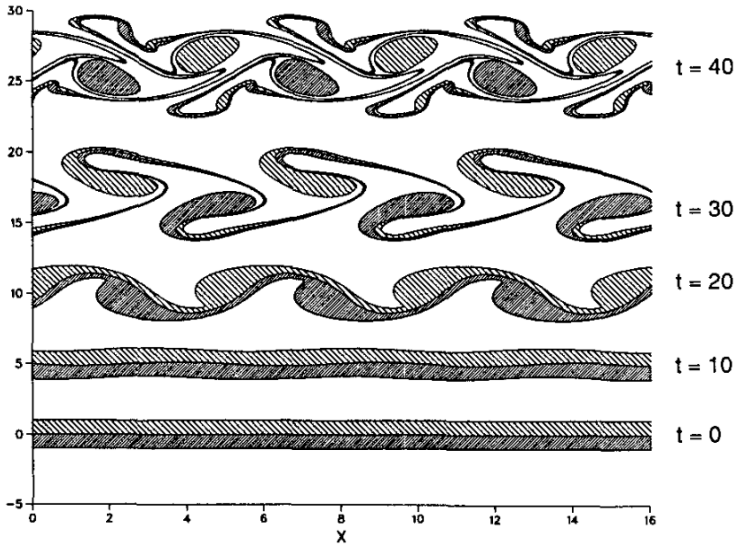

Figure 1.11: Mechanism of formation of dipoles suggested by *Bell & Pratt* [1992], which resulted in a "vortex street".

quently becoming bigger and transforming the initial flow in a sequence of vortex dipoles, that follow the basic flow.

Bell & Pratt [1992], also applying a contour dynamics model, explored the interaction of an unstable infinite zonal jet and a singular eddy using a jet with piecewise constant potential vorticity (in a 1-layer and $1^1/_2$-layers frameworks). They suggested that three ingredients are responsible for the stripping of potential vorticity from the near edges of the jet: (i) the existence of a regular eddy (a regular eddy is referred as having the velocity field it induces at the jet being opposite to the flow of the jet), (ii) the near edge of the jet must contain potential vorticity of opposing sign from the eddy, and (iii) a stagnation point must exist in the flow that remains inside the jet for a significant percentage of an eddy turnover time. When these three conditions are met, the eddy strips off an opposite eddy from the near jet edge and the resulting pair move upstream and away from the jet, forming what they called a "vortex street". Figure 1.11 shows the mechanism of dipoles formation suggested by the authors.

Schmidt [2004] investigated the interaction of an unstable WBC, eddies and the continental margin in idealized models of contour dynamics. Using similar scenarios to the southeast Brazilian coast, he explored the interaction of both a rectilinear and a curvilinear continental margin and a singular eddy that would represent the BC cyclonic and anticyclonic meanders. The author observed the formation of bipolar fea-

tures and suggested that the presence of the continental margin contributed to the formation of such dipoles. In the study of the interaction of a WBC jet with a rectilinear meridionally oriented continental margin, a hybrid model of contour dynamics was implemented. It consisted of allowing a barotropic configuration internally to the continental margin, and a $1^1/_2$-layer on the oceanic side. It was observed that unstable waves propagated phase and group towards north with the shelf on their left. Additionally, the narrower the shelf, the smaller are the propagation velocities of the unstable waves and their corresponding growth rates. Bands of defined unstable waves, with short and long wave limits, were obtained for all the analyzed flow configuration. The contour dynamics experiments showed that regardless of the disturbance being cyclonic or anticyclonic, the topographic eddies formed were always anticyclonic. His investigation in the curvilinear coastline was limited to the barotropic 1-layer approximation only, where he looked to the interaction between cyclonic and anticyclonic eddies with the continental margin. The bulk dynamical characteristics of the model runs, such as the formation of dipoles and topographic eddies, were not changed in this new configuration relatively to a meridionally oriented coast.

Stern & Whitehead [1990] looked to the problem of separation of a jet from a curvy coast. A semi-infinite jet was considered along a vertical wall in a rotating fluid, with the nose of the intrusion approaching a corner where the wall turns through an obtuse angle θ+180°. The jet separates at the corner and flows into the interior if θ exceeds a critical θ_c, otherwise part of the jet continues around the corner and flows along the downstream segment of the wall. The separation criterion was computed using an inviscid and piecewise-uniform-vorticity model. The separation effect was also demonstrated by a laboratory experiment in which a two-dimensional jet flows along the wall from a source. Their calculations suggested that the separation mechanism is independent of local viscous forces, although the cumulative effect of lateral eddy stresses in the jet is important in establishing the value of θ_c immediately upstream from the corner. The resulting scenario for the separating jet was the formation of a dipolar vortex which propagated into the interior, and thereby established the path for the trailing jet. In the non-separating jet case, the flow continued along the downstream segment of the wall and formed a strong wall current at and downstream from the corner. This

was accompanied by a large counterclockwise offshore eddy, and no evidences of bipolar features were seen. In this case, all the initial conditions were the same as in the first one, except that θ_c was reduced by half. Hence, they argue that this separation effect is not merely a simple consequence of the forward momentum of the jet, and actually it is strongly dependent on the angle of the change in the coastline.

1.1.4 Scientific questions

In the above paragraphs we tried to summarize all the knowledge related to the BC dynamics south of Cape Frio and point out the missing issues. We were mostly motivated by the occurrence of bipolar features, that lack investigations regarding their dynamics in term of formation, growth and interaction with the continental margin. The recent observational study of *Pereira* [2009] showed an unique observational evidence of a BC dipole captured by direct-velocity measurements and hydrographic datasets. In this context, some scientific questions can be pointed out:

- What is the role of lateral boundary variations in the formation and growth of bipolar features frequent observed off southeast Brazil?
- Is barotropic instability the mechanism responsible for the formation of these bipolar features?

The questions formulated above motivated us to develop the present research, and the goals will be presented in the next section. Besides the gap of knowledge regarding dipoles formation off southeast Brazilian coast, it is important to highlight some other interesting and important aspects of this location. We have mentioned the complexity of the topography, which presents contrasting characteristics between the north and the south of Cape Frio. Associated with that, a relatively intense coastal upwelling system takes place off Cape Frio and Cape São Tomé, being the most important present along the Brazilian coast. Coastal upwelling is not common at the eastern coasts of the continents, as it is at the western coasts, and it is another interesting oceanographic characteristic of southeastern Brazil region. Although it is not the focus of our study, the interaction of such phenomenon with BC and its eddies has been investigated. This

set of attributes (WBCs system + topography + coastal upwelling) makes the southeastern Brazilian continental margin an interesting area for oceanographic investigations, and exert some influence in the economic aspects of the region, since it is one of the main locations of offshore oil prospection and fishery economy in Brazil. For instance, offshore platform installation and operation depends on the knowledge regarding the oceanic circulation, and fishery activity might be dependent on the biomass production related to the rich-nutrient upwelled waters.

1.2 Thesis Objectives

The rich mesoscale activity and the complex topographic characteristic off southeast Brazil motivated us to investigate the dynamics of BC dipoles and the role of topography on it. Given the lack of studies that have investigated the physical processes that drive the formation and growth of such dipoles, and considering the questions formulated in the previous section, we proposed a semi-theoretical and idealized investigation of the interaction of the BC flow and topography, looking to the development of geostrophic instabilities able to form dipoles and likely features. The work discussed here attempts to improve our theoretical understanding of the role of topography (focusing on lateral boundary variations primarily) in the time-dependent dynamics of a meridionally evolving, strongly inertial, unstable jet in a configuration and parameter regime that is relevant to the BC jet system, as well as other relatively weak WBCs (while attached to the continental margin).

Therefore, the objectives are:

1. to characterize an approximately non-perturbed BC jet captured by an hydrographic dataset that comprised Cape Frio oceanic region. Here we aim to describe the flow in terms of horizontal and vertical extensions, cinematic characteristics and horizontal cross-jet structure of velocity and potential vorticity;

2. to obtain the linear instability properties of the BC jet, such as phase and group velocities and growth rate of the perturbations;

3. to isolate the barotropic instability effect and examine the nonlinear evolution of

a unstable meridional jet attached to a rectilinear western boundary;

4. to examine the interaction of a barotropically unstable meridional jet and a western boundary in idealized configurations relevant to BC jet system, in particular the role of lateral boundary variations;

5. to examine eddy-jet-topography interactions of a meridional evolving jet inside a realistic topography scenario.

The present study is based on quasigeostrophic theory, and all the dynamical parameters computed and discussed here are done assuming this physical simplification, which is reasonable to the phenomenon scale in question. Nevertheless, through observational data analyses, we will be able to validate such approximation.

In order to accomplish those goals, we consider the geophysical instability theory to obtain the linear instability properties of the BC jet. This is also the reason why we aim to describe firstly an approximately non-perturbed BC jet. Goals 3, 4 and 5 are all nonlinear analyzes. Following the presented order, in each one, we aim to make use of more complex frameworks and methodologies and, therefore, try to construct a theoretical understanding of dipole formation through the isolation of physical processes. Then, item 3 makes use of the contour dynamics technique where a piecewise constant potential vorticity field is constructed based on the BC jet characteristics and evolves nonlinearly in time. Item 4 makes use of a quasigeostrophic numerical model where the potential vorticity field is quasi-continuous and the effect of a curvy western boundary is inserted. Finally, for goal 5 we make use of a primitive equations numerical model framework where we also include an idealized BC jet, but using a realistic topography scenario. The methodologies briefly described above will be fully presented on their correspondent chapters.

It is the hope that the semi-theoretical approach of studying idealized models will permit more insight on the essential physics of the system, while the observational analysis can provide the necessary reality check to help understand the relevance of the idealized system and the theoretical framework derived from it to the real oceanic system. Taken together, the goal is to construct a tractable theoretical framework in which to think about eddy-jet-western boundary interactions in WBC jet systems, that

gives both an understanding of the dynamics from first principles, as well as an understanding of its relevance to the actual oceanic system.

1.3 Thesis Outline

Work towards achieving these goals is presented in the following five chapters. Chapter 2 presents a brief overview regarding the theory in which we based our study. Moreover, we present the BC potential vorticity structure from observational data. Yet, we validate the theory we are applying in this study using the cited dataset. Based on the observational evidences of the BC, in Chapter 3 we apply the technique known as contour dynamics. Therefore, we perform a linear evaluation of the observed jet and analyze the evolution of a idealized meridional jet in a piecewise potential vorticity field. Advancing our analyses into the nonlinear theory, Chapter 4 presents the nonlinear, time-dependent development of a meridional unstable jet attached to a western boundary in a quasigeostrophic numerical model, where the potential vorticity field is now continuous. Finally, Chapter 5 consists in the evaluation of a BC-like jet in a primitive equation numerical model. The modeled scenario consists of a continuously stratified ocean with nearly-real topography. A general discussion and conclusions are presented in Chapter 6.

Chapter 2

Quasigeostrophic approximation of Brazil Current

2.1 Theoretical background

As mentioned in Chapter 1, WBCs are defined as confined geostrophic jets, part of the large scale wind-driven circulation at subtropical latitudes, and correspond to the return of Sverdrup transport integrated for the ocean basin. However, WBCs can not be essentially described using the geostrophic approximation, since it is very idealized. Oceanic jets such as WBCs usually are characterized as robust flows that may develop deviations or perturbations along its track, which are translated in the formation of meanders or vortices (theses last ones may develop when the perturbation grow). Those jets present low Rossby number, which means Earth rotation is highly important for their dynamics. Oceanic motions under this characteristic can be studied and better described by quasigeostrophic (QG) theory, which in summary means to allow deviations of the steady geostrophic motion. Consequently, it is possible to investigate the formation of meanders, eddies and geophysical instabilities along the jet.

Therefore, our study is based on QG theory, given the suitability of investigating WBCs dynamics by such approximation, and we will follow *Pedlosky* [1987]. It is important to point out that we are trying to investigate the development of geophysical instabilities in a geostrophic flow, and the first consideration the QG theory assumes is that perturbations start growing from a initial basic state, e.g. a mean steady state

flow. The linear theory explains the development of these perturbations while their velocities are considered much smaller than the mean flow velocities. At the point these perturbations become too strong (e.g. the perturbed velocities have same order that the basic velocities), the nonlinear theory comes to solve the missing issues. Therefore, the geostrophic system of equations (which describes a horizontal steady state motion) are complemented by the temporal and advective derivatives, and from the combination of the equations of motion considering those terms, we obtain the time-dependent potential vorticity equation:

$$\frac{Dq}{Dt} = \left(\frac{\partial}{\partial t} + u\frac{\partial}{\partial x} + v\frac{\partial}{\partial y}\right) q = 0, \tag{2.1}$$

where u and v represent, respectively, the zonal and meridional geostrophic velocities.

This equation defines the main statement of the QG theory, which is conservation of potential vorticity (PV) q. For the 1-layer barotropic ocean under the short-wave approximation, q is define as

$$q = \nabla^2\psi + \beta y, \tag{2.2}$$

and for a $1^1/_2$-layer (or equivalent-barotropic) ocean,

$$q = \nabla^2\psi - \frac{\psi}{R_d^2} + \beta y, \tag{2.3}$$

where ψ is the geostrophic streamfunction and $\beta = {}^{\partial f}/_{\partial y}$ is the variation of the Coriolis parameter f. R_d is the Rossby deformation radius, defined as $R_d = \frac{\sqrt{\frac{\Delta\rho}{\rho_0} gH}}{|f_0|}$, whereas $\Delta\rho$ represents the density difference between the layers, H is the mean active layer thickness and g is the gravity acceleration. In the equivalent-barotropic approximation, it represents the first baroclinic deformation radius.

Here one can see the major advantage in using the QG framework. All the dynamics is reduced to a single equation that is a function of ψ, which is a scalar variable and makes the problem easier to be solved. It's important to highlight here that all this system of equations describes a horizontal motion. Equation 2.4 presents the relation between the geostrophic velocities and ψ:

$$u = -\frac{\partial\psi}{\partial y} \;\; ; \;\; v = \frac{\partial\psi}{\partial x}. \tag{2.4}$$

where u and v are the geostrophic velocities defined in the zonal (x) and meridional (y) directions.

In Equations 2.2 and 2.3, $\nabla^2\psi$ is the geostrophic relative vorticity, $\psi/_{R_d^2}$ is the stretching vorticity and βy is the planetary vorticity variation. Combining the expressions 2.1 and 2.4, we obtain a new equation for q as

$$\frac{Dq}{Dt} = \left(\frac{\partial}{\partial t} - \frac{\partial\psi}{\partial y}\frac{\partial}{\partial x} + \frac{\partial\psi}{\partial x}\frac{\partial}{\partial y}\right) q = 0. \tag{2.5}$$

or

$$\frac{\partial}{\partial t}q + J(\psi, q) = 0, \tag{2.6}$$

where the Jacobean operator is defined as $J(A, B) = \frac{\partial A}{\partial x}\frac{\partial B}{\partial y} - \frac{\partial A}{\partial y}\frac{\partial B}{\partial x}$.

In the next section, we will present a recent hydrographic dataset which comprised the BC system off southeast Brazil. We used this data to characterize the system under investigation in terms of vertical and horizontal structure, focusing the data analysis in guiding us to the development of the dynamical analyzes we proposed.

2.2 Brazil Current potential vorticity structure and quasi-geostrophic validation

The beginning of our analyzes will start from the evaluation of a hydrographic dataset which comprised the BC vertical and horizontal structure off Cape Frio. This dataset was obtained from a hydrografic cruise conducted in July, 2001 and was the second of the Project "Dinâmica do Ecossistema da Plataforma da Região Oeste do Atlântico Sul" (DEPROAS II). The cruise consisted of a transect off Cape Frio, composed by 26 hydrografic station, but only 6 comprised the BC flow, e.g. the continental shelf break and slope regions. The data acquisition was performed through the use of CTD top-bottom profiling. The CTD equipment (Conductivity-Temperature-Depth Profiler) measures temperature and salinity (T-S) along the water column. The cruise stations are illustrated in Figure 2.1.

We opted for choosing this dataset due to the presence of a BC flow apparently free of perturbation, e.g. no eddies or frontal meanders were associated with its flow. So,

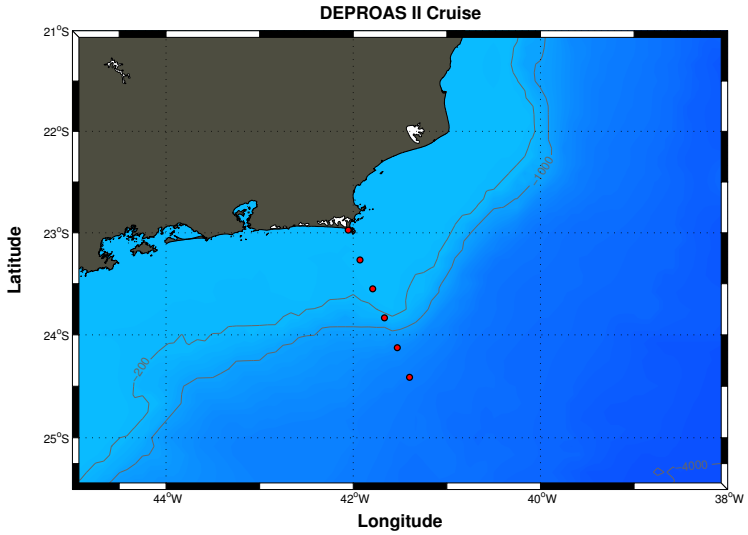

Figure 2.1: Representation of topography at southeast Brazilian continental margin (centered in Cape Frio). The dots represent the location of the hydrographic stations of DEPROAS II cruise conduct in July 2001 across Cape Frio.

we are considering here that this current represents the quasi-mean state of the BC off Cape Frio. This is important to our evaluation since we will prove that a quasi-mean flow is barotropically potentially unstable, so we will be able to validate the use of this data.

The dataset provided us density field information to allow us to compute baroclinic geostrophic velocities. Instead of following the traditional way of obtaining it through the Dynamic Method, we applied the POMsec (Princeton University Oceanic Model in its sectional version) to obtain vertical sections of absolute baroclinic geostrophic velocities. The method, according to *Lima* [1997] and *Silveira et al.* [2004], is independent of a reference level (for that reason it is called "absolute"), and we followed the above authors for our calculation. The use of baroclinic geostrophic velocities for our study is adequate, since the BC is a very baroclinic current, as discussed in Chapter 1.

Regarding the goals of our study, here we are interested in the kinematics structure of the BC system. Some properties, related to the cross jet and vertical velocity structures, are important information to help us in both determining the linear instability properties of the jet, and in prescribing the initial idealized conditions for the nonlinear evaluations. Moreover, we may determine if the jet is potentially unstable to develop geophysical instabilities, insofar as such conditions may trigger the development of mesoscale features. Therefore, we will use the baroclinic geostrophic velocity output

described above to develop all the following analyzes.

Firstly, we shall present the vertical section of meridional velocity obtained across Cape Frio, illustrated in Figure 2.2. In the figure, the reddish colors and negative values represent the BC flow, while the bluish colors and positive values are representative of the IWBC. From this figure, one can see the BC occupying the first 450 m of water column, flowing southwestward right above the continental slope. Underneath it, the IWBC is flowing northeastward, between 500 m and 1400 m.

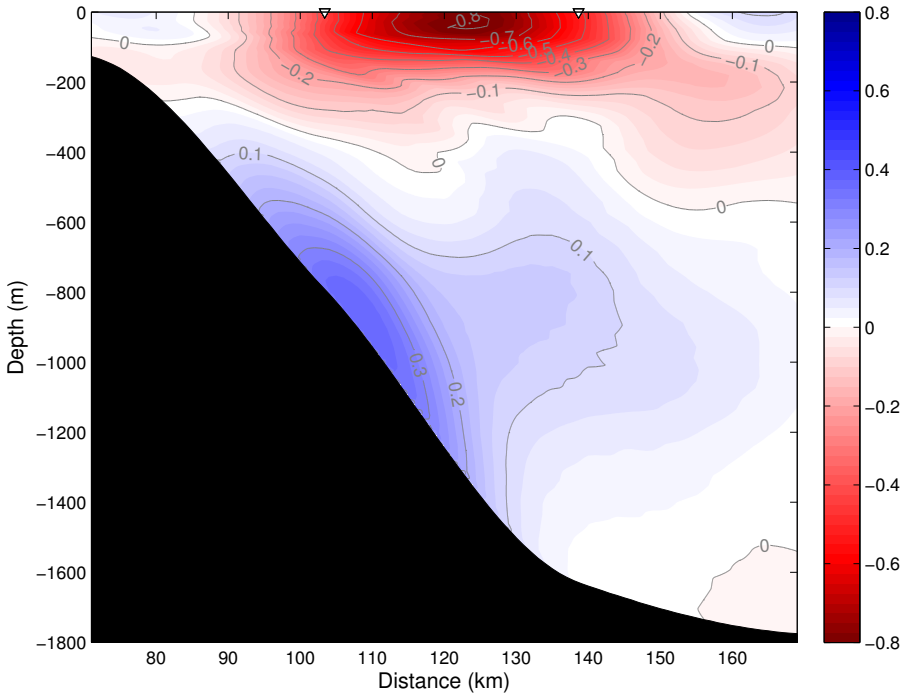

Figure 2.2: Vertical section of baroclinic geostrophic velocity along the transect across Cape Frio. Hydrografic data obtained from DEPROAS II cruise.

In having the velocity field, we shall validate the application of QG theory for the observed system we are analyzing. Therefore, we followed *Pedlosky* [1987] and checked the conditions for the QG approximation. The first condition is the Rossby number to be very small, e.g. $Ro = \frac{|\zeta|}{|f_0|} \ll 1$. Here ζ is the vertical component of relative vorticity vector defined as $\zeta = \left(\frac{\partial v}{\partial x} - \frac{\partial u}{\partial y}\right)$, and only the first right-hand side term is valid for the present case. Our calculation gave us a mean Ro = 0.18, which cannot be considered very small (e.g., smaller than 0.1), but leads to the information that the relative vorticity represents only 20% of the absolute vorticity. This value is comparable to other estimates that employed QG theory for the study of other WBCs, such as

the Florida Current and the North Brazil Undercurrent [*Xue & Mellor*, 1993; *Meacham*, 1991; *Silveira et al.*, 1999]. The second one would be the β plane approximation, e.g. $\hat{\beta} = \frac{\beta L}{|f_0|} \ll 1$. L should be the typical length scale of the BC width and its eddies, that we considered as having order 100 km. This gave us $\hat{\beta}$ = 0.04, which satisfies not only the β plane approximation, but we can securely ensure the f plane approximation is also valid.

After assuring the QG approximation can be applied to our study, we shall compute the QGPV (q) profile. To do so, we shall introduce the dynamics we are going to retain in our idealized QG ocean, where we will be basing all the following analyzes. Considering that the BC system presents an undercurrent below the BC flow and since we want to test the possibility of barotropic instability in triggering the formation of vortices and dipoles, we opted for considering a $1^1/_2$-layer model (also known as reduced-gravity approximation). This approximation allows us to incorporate both the condition for barotropic instability and the stratification effect in its minimal form. In other words, we keep the baroclinic scales of geostrophic adjustment but isolate the BC from interacting with the IWBC, and therefore, not allowing baroclinic instability to occur. Figure 2.3 exhibits our reduced-gravity model configuration. In the model, the rigid lid approximation is valid and the dynamically active layer corresponds to the BC layer (ρ_1). In Figure 2.3, such layer is represented with thickness H. Yet, $h = H + \eta$, where η is the vertical variation of the interface between ρ_1 and ρ_2. Within each layer, the Taylor-Proudman theorem is valid, e.g., the layers are homogeneous. The lower layer (ρ_2) is considered infinite and at rest. Hence, the QG velocities are null ($u = v = 0$), while the dynamically active layer of potential density (ρ_1) is in motion. Thus, Equation 2.3 under the f plane approximation becomes

$$q = \nabla^2\psi - \frac{\psi}{R_d^2}. \tag{2.7}$$

Since we are dealing with a vertical section, instead of following the traditional method of computing q through the streamfunction ψ, we opted for an alternative way and considered the Ertel PV equation for our calculations. For the $1^1/_2$-layer ocean, the

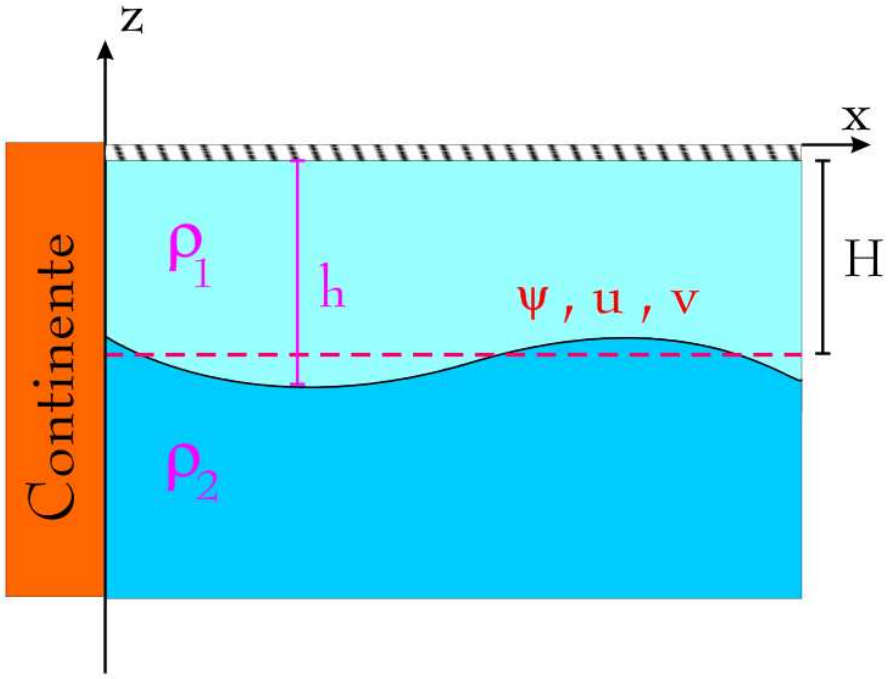

Figure 2.3: Schematic representation of the density structure of the QG $1^1/_2$-layer model. H is the water column rest thickness. From: *Leal Silva* [2000].

Ertel PV equation is represented by Equation 2.8:

$$\frac{D\Pi}{Dt} = 0 \tag{2.8}$$

and

$$\Pi = \frac{\zeta + f}{h}, \tag{2.9}$$

where ζ is the relative vorticity and h is the dynamical active layer thickness (see Figure 2.3. After estimating ζ and h, we shall use Equation 2.8 to obtain Ertel PV. From that, we may subtract the basic PV, assumed not to be dynamically relevant, e.g. we are interested in the Π perturbation. Therefore, q can be written as

$$q = H \;\; \Pi - f_0, \tag{2.10}$$

where H is the mean upper layer thickness in the QG model (same as H of Figure 2.3), indeed, a proxy for the QGPV q.

The first step to obtain q is determining the mean cross-jet velocity profile inside the active layer. Such layer was considered as the one defined by the SACW thickness, which comprises the pycnocline layer. Therefore, it is located below the mixed layer where ageostrophic processes may be relevant. The SACW layer is usually defined as

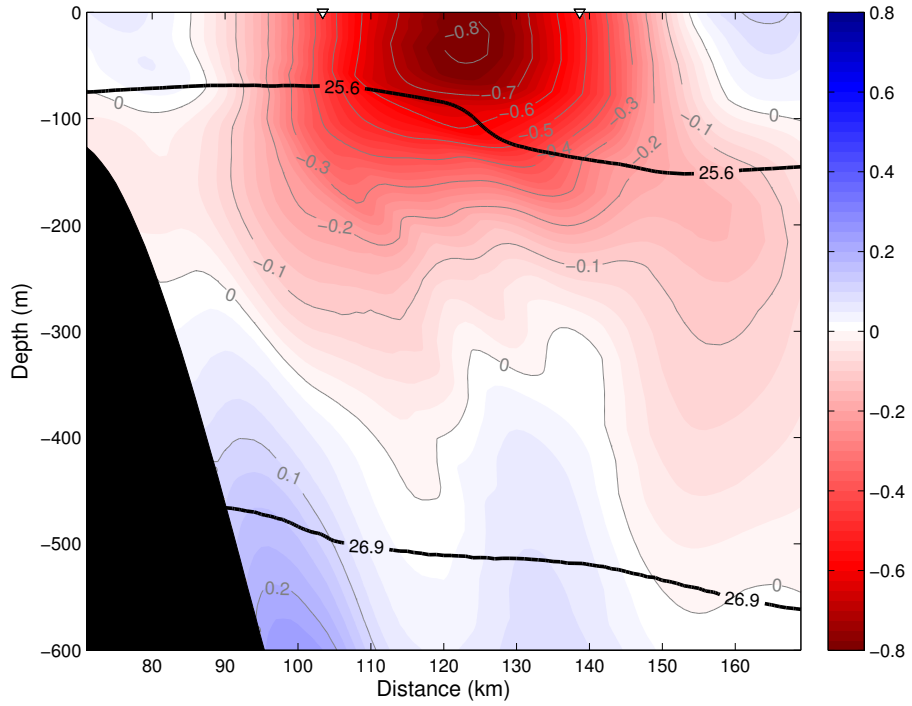

Figure 2.4: Vertical section of baroclinic geostrophic velocity along the transect across Cape Frio. Hydrografic data obtained from DEPROAS II cruise. TW-SACW interface is indicated by the isopycnal of 25.6 kg m^{-3}, and SACW-AIW interface is indicated by the isopycnal of 26.9 kg m^{-3}.

the one in between the 25.6 and 26.9 kg m^{-3} isopycnals [*Mémery et al.*, 2000; *Silveira*, 2007]. We computed the mean vertical velocity considering the 26.9 kg m^{-3} isopycnal mean level, which was about 500 m of depth. Figure 2.5 illustrates the SACW vertical layer we are considering here. Figure 2.4 illustrates the BC velocity vertical section where we plotted the SACW upper and lower limits.

The velocity profile is illustrated in Figure 2.6 and gave us a jet width of 80 km and a maximum along-stream velocity of -0.33 m s^{-1}. Then, considering the velocity profile obtained in Figure 2.6, we calculated ζ, that is represented by Figure 2.7 (left panel). Figure 2.7 (right panel) illustrates the cross-jet q profile. At a first glance, one can see that such profile changes sign along the cross-jet direction. Considering x direction perpendicular to the jet axis and y direction parallel to the jet axis, we checked the Rayleigh condition in this profile. Rayleigh condition says $\partial q/\partial x$ profile must have at least one inversion of sign inside the jet domain, and this defines the necessary but not sufficient conditions for barotropic instability. An additional and more robust condition for barotropic instabilities is known as Fjørtoft condition, that requires the $(\bar{v} - v_c)\partial q/\partial x$

profile to be positive in one portion of the domain ($\bar{v}$ is the mean along-stream velocity component and v_c is the velocity value correspondent to the inflexion point of $\partial q/\partial x$). Figure 2.8 illustrates both the Rayleigh and Fjørtoft conditions computed for the q profile in Figure 2.7. Looking to them, one can see that both conditions are met. Therefore, we can conclude that the observed BC is potentially barotropically unstable, e.g. it is characterized as a jet able to develop barotropic instabilities. From that, we may go forward in our analyzes, having velocity and PV structure as import parameters. It is also relevant to point out that goal number 1 (presented in Section 1.2) was accomplished, e.g. we characterized an approximately non-perturbed BC jet captured by an hydrographic dataset off Cape Frio in terms of horizontal and vertical extensions, cinematic characteristics and horizontal cross-jet structure of velocity and potential vorticity.

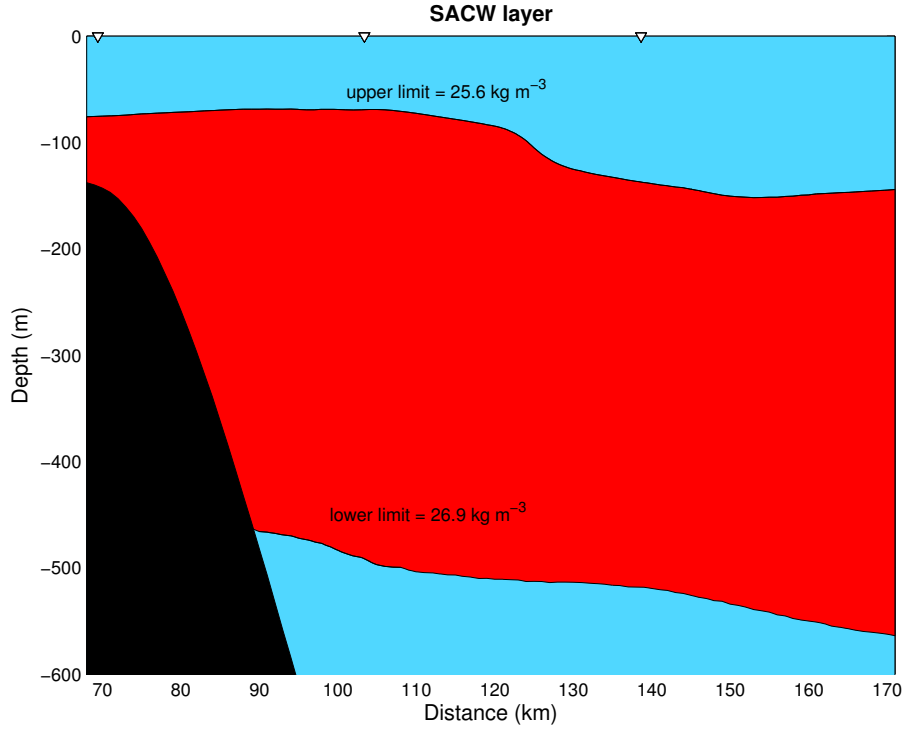

Figure 2.5: Schematic representation of the vertical layer comprised by the SACW in terms of density anomaly values. The lower limit 26.9 (kg m^{-3}) represents the limit between the BC and the IWBC flows.

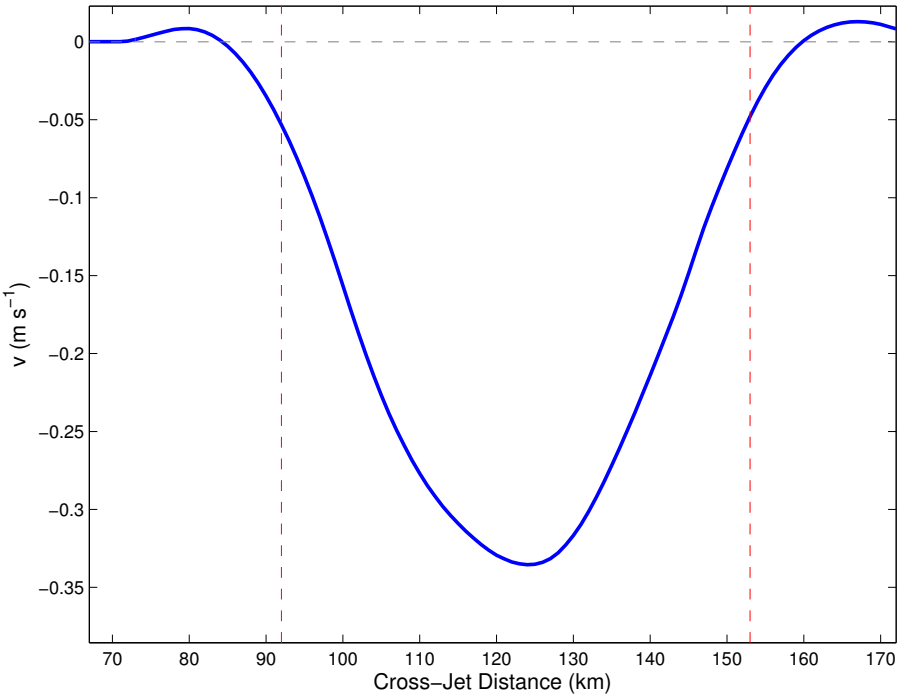

Figure 2.6: Vertical mean cross-jet velocity profile across Cape Frio, integrated within the SACW vertical layer. The red-dashed lines correspond to the -0.05 m s^{-1} and limit the jet area.

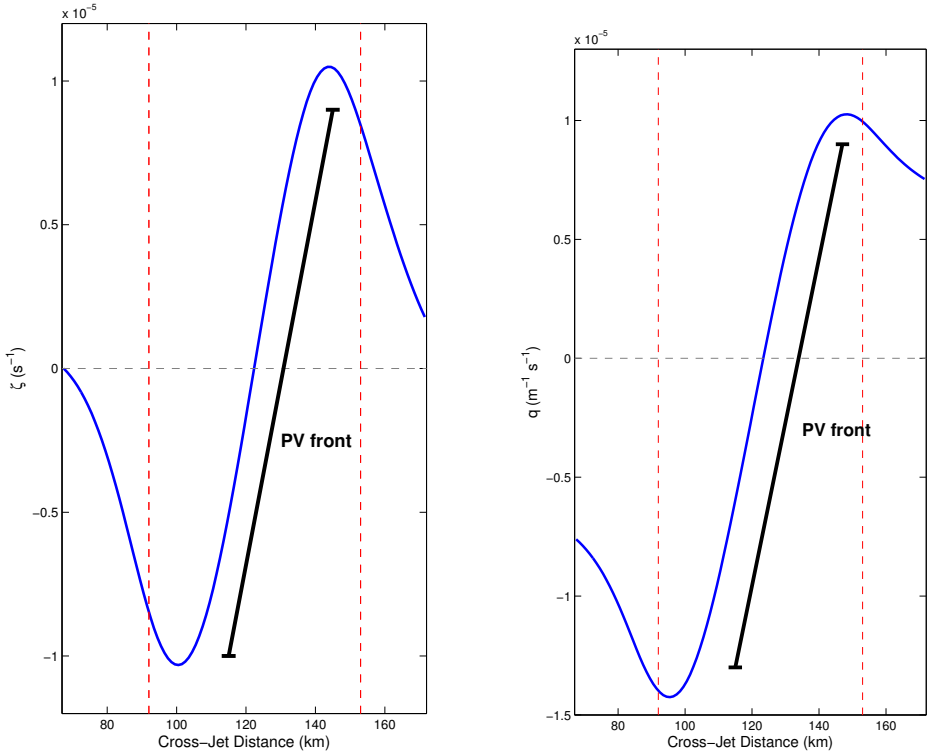

Figure 2.7: Relative vorticity ζ (left panel) and QG potential vorticity q (right panel) mean cross-jet profiles computed from the mean velocity profile of Figure 2.6. The black line highlights the vorticity front present in the jet. The red-dashed lines correspond to the -0.05 m s^{-1} and limit the jet area.

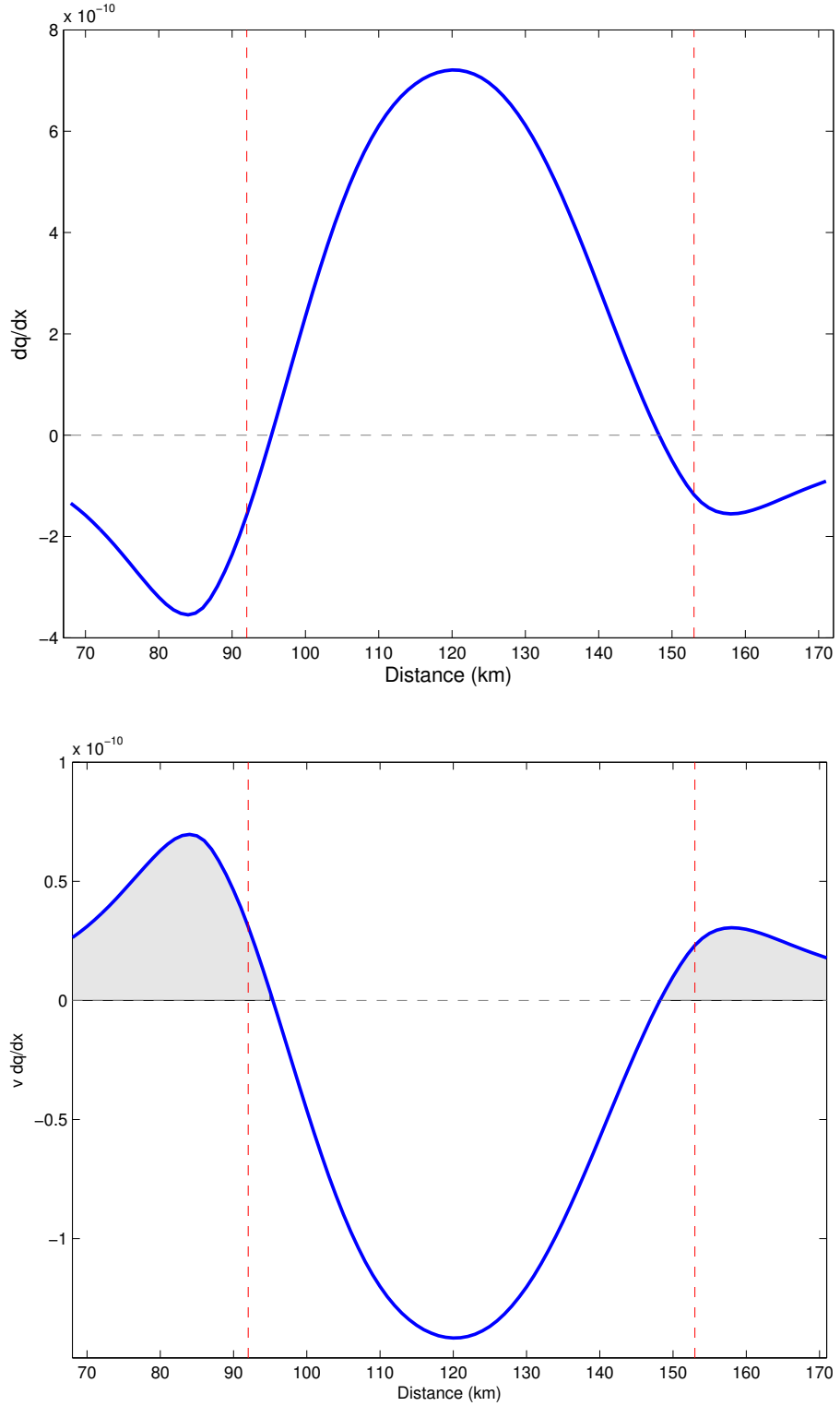

Figure 2.8: Necessary but not sufficient conditions for barotropic instability. Upper panel: Rayleigh condition ($^{dq}/_{dx}$ profile). Lower panel: Fjørtoft ($(\bar{v} - v_c)^{dq}/_{dx}$ profile). The gray-shaded regions indicate positive values for the Fjørtoft condition. The red-dashed lines correspond to the -0.05 m s^{-1} and limit the jet area.

Chapter 3

The contour dynamics model

The present chapter aims to describe the first step into the investigation of the dynamics of the BC and the formation of bipolar features. Using a dynamical approximation in accordance with the observed jet scenario off southeast Brazilian coast, we started from the application of the method known as contour dynamics (CD), where a piecewise constant PV field is evolved in a model that considers a meridional southward jet flowing along a straight western boundary wall. The idea of the present chapter is to start from the simplest analysis, where we retain the physics we are interested in and where we have the control of the processes that are governing the results. Advancing to the next chapters, we go towards the application of methodologies that bring more dynamical complexity to the study. Therefore, at each degree of complexity we advance into, the previous analysis certainly works as a control scenario and a baseline for the next one.

3.1 Methodology

The classical application of QG models is the use of the method known as CD, vastly used in studies that tried to investigate the dynamics of geophysical flows, including WBCs. Since geophysical flows are associated with PV fronts, the use of step function is a reasonable approximation. The technique was developed by *Stern* [1985] and *Pratt & Stern* [1986], and some important applications are in *Polvani et al.* [1988], *Polvani et al.* [1989], *Meacham* [1991], *Pratt et al.* [1991], and others. This method consists in

assuming that the PV horizontal field is discretized in layers of uniform vorticity. The front separating each layer is called a contour, and PV is conserved along each contour. Moreover, the velocity is continuous across each front, but the PV is discontinuous. Then the CD technique consists in simply following the evolution of these contours. Since PV is conserved, these contours are material curves.

The geostrophic velocities can be written as contour integrals which are dependent upon the position of the contours, through the inversion of q [*Pullin*, 1992]. It is possible to see how the advection changes the modeled ocean structures through the evolution of q anomalies and the currents induced by them. The advantage in using CD is characterized by the principle of inversion of q, and then the problem (originally in two or three dimensions) is reduced to a set of linked unidimensional problems.

Silveira et al. [1999] utilized a configuration of q with only one PV front (one contour) in a equivalent-barotropic ocean in order to study converging jets along a western boundary. *Silveira & Flierl* [2002] investigated the same problem in a $2^1/_2$-layers configuration, and considering a three-front jet. Following both studies, here we implemented the technique for a 3-front meridional jet flowing along a western boundary in a $1^1/_2$-layers ocean. The initial conditions of the CD model were constructed based on the jet structure and kinematics characteristics obtained in Chapter 2. The CD technique is composed by two parts. The first consists of a linear analysis, where the linear theory considers the magnitude of the flow perturbations much smaller than the magnitude of the mean flow velocities. This allow us to obtain the linear instability properties of the jet. The nonlinear analysis allow these perturbations to grow and give us the time evolution of the piecewise constant PV field. In the next section, we present the development of the CD methodology for the case of a n-fronts meridional jet flowing along a meridionally-oriented western boundary.

3.1.1 The linear model

Here we will present the equations considering a meridional jet attached to the western boundary. Since the BC flows in the southwest direction, we will consider y as the direction parallel to the jet and x as the direction normal to the jet. Within the jet domain, we assumed conservation of q, in accordance with $1^1/_2$-layers QG theory. Therefore,

we shall recall Equation 2.6 and the q inversion relationship given by Equation 2.3. The CD technique, besides using the q inversibility relation, requires the utilization of the equations in their non-dimensional form. Therefore, we may scale some important parameters that will be used in the linear model. The scales utilized in this study are presented in Table 3.1. Therefore, Equation 2.3 in its non-dimensional form and assuming f plane is

$$(\nabla^2 - 1)\psi \;=\; q. \tag{3.1}$$

It is important to point out that, since we are dealing typically with mesoscale structures, we utilized R_d as the characteristic horizontal length scale. As we presented in Section 2.2, it was previously computed as having 36 km.

Table 3.1: Non-dimensional scales.

QUANTITY	SCALE
horizontal length	R_d
horizontal velocity	V
time	$R_d V^{-1}$
potential vorticity	$V R_d^{-1}$
horizontal PV gradient	$V R_d^{-2}$
V = jet core velocity	

The linear model here consists in a set of calculations we utilized to determine the gradient of PV and the zonal profile of the meridional velocity, which are function of the choices of mean velocity values at the contours. Here we also developed the set of equations that have considered the western boundary close to the flowing jet, which means the continent has influence on the dynamics of the fronts (contours). Following *Silveira et al.* [1999], the q fields can be expressed as

$$q(x) \;=\; q_0 \;+\; \sum_{i=1}^{3} \Delta_i \, \mathcal{H}[x - \bar{x}_i - \xi_i(y,t)] \; . \tag{3.2}$$

In Equation 3.2, the contours are enumerated in sequence with index in the range 1 to 3. The Δ_i values correspond to the q jumps (e.g. the gradients), $\bar{x}_i$ are the contours mean positions, and ξ_i their deviations. $\mathcal{H}$ represents the Heaviside step function, where

$$\mathcal{H}(x) = 0 \text{ for } x < 0$$
$$\mathcal{H}(x) = 1 \text{ for } x > 0\,.$$

It is possible to replace the choices of Δ_i by choices of $\bar{v}_i$, e.g., the basic meridional velocity values at the contours. Then, through the initial choice of $\bar{x}_i$ and $\bar{v}_i$, the linear instability properties can be obtained. The reader should note that we opted to use a PV structure of four regions of piecewise constant q separated by three fronts. This choice was made in order to correctly approximate the PV structure on the cyclonic and anticyclonic borders of the WBC jet. Moreover, the application of the technique is reasonable and it is relatively easier to solve the integrations for a three-fronts jet. As you increase the number of fronts, the problem becomes much more complex because you introduce a higher number of degrees of freedom.

The inversion relationship that solves the problem is Equation 3.1. Splitting such solution in two parts, we can have one part related to the basic state $\bar{\psi}$ (the undisturbed and straight front), and the other related to the perturbed state ψ' (this last one is associated to small amplitude waves). Therefore, we obtain

$$\psi = \bar{\psi}(x, y) + \psi'(x, y, t). \tag{3.3}$$

Considering a wave solution type for ψ', we can write

$$\psi' = \phi(x) e^{il(y-ct)}, \tag{3.4}$$

where c is the phase velocity and l is the wavenumber parallel to the jet. Therefore, the solutions for ξ and u' are also a wave solution type

$$\xi_i = \hat{\xi}_i e^{il(y-ct)} \tag{3.5}$$

and

$$u' = \hat{u} e^{il(y-ct)}. \tag{3.6}$$

Similarly to Equation 3.3, we shall split q as

$$q = \bar{q}(x) + q'(x, y, t). \tag{3.7}$$

where

$$\bar{q} \;=\; q_0 \;+\; \sum_{i=1}^{3} \Delta_i \, \mathcal{H}(x - \bar{x}_i) \tag{3.8}$$

and

$$q' \;=\; \sum_{i=1}^{3} \Delta_i \left[\mathcal{H}(x - \bar{x}_i - \xi_i(y,t)) - \mathcal{H}(x - \bar{x}_i) \right] . \tag{3.9}$$

Given the solutions above, we can write the inversion relationship for both solutions $\bar{q}$ and q', where

$$\left(\frac{\partial^2}{\partial x^2} - 1 \right) \bar{\psi} \;=\; \bar{q} \tag{3.10}$$

and

$$(\nabla^2 - 1)\psi' \;=\; q'. \tag{3.11}$$

Applying the equation that relates ψ, u and v (Equation 2.4) in Equations 3.10 and 3.11, linearizing and assuming small amplitude waves, we obtained for the basic state

$$\left(\frac{\partial^2}{\partial x^2} - 1 \right) \bar{v}(x) \;=\; -\sum_{i=1}^{3} \Delta_i \delta \left(x - \bar{x}_i \right) \tag{3.12}$$

and for the perturbed state

$$(\nabla^2 - 1)u' \;=\; -\sum_{i=1}^{3} \Delta_i \delta \left(x - \bar{x}_i - \xi_i \right) \left(\frac{\partial \xi_i}{\partial y} \right) . \tag{3.13}$$

Combining the conservation of q equation (Equation 3.1) and the linear wave solution type Equation 3.6, we obtain

$$u' \;=\; \frac{\partial \xi_i}{\partial t} \;+\; v \frac{\partial \xi_i}{\partial y}. \tag{3.14}$$

Replacing ξ_i and u' in Equations 3.13 and 3.14 for the wave solutions and linearizing the equations, we obtain, respectively,

$$(\nabla^2 - 1)\hat{u} \;=\; -il \sum_{i=1}^{3} \left[\Delta_i \delta(x - \bar{x}_i) \frac{\partial \hat{\xi}_i}{\partial y} \right] \tag{3.15}$$

and

$$\hat{u} \;=\; il \, \hat{\xi}_i \left[\bar{v}(x) - c \right]. \tag{3.16}$$

The solutions for 3.12 and 3.15 are obtained from the Green's function method, that satisfies

$$\frac{\partial^2}{\partial x^2} + (l^2+1)\, G(x|x') \;=\; \delta(x-x'). \tag{3.17}$$

The solution for Equation 3.17 in the presence of a western boundary placed at x = 0 is

$$G_l(x|x') \;=\; G_{l+}(x|x') + G_{l-}(x|x'), \tag{3.18}$$

where

$$G_{l+} \;=\; \frac{1}{2\sqrt{l^2+1}} e^{-\sqrt{l^2+1}\,|x-x'|}, \tag{3.19}$$

and

$$G_{l-} \;=\; -\frac{1}{2\sqrt{l^2+1}} e^{-\sqrt{l^2+1}\,|x+x'|}. \tag{3.20}$$

The G_{l-} is associated with the vortex images necessary to satisfy the boundary condition at x = 0. For the particular case of $l = 0$, the Green's function becomes

$$\begin{aligned} G_0(x|x') \;&=\; G_{0+}(x|x') + G_{0-}(x|x') \\ &=\; \frac{1}{2} e^{-|x-x'|} - \frac{1}{2} e^{-|x+x'|}. \end{aligned} \tag{3.21}$$

Applying 3.18 and 3.21 in $\bar{v}$ and u' equations, we obtain

$$\bar{v} \;=\; \sum_{i=1}^{3} \Delta_i G_0(x|x') \tag{3.22}$$

and

$$u' \;=\; -il \sum_{i=1}^{3} \Delta_i\, G_l(x|x')\, \hat{\xi}_i. \tag{3.23}$$

Having Equations 3.16, 3.22 and 3.23, we can find the dispersion relation through the applications of 3.16 in each contour and

$$M_l\, \hat{\xi}_i \;=\; 0. \tag{3.24}$$

M_l is the squared matrix 3×3 given by the three equations mentioned above. The non-trivial solution for c is found considering

$$\det(M_l) \; = \; 0. \tag{3.25}$$

From the dispersion relation equation, we obtain a complex number c, in which the real and imaginary parts are related, respectively, with the phase velocity (c) and with the wave growth rate (σ). The non-trivial solutions for c is obtained as

$$c \; = \; c_r + ic_i \; = \; c_r + \frac{i\sigma}{l}. \tag{3.26}$$

We can also obtain the wave frequency (ω) and its group velocity (c_g), expressed by

$$\omega \; = \; lc \tag{3.27}$$

and

$$c_g \; = \; \frac{d\omega}{dl}. \tag{3.28}$$

Having Equation 3.22, we can obtain the zonal profile of the meridional jet . In practical terms, such equation is solved in a inverted form, since the choice of $\bar{v}(\bar{x}_i)$ is more intuitive than the q jumps choice in each front (Δ_i).

The set of equations presented above characterizes the linear analysis, and we have shown how to obtain the linear instability properties, which are the zonal profile of the meridional jet, growth rate of the unstable waves and phase and group velocities.

3.1.2 The nonlinear model

The nonlinear model is the second part of the CD technique. It determines the non-linear evolution of the system from a initial PV distribution. The conservation of q equation is Equation 3.1. Then, we again split the q and ψ fields in two parts, such as Equation 3.3:

$$\psi \; = \; \bar{\psi}(x, y) + \psi'(x, y, t). \tag{3.29}$$

where $\bar{\psi}$ is associated to the rectilinear q fronts positions. The inversibility relation that associates $\bar{q}$ and $\bar{\psi}$ is according to Equations 3.8 and 3.10:

$$(\nabla^2 - 1)\bar{\psi} = \bar{q} \tag{3.30}$$

$$= q_0 + \sum_{i=1}^{3} \Delta_i \mathcal{H}(x - \bar{x}_i). \tag{3.31}$$

The ψ' component is the perturbed part of the solution, and it is correspondent to the streamfunction field associated to space-temporal deviations of ψ. Therefore, as defined in Equation 3.9 and 3.11,

$$(\nabla^2 - 1)\psi' = q'$$

$$= \sum_{i=1}^{3} \Delta_i \left[\mathcal{H}(x - \bar{x}_i - \xi_i) - \mathcal{H}(x - \bar{x}_i)\right]. \tag{3.32}$$

According to *Pratt & Stern* [1986], in order to set appropriate boundary conditions, the Green's function takes the form

$$G = G_+ + G_- = -\frac{1}{2\pi} K_0(r_+) + \frac{1}{2\pi} K_0(r_-)\,, \tag{3.33}$$

where K_0 is the modified Bessel function of the second kind of order zero, G_- represents the image point required to satisfy $\psi' = 0$ at the western boundary and

$$r_+{}^2 = (x - x')^2 + (y - y')^2\,,$$

$$r_-{}^2 = (x + x')^2 + (y - y')^2\,.$$

The disturbed velocity field is determined from Equation 3.32, according to stream function definition

$$(u', v') = (-\frac{\partial}{\partial y}, \frac{\partial}{\partial x})\psi'\,, \tag{3.34}$$

and using Equation 3.33.

The contour dynamics technique requires Equation 3.34 be written in terms of contour integrals. According to *Pratt & Stern* [1986], we need to express the x and y derivatives in terms of x' and y'. We then follow *Silveira & Flierl* [2002] derivation in using the

symmetry properties of the Green's function to write

$$\frac{\partial}{\partial x}G_+ = -\frac{\partial}{\partial x'}G_+ \tag{3.35}$$
$$\frac{\partial}{\partial x}G_- = \frac{\partial}{\partial x'}G_- \tag{3.36}$$
$$\frac{\partial}{\partial y}G_+ = -\frac{\partial}{\partial y'}G_+ \tag{3.37}$$
$$\frac{\partial}{\partial y}G_- = -\frac{\partial}{\partial y'}G_- \,. \tag{3.38}$$

We then invoke the divergence theorem,

$$\begin{aligned} v' &= 2\int\int_D \nabla\cdot(G_+\vec{i}' - G_-\vec{i}')\,dx'\,dy' \\ &= 2\int_{\partial D}(G_+ - G_-)(\vec{i}'\cdot\vec{n}')\,dr' \\ &= -2\int_{\partial D}(G_+ - G_-)\,dy' \,, \end{aligned}$$

where ∂D is the contour enclosing D, $\vec{n}'$ is the unit vector normal to ∂D, dl' is the infinitesimal increment along ∂D, and $\vec{i}'$ is the unit vector in the x'-direction.

An analogous procedure can be applied to obtain the disturbed cross-shore velocity u' in terms of contour integrals. Using the Green's function definitions (3.33) in the velocity expressions yields

$$u' = \frac{1}{\pi}\int_{\partial D}[K_0(r_+) - K_0(r_-)]\,dx' \tag{3.39}$$

$$v' = \frac{1}{\pi}\int_{\partial D}[K_0(r_+) + K_0(r_-)]\,dy' \,. \tag{3.40}$$

The partitioning of the streamfunction field was chosen so that Equations 3.32, 3.39 and 3.40 do not involve improper integrals, which potentially behave poorly [*Pratt & Stern*, 1986]. Rather, ∂D in Equations 3.39 and 3.40 has finite boundaries.

However, Equations 3.39 and 3.40 still have a logarithmic singularity because $K_0(r) \simeq -\ln(r)$ when r is very small. The singularity is circumvented following *Polvani et al.* [1988] through a simple integration by parts of Equations 3.39 and 3.40, leading to the non-singular expressions

$$u' = \frac{1}{\pi}\Big[\int_{\partial D}(x - x')\,K_1(r_+)\,\frac{{dr_+}^2}{2r_+} + \int_{\partial D}(x + x')\,K_1(r_-)\,\frac{{dr_-}^2}{2r_-}\Big] \tag{3.41}$$

$$v' \;=\; \frac{1}{\pi}[\int_{\partial D}(y-y')\,K_1(r_+)\,\frac{{dr_+}^2}{2r_+} \;+\; \int_{\partial D}(y-y')\,K_1(r_-)\,\frac{{dr_-}^2}{2r_-}]\,, \tag{3.42}$$

where K_1 is the modified Bessel function of the second kind of order one.

Finally, having the q contour values, they can evolve in time according to

$$\frac{d}{dt}\xi_i \;=\; u_i \;=\; \frac{d}{dt}\psi(x_i, y+\xi_i(y,t),t). \tag{3.43}$$

It is important to notice that the above equations are nonlinear. However, since the second term in the Taylor series expansion of $\mathcal{H}$ is the delta function, the above system can be easily linearized. It is important to highlight that the separation of ψ in components, according to *Silveira et al.* [1999], is done to facilitate the application of the CD technique in semi-infinite domains.

3.2 Linear analysis results

Recalling the cross-jet velocity profile of Figure 2.6, we computed a BC width of approximately 80 km. In that figure, one can notice the BC jet is almost symmetric, with its core located at about 50 km from the shelf break. The coastal side of the jet is at about 90 km distance from the nearest point in the coast and the offshore side at about 160 km. Getting the maximum velocity value in this profile and considering R_d as the horizontal length scale, we scaled the parameters of the model according to Table 3.1, using R_d = 36 km and $|v_{max}| = V$ = 0.33 m s^{-1}. Figure 3.1 presents again the original velocity profile with the indication of the three contours positions used for the linear model. Still in the figure, the non-dimensional velocity profile is illustrated, also with the indication of the three contours positions. The non-dimensional values used as input parameters for the linear model are presented in Table 3.2, where i refers to each front (i = 1 is the continental-side front, i = 2 is the jet core front, and i = 3, the deep ocean side front). $\bar{x}_i$ are the front positions, v_i are the velocities at each front, and Δ_i are the PV jumps.

Having that, we applied the linear model. The modeled jet profile is illustrated in Figure 3.2 (left panel), where we also plotted the original observed one for comparison. The model also gave us the q jumps (Δ_i), also presented in Table 3.2. It is

Table 3.2: Input data for the linear model.

QUANTITY	**i=1**	**i=2**	**i=3**
$\bar{x}_i$	0.55	1.55	2.55
v_i	0	-1	0
Δ_i	0.85	-2.62	0.85

important to highlight the change of sign in the Δ_i values, which satisfy the Rayleigh necessary conditions for barotropic instability. Figure 3.2 (right panel) illustrates the non-dimensional q profiles, the modeled over the observed one (presented in Chapter 2).

The linear instability properties of the modeled jet are represented by Figure 3.3. The upper panel illustrates the phase and group velocities of the unstable wave, while the lower panel refers to the growth rate of the unstable wave. The higher value of growth rate (0,14) corresponds to a wavenumber of 1.29, which gives a wavelength of 4.87 R_d. If we re-scaled this value by R_d, we obtain a dimensional wavelength of 175 km. This value in within the range of the BC paired eddies depicted in Figure 1.9. The wavelength of 175 km is correspondent to the most unstable wave obtained by the linear model, and might indicate that the BC is potentially unstable for the generations of a unstable wave of the same order of the previously observed mesoscale features. The phase velocity plot confirm the propagation of the unstable wave southward, since it presents negative values only. The mean phase velocity was of -0.18, while the mean group velocity was of -0.31.

3.3 Nonlinear results and discussion

Here we present the experiment conducted for the nonlinear model. The initial conditions of this model were obtained from the linear model, where we used the informations of front positions $\bar{x}_i$ and the PV jumps Δ_i (see Table 3.2). We considered that the cyclonic eddy off Cape Frio, which is a recurrent feature present in the area, can trigger barotropically unstable waves inside the southeast Brazilian oceanic region. Hence, we assumed the meander can make the jet unstable and, because of that, we used appro-

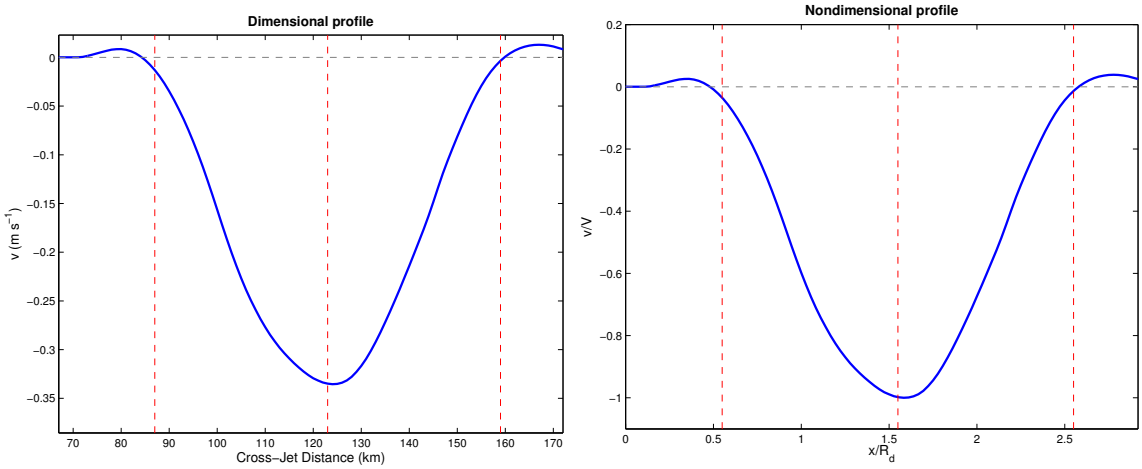

Figure 3.1: Mean velocity profile obtained from the observational dataset and presented in Chapter 2. The three fronts used in the linear model are indicated by a red-dashed line. Left panel: dimensional profile; right panel: non-dimensional profile.

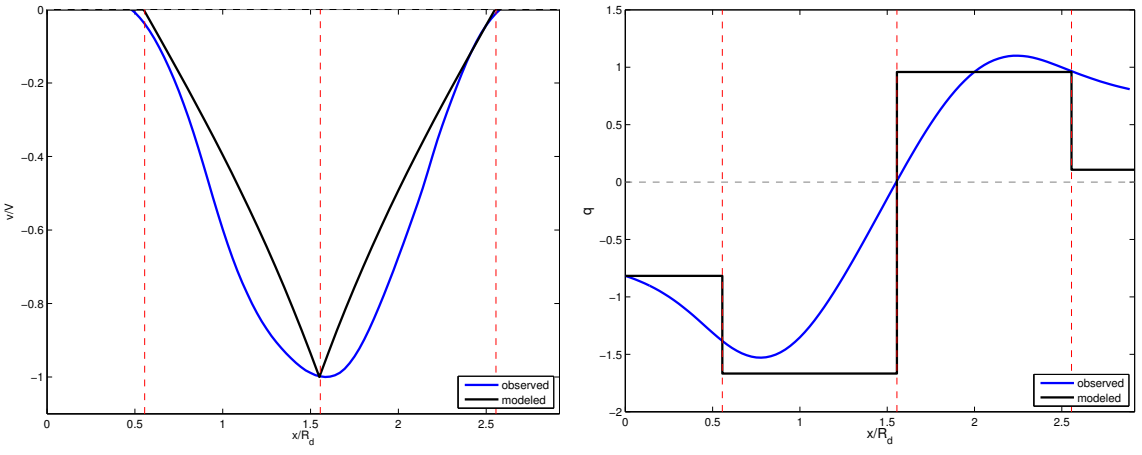

Figure 3.2: Left panel: non-dimensional velocity profile of the modeled jet (black) over the observed non-dimensional profile (blue). Right panel: non-dimensional q profile of the modeled jet (black) over the observed non-dimensional profile (blue).

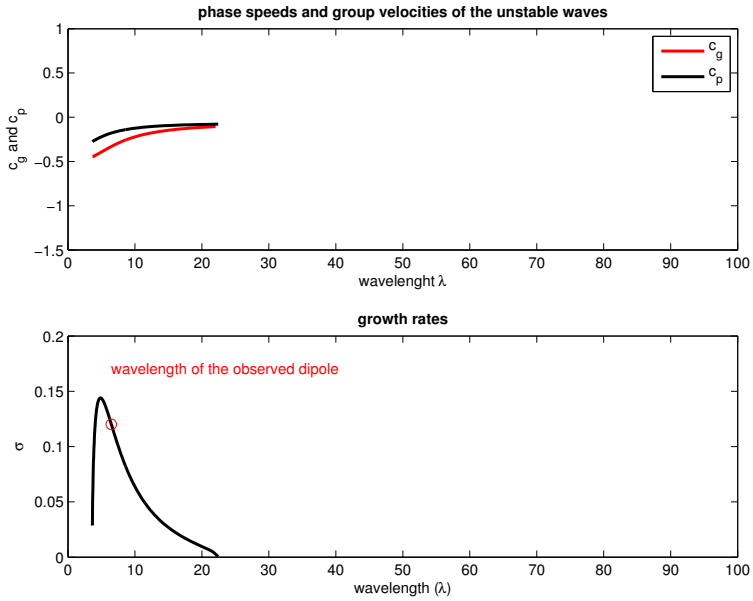

Figure 3.3: Linear instability properties of the three-fronts jet. Upper panel: phase velocity c_p (black) and group velocity c_g (red) of the unstable wave. Lower panel: growth rate σ of the unstable wave. The wavelength of the observed dipole (Figure 1.9) is indicated in the figure.

priate values to excite the jet within possible wavenumbers from Cape Frio eddy. In the absence of mechanisms to generate a Cape Frio-like eddy in the model, we used a initial perturbation in the jet in the form of a $\cos$ bump. The perturbation equation is presented in Equation 3.44

$$b == Aexp\left[\frac{-(y)^2}{w^2}\right]\cos(k_0 y). \tag{3.44}$$

where we used as the wave amplitude A = 1, the function width w = 1.5 and the most unstable wavenumber (from the linear model) k_0 = 1.29 (all the values are non-dimensional). This multilobed anomaly sets k_0 as the dominant wavenumber, and the width w determines the extent to which wavelengths neighboring k_0 are present.

The results of the temporal evolution of the initial disturbance are illustrated in Figure 3.4. The jet is meridionally oriented and it is propagating southward. The upper left panel illustrates the initial state of the model, where there is a bump perturbation upstream. The central front (at x = 1.55) represents the jet core. We can see the downstream evolution of the fronts the in following days. In day 10, an eddy was formed at each side of the jet. In day 15, a dipole start to grow upstream, while eddies continue to be formed right downstream. At the end of the simulation (day 25), the jet evolved to a

scenario where paired eddies were generated upstream, close to the perturbation location. This result correspond to the results obtained by *Pereira* [2009] and *Velhote* [1998], where the dipole (paired eddies) were observed close to Cape Frio. Downstream, the pattern is like a vortex street (*Bell & Pratt* [1992]), such as the scenario described by *Campos et al.* [1996] in the southeast region of the Brazilian continental margin.

It is possible to note that the presence of the western wall limits the spatial growth of the features in the coastal side. We performed a simulation with the same jet characteristics, but in a open ocean domain (no boundaries), and could see the differences. In the open domain, the same structures were formed, but they could spatially grow and became more organized. In the case presented here, the features seem to shrink due to the solid wall, and the eddies are more distorted.

The wave typical length scale in our simulation was about 4.5 R_d, which gives a dimensional value of 162 km. The most unstable wave obtained in the linear model results were of 175 km (4.8 R_d). Therefore, the nonlinear evolution could reproduce a pattern in accordance with the linear characteristics of the jet.

The results presented here conducted us to verify that a barotropically unstable jet within a simple and limited framework of piecewise constant PV fronts can generate dipoles and also a sequence of non-paired eddies that propagate downstream. In other words, a model with a PV structure that is able to support the vortex dipole formation in its minimal form satisfactorily reproduced the main characteristics of the BC dipoles described in the literature from observations. In the next chapter, we will relax the oversimplified piecewise constant PV field and allow the q structure to be quasi-continuous horizontally. Also, we will seek to examine the dynamical effect of a curvy coastline besides the investigation of WBC jets flowing adjacent to a meridional coast. In order to do that, we will calibrate the model with the jet characteristics obtained in Chapter 2 and we will consider that wavelength of approximately 175 km can occur (e.g. eddies of about 87 km), which is the wavelength of the most unstable barotropic waves that the BC jet can excite.

Finally, it is important to highlight that our goals number 2 and 3 presented in Section 1.2 were accomplished in the present chapter, e.g we obtained the linear instability properties of the observed jet, isolated the effect of barotropic instability and examined

the nonlinear evolution of the jet in a CD model.

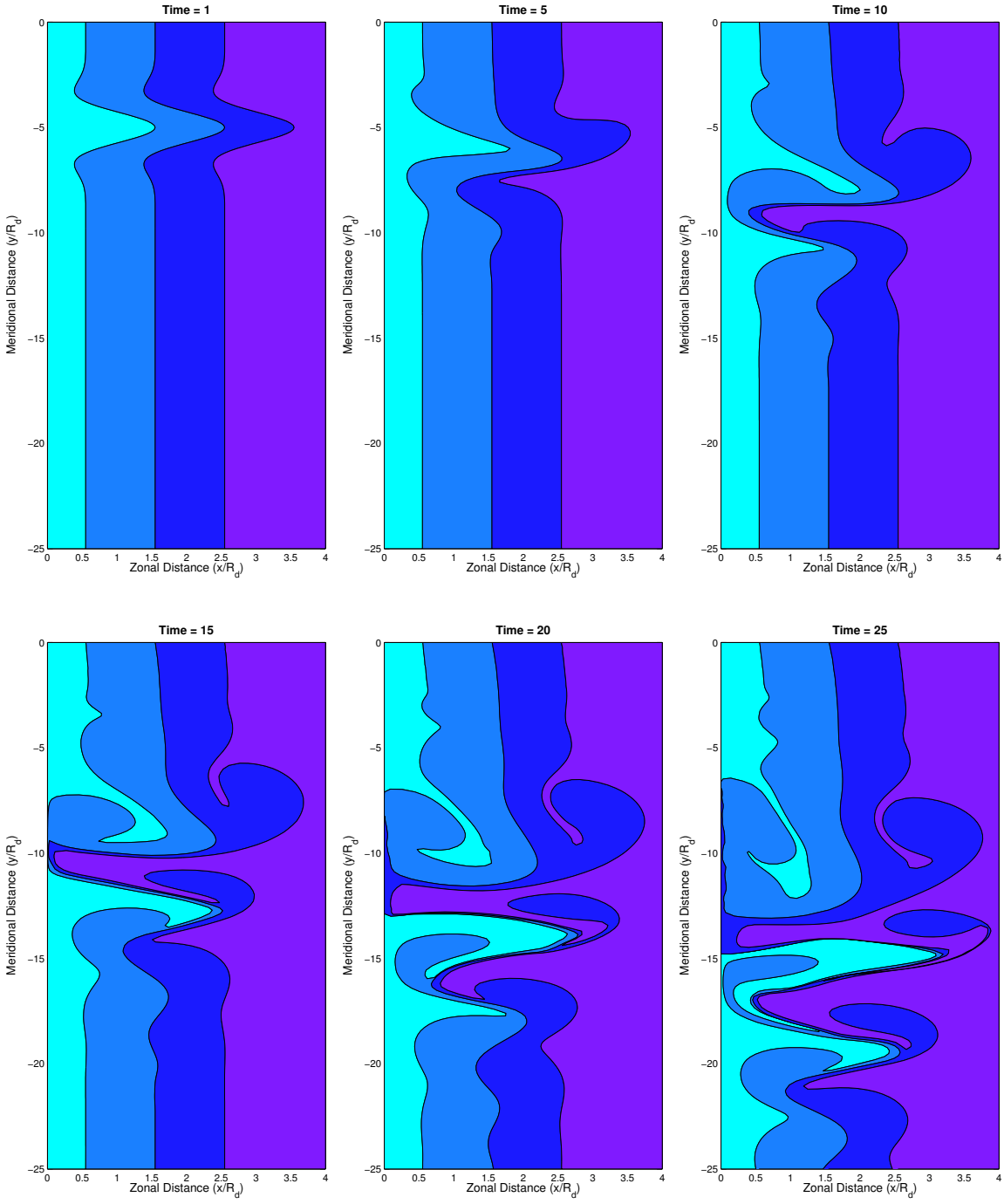

Figure 3.4: Nonlinear model results for t = 1, 5, 10, 15, 20 and 25 days. Four PV regions are separated by three fronts. The cyan color represents the coastal side of the model, while the purple color represents the deep ocean side of the model. The central front represents the jet core.

Chapter 4

The quasigeostrophic numerical model

In order to bring more complexity and reality to our idealized physical system, here we will present the methodology developed and the analysis conducted for a multi-front (quasi-continuous) PV field. Given the fact that being more realistic regarding the horizontal structure of the idealized ocean, the CD technique would become very complex to solve. The other approach presented here is essentially a numerical model under the quasigeostrophic (QG) approximation. It allows, besides a quasi-continuous PV field, the implementation of solid boundaries, both rectilinear and curvilinear.

We intended to investigate the downstream evolution of an idealized prescribed jet which was set to be potentially barotropically unstable, in order to see the possible development of instabilities translated in eddies and/or dipoles. Since our statement (presented in Chapter 1) is that bipolar features are formed due to barotropic instabilities, here we aimed to isolate this phenomenon in a 2-dimensional QG model. Using the information obtained in Chapter 2, this jet was calibrated with the BC characteristics in terms of horizontal scale and velocity magnitude.

We investigated the behavior of a meridional southward jet under the barotropic and equivalent-barotropic approximations. Trying to start from the simplest scenario and evolve to a more complex one, we considered 3 different cases. The first consisted of a meridional jet centered in a open domain. The second consisted of meridional jet flowing along a straight western boundary inside a meridional channel. In the third one, we added a variant coastline, and we investigated the behavior of the jet interacting with this perturbation, again inside a meridional channel. The idea was to con-

struct a theoretical understanding regarding the development of barotropic instabilities in a BC-like jet through the investigation of the two simplest QG dynamical cases: the 1-layer barotropic case and the $1^1/_2$-layer equivalent-barotropic case. Although the latter consists of a dynamical simplification more in accordance with the BC system off Cape Frio, the barotropic study will be the baseline in which we know the interaction of a meridional simple jet with a more complex western boundary. Moreover, although the dipoles formation is located in a region where the CB is very baroclinic, there are evidences of the downstream propagation of these structures (resembling a wave pattern composed by cyclones and anticyclones) into a region where the BC tends to be more barotropic, since the current vertical extension reaches deeper levels as it flows southwestward.

4.1 Methodology

The model is essentially the quasigeostrophic one described in *Jayne et al.* [1996] and *Waterman & Jayne* [2011]. However, while the authors investigated a zonal eastward jet along an infinite zonal channel, here we considered a meridional southward jet. Then, our analysis is based on the along-stream evolution of an idealized WBC jet using a numerical model of an unstable, boundary forced jet in a meridionally-oriented channel. The QG model is on the f plane, and fully nonlinear, with x (zonal direction), y (meridional direction) and time dependence, and it is dimensional. The model is forced at the northern boundary by imposing a jet inflow directed southward and it is scaled appropriate to the BC extension. We solve a modified conservation of PV equation, where, instead of considering the balance in Equation 2.6, we opted to include a dissipation term. This was done in order to facilitate dealing with some numerical issues, such as giving stability to the model and to configure an inflow-outflow condition. Hence, our new PV equation (for a inviscid ocean) is

$$\frac{\partial}{\partial t}q + J(\psi, q) = -R\nabla^2\psi, \tag{4.1}$$

where R is the bottom friction coefficient (which scales as t^{-1}) and ∇^2 is the horizontal Laplacian operator. Again, q is our QG potential vorticity (QGPV) and ψ is the

streamfunction. Then, q is defined in the 1-layer (2-dimensional) case as

$$q = \nabla^2 \psi, \tag{4.2}$$

and for the $1^1/_2$-layer case (for the dynamical active upper layer)

$$q = \nabla^2 \psi - \frac{\psi}{R_d^2}. \tag{4.3}$$

where R_d is the first baroclinic deformation radius.

Therefore, Equation 4.1 is applied in a 2-dimensional channel with size L x W, where W = L/2, and has a uniform grid spacing of dx = dy = 15 km. We have tested a few values for L, since according to *Berloff & McWilliams* [1999], the channel length and width may influence the dynamics of the interior because they are a parameter of the model. So we tried to investigate the proper size willing to chose a length big enough to avoid such influence. Based on that, and following *Jayne et al.* [1996], we used L = 6000 km. Additionally, we chose 15 km of resolution since we are expecting wavelengths of order 175 km (according to the previous chapter), which would allow eddies of about 87 km of diameter. Therefore, 15 km seems to be an appropriate value to allow the occurrence of those eddies. In other words, such grid spacing is nearly "eddy-resolving" for the eddy dimensions we are expecting to obtain.

Integration in space is done using a scheme that is center differenced in the two spatial dimensions (an "Arakawa C-grid") with flux-limited advection. The integration in time is done using a second-order Adams-Bashforth scheme. The model is forced by inflow-outflow conditions. The inflowing jet is potentially barotropically unstable, i.e. it satisfies the Rayleigh necessary condition for instability, requiring the potential vorticity gradient profile to change sign in the horizontal. The inflowing mass must be removed from the domain at the southern boundary, and it is important to the relevance of this study to the along-stream development of a WBC jet that the northern boundary condition does not control the upstream dynamics we study. We make the upstream dynamics qualitatively insensitive to the outflow condition by making the meridional extent of the domain long relative to the meridional extent we examine and through a meridionally broad northern boundary sponge layer, which allows the jet to adjust to the outflow condition near the northern boundary. The bottom friction coefficient varies linearly within the channel, and it was chosen to make the inflow-outflow

regions stable (steady-state condition), and to make the interior flow to be marginally stable (allowing only weak instabilities). Then R $\approx$ (900 days)$^{-1}$ within the sponge layers and R $\approx$ (1 day)$^{-1}$ in the interior (such as in *Jayne et al.* [1996]). No normal flow is allowed at the eastern and western walls and, following again *Berloff & McWilliams* [1999], no-slip boundary condition is applied at the western one. According to the authors, the no-slip boundary condition is adequate to allow jet instabilities, and it is not the case of the free-slip one, which has a stabilizing effect on the flow in a nonlinear regime. *Verron et al.* [1991] also used no-slip boundary condition in the investigation of a flow past a cape in a QG framework, and mentioned that in the free-slip, no eddy-shedding is observed (see *Berloff & McWilliams* [1999] for a discussion). In the scenario we have a variant (curvy) western boundary, the same boundary conditions apply, and the coastline is handled with a capacitance matrix approach.

Therefore, we allow the jet to evolve freely in the meridional direction from the northern edge of the domain, and remove it at the southern edge a long way downstream and in a manner that does not affect the upstream (interior) dynamics we study. Note that, although we do not run the model for a long integration time, the presence of the sponge layer on the northern boundary in particular has the effect of eliminating any feedback of possible recirculation strength on the inflowing jet, and as such eliminates the potential for more complex behavior associated with the low-frequency variability or multiple dynamical regimes observed in WBC systems, a complicating feature we wished to eliminate from the system we studied.

The jet is a function of a $sech^2$ (e.g. a Bickley jet), where the steady-state meridional velocity is defined as

$$v(x) = v_o sech^2 \left(\frac{x - x_c}{\delta} \right), \tag{4.4}$$

where, v_o is a constant that determines the velocity magnitude, δ is a normalization factor (function decay) proportional to the jet width and x_c is the position of the core velocity. The Bickley jet was chosen based on studies that have investigated the stability problem of geophysical flows using this type of function. For instance, *Lipps* [1963] investigated the effect of the horizontal mass divergence upon the stability of a barotropic flow under the equivalent-barotropic approximation using a zonal jet pre-

scribed as

$$U(y) = V sech^2\left(\frac{y}{L}\right) + V_0, \tag{4.5}$$

where V,L and V_0 are constants. He derived the stability problem of this jet, obtained a sufficient condition for stability, and applied the stability theory to a Gulf Stream-like jet, where he could compute the most unstable wavelength. Other references that had applied a Bickley jet are *Mallier & Davis* [1999], *Jayne & Hogg* [1999], *Cunningham* [2000] and *Bouchut et al.* [2011].

All the results presented here consider we are in the Southern Hemisphere, e.g. $f < 0$. Therefore, we referenced "cyclonic" as clockwise circulation and "anticyclonic" as counter-clockwise circulation.

4.2 The barotropic case

All the evaluation done in the previous chapters considered the approximation of the BC observed jet in a $1^1/_2$-layer ocean. This consideration is more in accordance with the real BC scenario, where the BC flows above the IWBC. However, since we aim to verify whether barotropic instabilities can generate dipoles along the BC-like jet, the evaluation of the purely barotropic configuration is also relevant. However, the barotropic QG approximation of the observed BC flow would not be possible, since a vertical integration of transport in the BC-IWBC system would be nearly zero. As an alternative to that, we opted for prescribing a meridional jet by functions in which their constant parameters can be calibrated in order to generate a jet with the same kinematics characteristics as the observed BC of Figure 2.6. In the present barotropic case, we evolved Equation 4.1 considering q of Equation 4.2.

4.2.1 Open domain

It is natural to think that the investigation of the BC dynamics involves the presence of a western boundary. However, looking to the BC flow off Cape Frio scenario, the current, attached to the continental margin north of Cape Frio, encounters open waters when passing by this location. In an idealized study, we can think in a scenario where a jet, perturbed upstream, leaves the indentation and flows in a open domain. *Waterman*

& Jayne [2011] used a similar idea in their theoretical study on the role of eddy-mean flow interactions in the time-mean dynamics of a zonally evolving, unstable, strongly inertial jet in a configuration and parameter regime that is relevant to the Kuroshio extension (e.g., after the jet separates of the western boundary). Their idealized jet was perturbed upstream (at the inflow) and was allowed to evolve in a zonal channel configured as a open domain. Considering this idea, we believe the investigation of the open domain scenario as very relevant to our study, since we are trying to construct a theoretical understanding of the BC dynamics off Cape Frio region and we are focusing on process-based study.

Therefore, the $sech^2$ jet (Equation 4.4) was run in a channel of open boundaries in a grid size of 6000x3000 km, which was big enough so the boundaries did not have any influence on the dynamics of the interior, and the features that had appeared during the runs remained in the interior of the channel. The integration time was 300 days (about 1 year), so we could see the model reach an equilibrium state, that will be discussed ahead. We placed the jet flowing along the center of the channel. Hence, one experiment was conducted with a jet that presented BC kinematics characteristics. Such experiment is presented in Table 4.1, in which the values are correspondent to the inflowing steady-state jet. The parameters based on the BC characteristics are: v_o, x_c, δ (described in Equation 4.4 and $jetw$ (jet width). The parameter δ was set with the same value of the deformation radius computed for the BC in Chapter 2 ($R_d = 36$ km).

Table 4.1: Experiment run in the 1-layer barotropic open ocean QG model.

v_o (m s^{-1})	x_c (km)	$jetw$ (km)	δ (km)
-0.5	0	220	36

Figure 4.1 (upper panel) shows the initial velocity profiles at the inflow for each case. Figure 4.2 illustrates the initial q and ψ horizontal fields. In all the following representation of the horizontal fields, only the dynamical relevant part of the channel will be shown (the interior). For the open ocean case, the jet was initially perturbed, otherwise, the jet would be totally stable in this configuration. The perturbation used here is in the form of a noise applied on the PV field.

As we have done for the BC profile in Chapter 2 and in the previous section, we computed the Rayleigh and Fjørtoft conditions, that give us the necessary but not sufficient conditions for barotropic instabilities. In Rayleigh condition, $^{\partial q}/_{\partial x}$ should change signal at least once in the horizontal cross-jet direction. In Fjørtoft condition, a similar expression states a more robust condition, which is $(\bar{v} - v_o)^{\partial q}/_{\partial x}$, and should be positive at least in one portion of the cross-jet direction. Figure 4.1 center panel shows the Rayleigh condition computed, and Figure 4.1 lower panel shown the Fjørtoft one. In the present case, $^{\partial q}/_{\partial x}$ and $(\bar{v} - v_o)^{\partial q}/_{\partial x}$ changes sign at least once in the cross-jet direction.

The time evolution of the 1-layer open ocean case is shown in Figures 4.3 and 4.4, q and ψ horizontal fields respectively. The jet starts meandering up to day 30, when it begins the formation of quasi-paired eddies of opposite signs at each side of the current, that propagate with the flow. Two bipolar features grow and last until the end of the run, and they can be seen in the velocity arrows over the ψ field of Figure 4.4. The jet gets broken in eddies, but the main flow still lasts, and the jet axis is kept. In general, the eddies formed until day 90 had size of approximately 200 km in diameter, same scale as the initial jet width. However, the two dipoles that developed later ended up growing and reached about 400 km. These large scale features presented a slow-propagating pattern by the end of the run, so we considered that, from this moment, the results were not relevant to our investigation anymore. The propagation of the features along the channel was approximately 11 km day^{-1}.

4.2.2 Straight western boundary

The $sech^2$ jet (Equation 4.4) was run in a channel with a straight western boundary , and in a 6000x3000 km size configuration, which was big enough so the boundaries did not have any influence on the dynamics of the interior, and the features that had appeared during the runs remained in the interior of the channel. The integration time was 300 days (about 1 year), so we could see the model reach an equilibrium state, that will be discussed ahead. We constructed several experiments in which we varied the distance of the jet core (x_c) from the coast, which gave us different jet profiles. We selected 4 cases: x_c = 100 km, x_c = 60 km, x_c = 30 km and x_c = 10 km. Table 4.2 summarizes

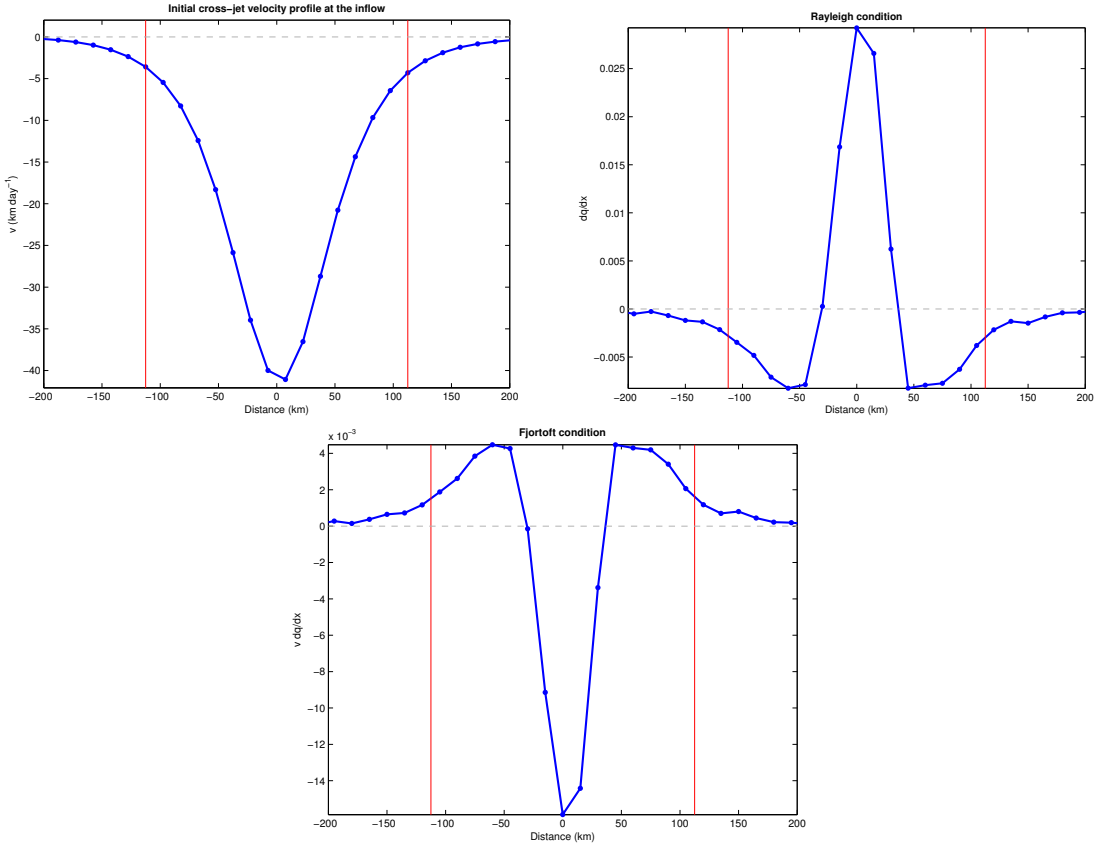

Figure 4.1: Top left panel: initial velocity profile at the inflow for the 1-layer open domain case. Top right panel: the Rayleigh necessary condition for barotropic instability ($^{dq}/_{dx}$). Lower panel: Fjørtoft necessary condition for barotropic instability ($(\bar{v} - v_o)^{dq}/_{dx}$). Values are in km and day units, and 0.5 m s^{-1} = 43.2 km day^{-1}.

these experiments, in which the values are correspondent to the inflowing steady-state jet. The parameters based on the BC characteristics are: v_o, x_c, δ described in Equation 4.4 and $jetw$ (jet width). In all the cases we fixed δ as having the same value of the deformation radius computed for the BC in Chapter 2 ($R_d = 36$ km).

Figure 4.5 shows the initial velocity profiles at the inflow for each case. Figure 4.6 and 4.7 illustrates the initial q and ψ horizontal fields. In all the following representation of the horizontal fields, only the dynamical relevant part of the channel will be shown, e.g. the inflow and interior areas. For the straight coast cases, the jet was initially perturbed, otherwise, without no source of instability, the jet would be totally stable in this configuration. The perturbation was the same used for the previous open ocean case (a small noise). Looking to these figures, one can see that the inflowing jet is directed southward. In each given x_c, the jet core gets closer to the wall.

As we have done for the BC profile in Chapter 2, we computed the Rayleigh and

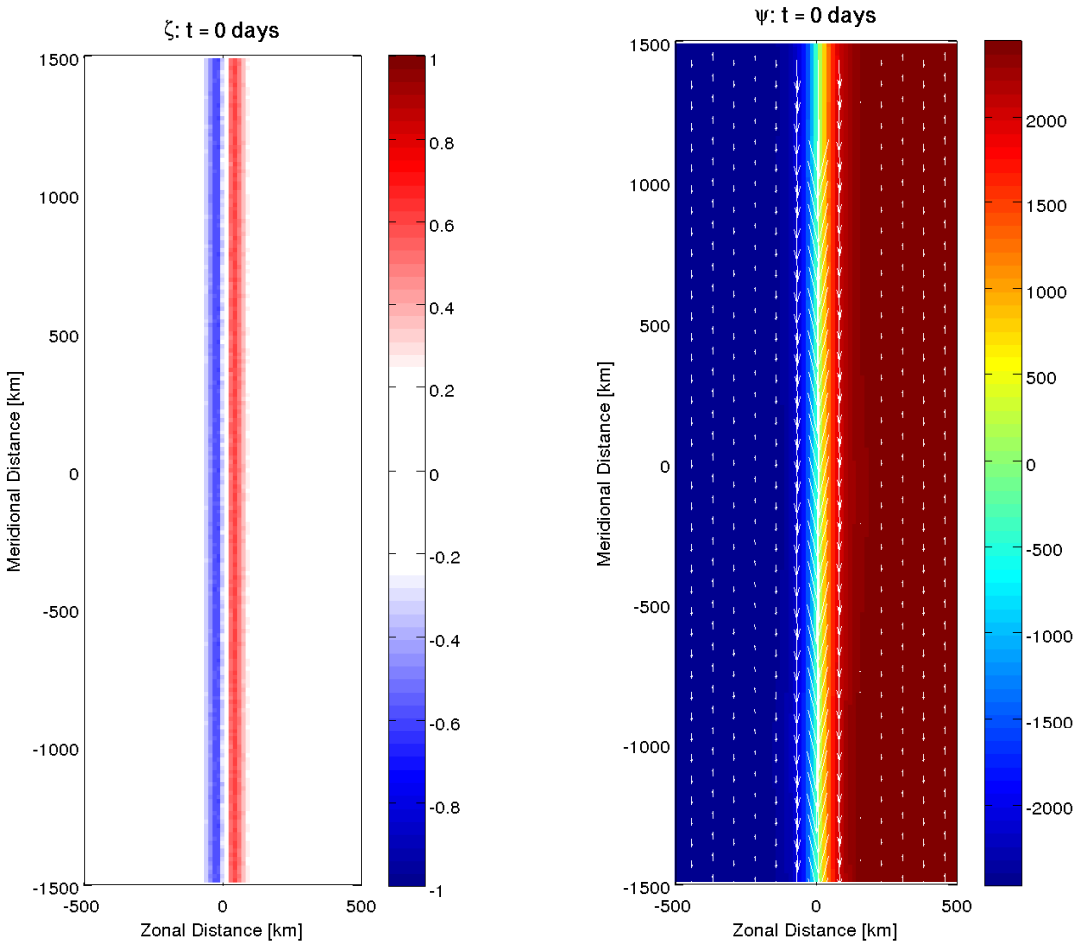

Figure 4.2: Initial fields for the 1-layer open domain case. Only interior region is shown. Left panel: q field. Right panel: ψ (color) and velocity (arrows) fields.

Table 4.2: Experiments run in the 1-layer barotropic QG model with straight coastline.

Coast shape	v_o (m s^{-1})	x_c (km)	$jetw$ (km)	δ (km)
Straight	-0.5	100	135	36
Straight	-0.5	60	127	36
Straight	-0.5	30	112	36
Straight	-0.5	10	83	36

Fjørtoft conditions, that give us the necessary but not sufficient conditions for barotropic instabilities. In Rayleigh condition, $^{\partial q}/_{\partial x}$ should change signal at least once in the horizontal cross-jet direction. In Fjørtoft condition, a similar expression states a more ro-

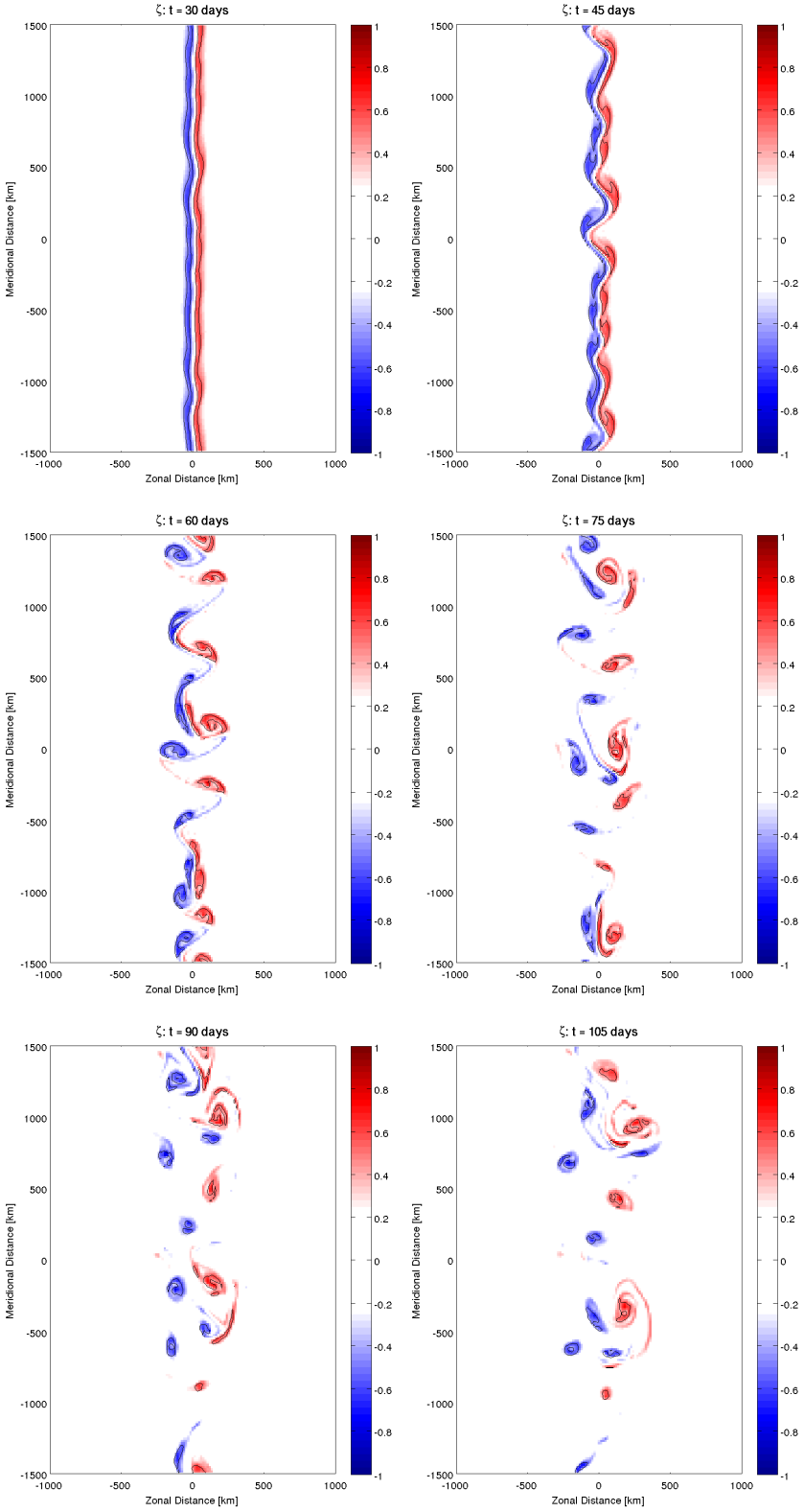

Figure 4.3: Time evolution of q field for the 1-layer open domain case. Only interior region is shown. From top left to bottom right, t = 30 days, t = 45 days, t = 60 days, t = 75 days, t = 90 days, t = 105 days.

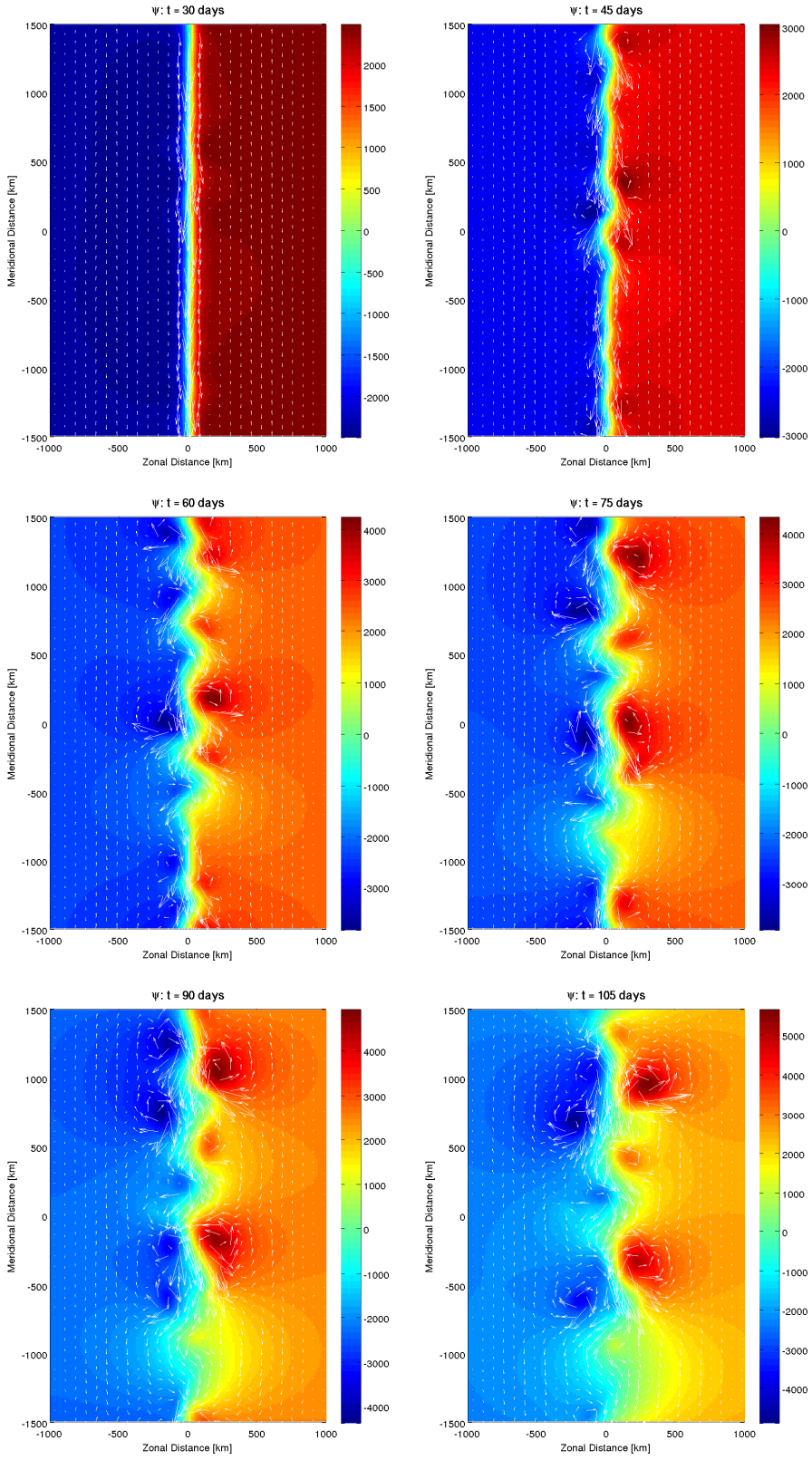

Figure 4.4: Time evolution of ψ field (color) over velocity (arrows) for the 1-layer open domain case. Only interior region is shown. From top left to bottom right, t = 30 days, t = 45 days, t = 60 days, t = 75 days, t = 90 days, t = 105 days.

bust condition, which is $(\bar{v} - v_o)^{\partial q}/\partial x$, and also should change signal at least once in the horizontal cross-jet direction. Figure 4.8 shows the Rayleigh condition we computed for each case, and Figure 4.9 shown the Fjørtoft one. In all the cases, $^{\partial q}/\partial x$ and $(\bar{v} - v_o)^{\partial q}/\partial x$ changes sign at least once in the cross-jet direction. However, as the jet gets far away from the coast, more sign changes occur, which may indicates that the jet is getting more potentially unstable.

The time evolution of the 4 cases are shown in Figures 4.10 to 4.17. The x_c = 100 km case is when the jet is more unstable. It starts meandering and afterwards breaking up in eddies and bipolar features. Those dipoles propagate with the flow and becomes non-paired after a while. In this case, a dipole detaches from the main current and recirculates in the interior. Moreover, after about 80 days, eddy-wall interaction takes place, forming a counter-current between the southward jet and the wall. This is the case we can consider that the jet was unstable enough to generate strong instabilities, and the nonlinear effects are predominant and dominate the dynamics of the system, mainly after 100 days. Before that, the propagation of the features along channel was approximately 6 km day $^{-1}$. The typical length scale of the eddies was approximately 130 km in diameter.

In x_c = 60 km, the jet gets unstable latter than the previous case. The initial dipoles propagate with the jet and leave the domain by the southern boundary. Upstream, close to the inflow area, a dipole forms and shifts the jet slightly to the interior, which gives space for a cyclonic eddy to develop between the wall and the jet, and a eddy-wall interaction starts. This eddy-wall process starts after 150 days, and at this point, the dipole formed recirculates in the interior. The cyclone, instead of evolving to a counter-current, stays stationary (centered in the 4000 km of the y axis) until the dipole totally recirculates and be absorbed by the jet. From this moment, the impinging dipole interacts with the jet and an eddy-wall interaction starts again, forming a counter-current from day 290. Downstream, the jet keeps flowing southward, characterized by a sequence of cyclone and anticyclones that leave the domain by the southern boundary. The propagation of the features along channel was approximately 7.5 km day $^{-1}$. The typical length scale of the eddies was approximately 120 km in diameter.

The jet behavior in x_c = 30 km case is very similar to the x_c = 60 km. The main

difference is in the time things start to happen, that is latter in the present one. In summary, the jet also develops vortex dipoles along the main axis, and one dipole detaches from the current and recirculates. However, it seems there is a tendency of the jet to stabilize after about 270 days. Moreover, the recirculated dipole is absorbed by the current and does not trigger any new instability in the jet. The propagation of the features along channel was approximately 7 km day $^{-1}$. The typical length scale of the eddies was approximately 130 km in diameter.

In x_c = 10 km case, the jet is much more stable, meandering and forming less eddies. The anticyclonic ones are predominant, since there exists only the anticyclonic part of the jet in this case. Any eddy detaches from the main flow, and they propagate with the current southward and leave the domain throughout the southern boundary. The jet starts getting stable upstream as the time goes by, and the formation of eddies stays restricted to the downstream region. The propagation of the features along channel was approximately 15 km day $^{-1}$. The typical length scale of the eddies around day 50 was approximately 120 km in diameter. Latter (by day 140), the eddies presented some growth and reached about 220 km.

In all the four case, the model reached what we considered an equilibrium state by day 300, e.g. in x_c = 10 km, the jet presented a steady-state pattern, while in the others, it was observed the presence of large scale features which were having a nearly steady-state behavior as well (no growth and no propagation). In both situation, we considered the dynamics as not relevant to our analyzes anymore.

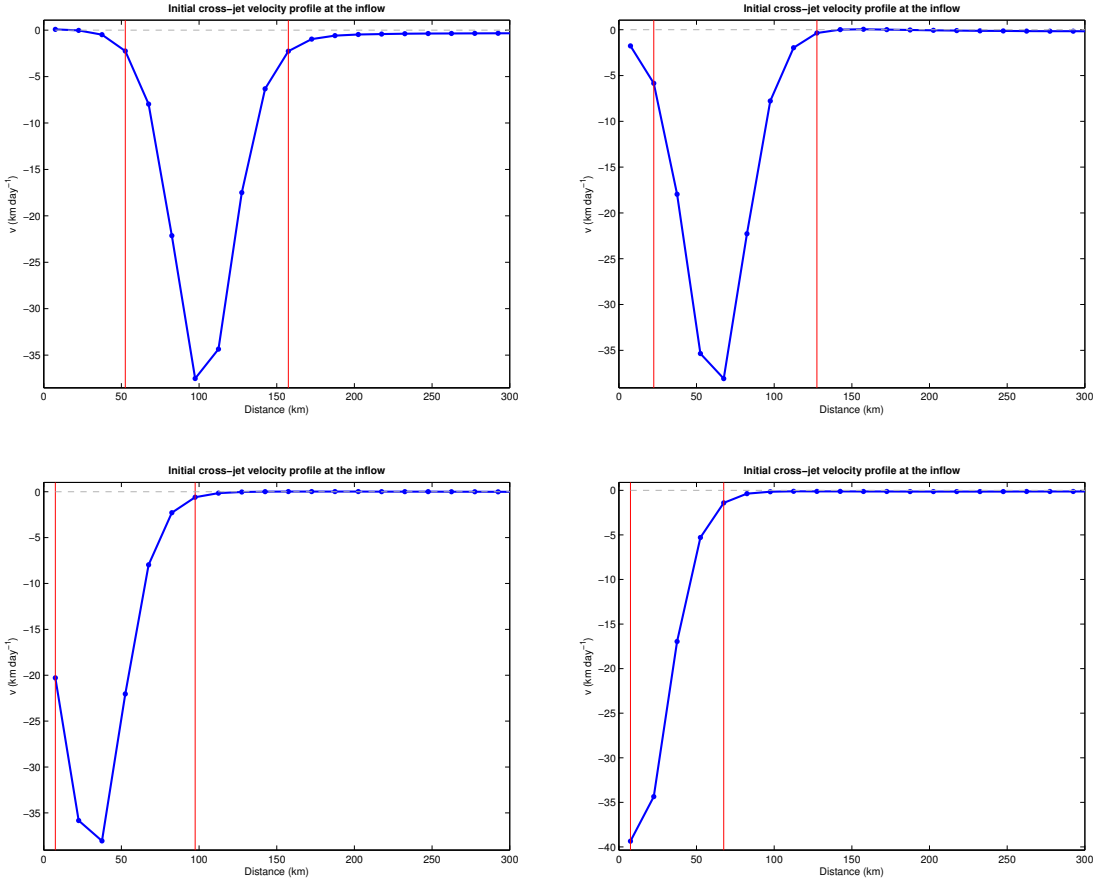

Figure 4.5: Initial velocity profile at the inflow for the 1-layer straight coast case. The sequence of 4 profiles are correspondent to x_c = 100 km (top left), x_c = 60 km (top right), x_c = 30 km (bottom left) and x_c = 10 km (bottom right). Values are in km and day units, and 0.5 m s^{-1} = 43.2 km day^{-1}.

4.2.3 Curvy western boundary

In the curvy western boundary scenario, the coast shape was idealistic constructed to resemble the southeast Brazilian coastline. Then we used a $tanh$ function and chose appropriate values to meet the curvature radius of the real coast. The meridional coastline profile prescribed is represented by Equation 4.6:

$$c(y) = dx + 300 - 300tanh\left(\frac{(y - {}^{L}/_{4})}{100}\right), \tag{4.6}$$

where dx is the zonal grid spacing and L is the channel length.

The curvature of the curve in Equation 4.6 was computed as

$$K(y) = \frac{\left|\frac{\partial^2 c}{\partial y^2}\right|}{\left[1 + \left(\frac{\partial c}{\partial y}\right)^2\right]^{\frac{3}{2}}}, \tag{4.7}$$

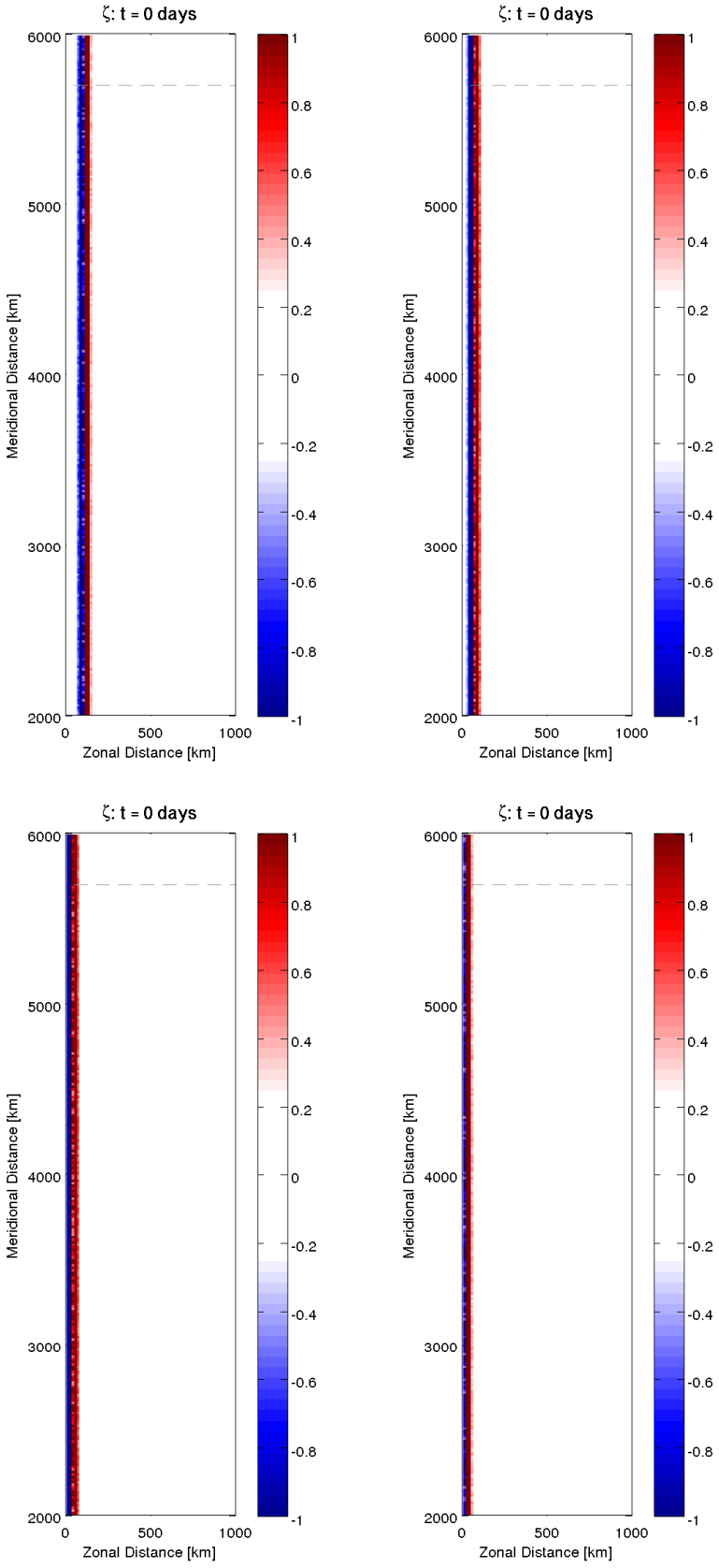

Figure 4.6: Initial q field for the 1-layer straight coast case. Only inflow and interior regions are shown. The gray-dashed line indicates the inflowing steady-state region. The sequence of 4 profiles are correspondent to x_c = 100 km (top left), x_c = 60 km (top right), x_c = 30 km (bottom left) and x_c = 10 km (bottom right).

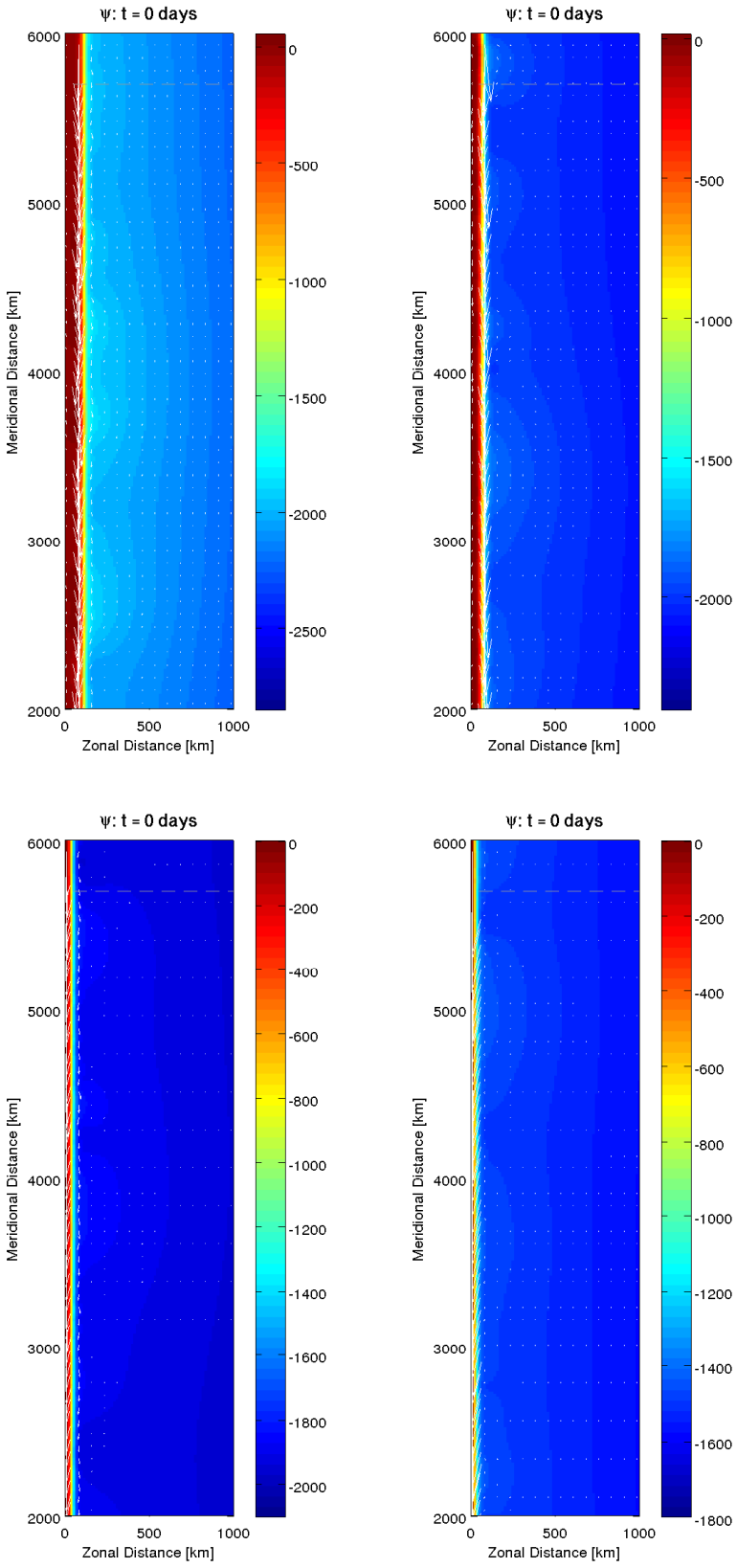

Figure 4.7: Initial ψ (color) and velocity (arrows) fields for the 1-layer straight coast case. Only inflow and interior regions are shown. The gray-dashed line indicates the inflowing steady-state region. The sequence of 4 profiles are correspondent to x_c = 100 km (top left), x_c = 60 km (top right), x_c = 30 km (bottom left) and x_c = 10 km (bottom right).

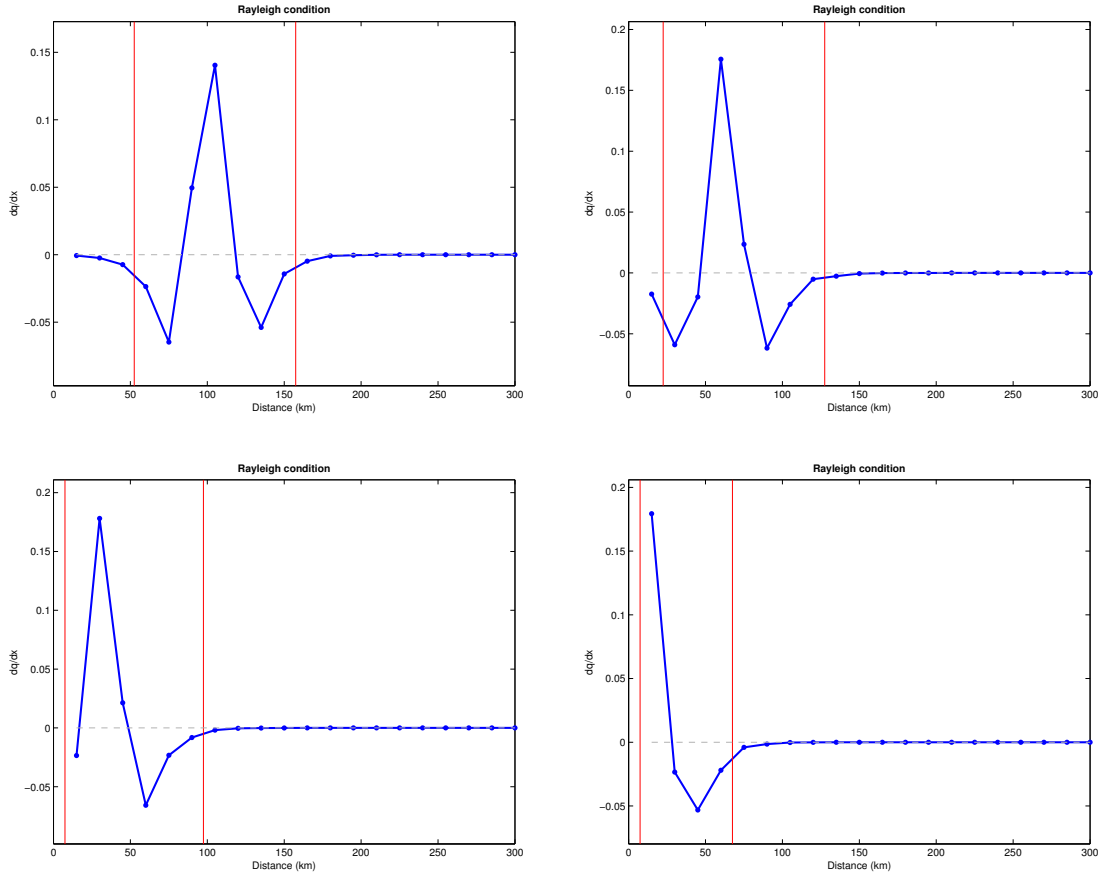

Figure 4.8: Necessary but not sufficient conditions for barotropic instability: the Rayleigh condition (dq/dx). The sequence of 4 profiles are correspondent to x_c = 100 km (top left), x_c = 60 km (top right), x_c = 30 km (bottom left) and x_c = 10 km (bottom right). Values are in km and day units.

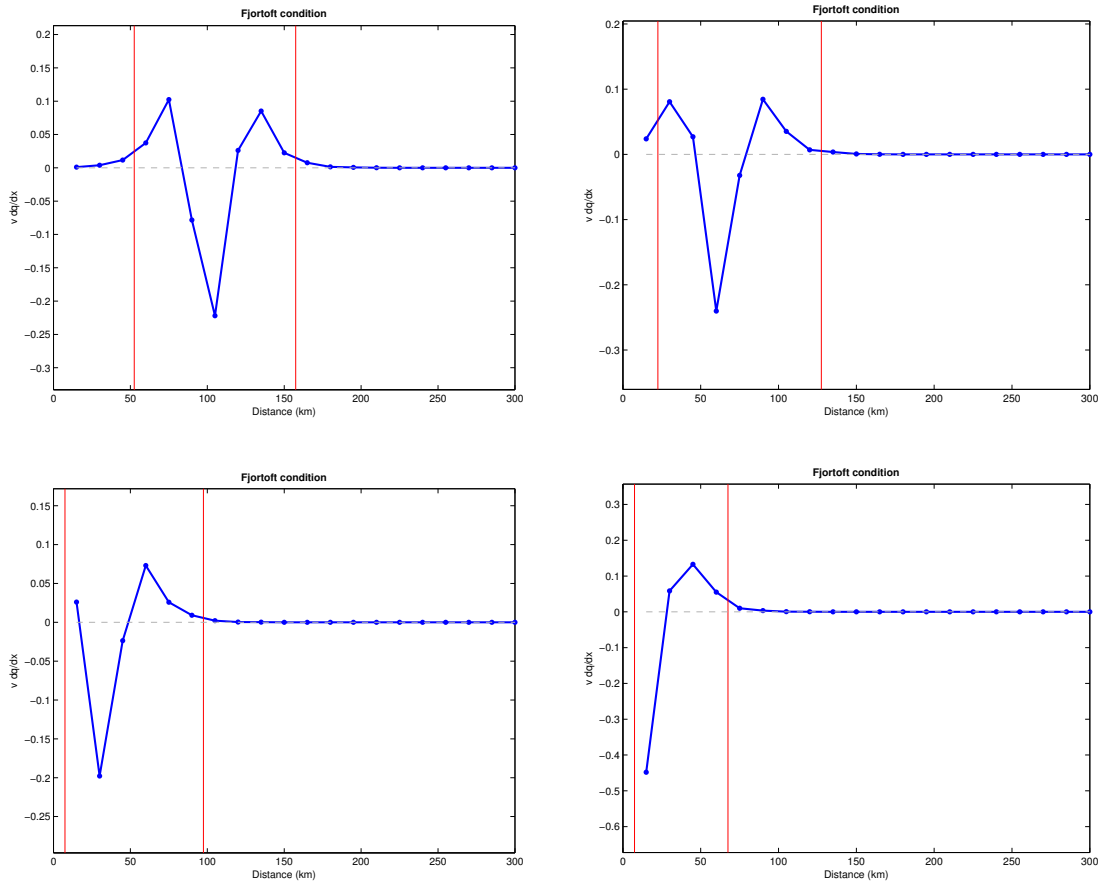

Figure 4.9: Necessary but not sufficient conditions for barotropic instability: the Fjørtoft condition ($(\bar{v} - v_o)^{dq}/_{dx}$). The sequence of 4 profiles are correspondent to x_c = 100 km (top left), x_c = 60 km (top right), x_c = 30 km (bottom left) and x_c = 10 km (bottom right). Values are in km and day units.

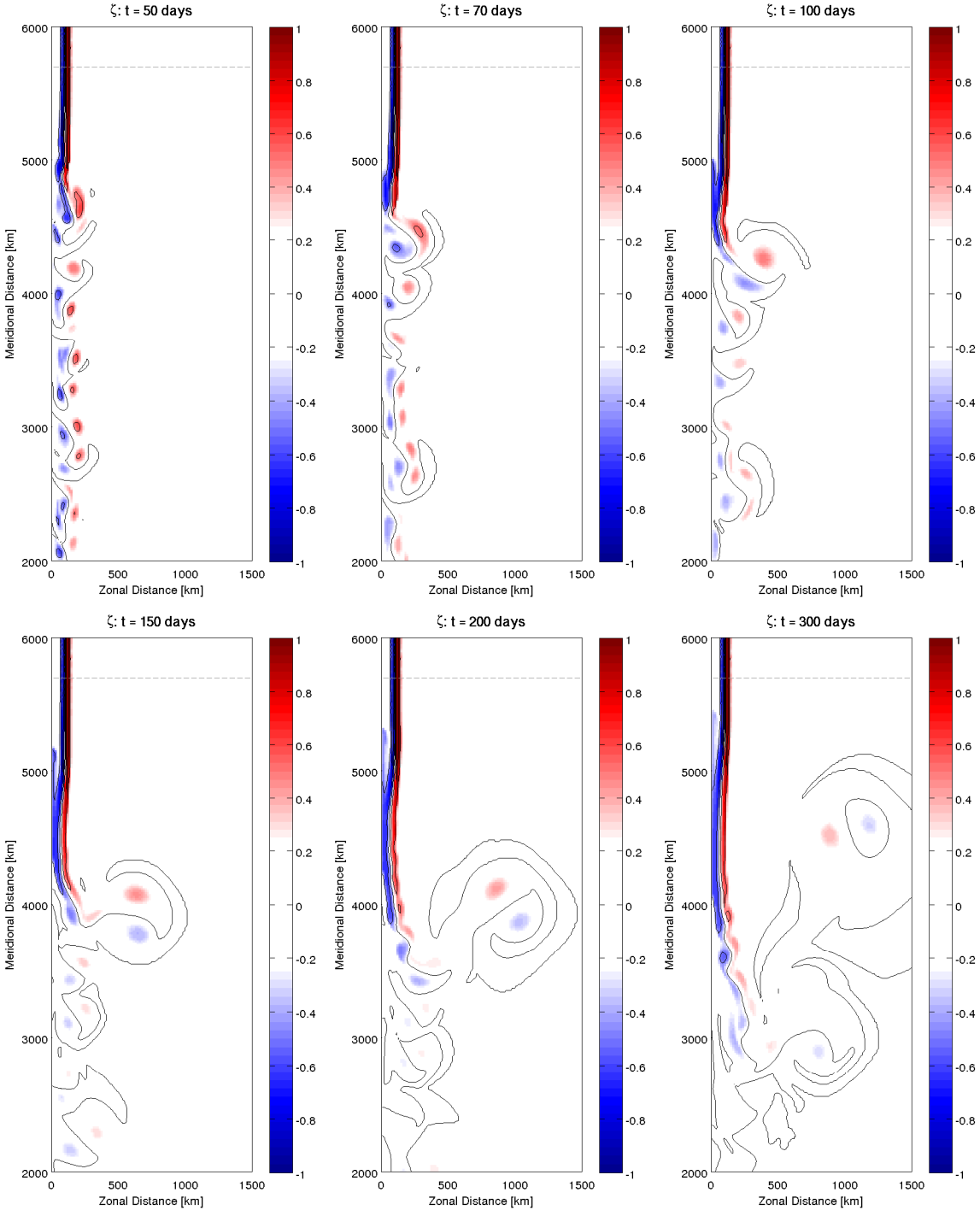

Figure 4.10: Time evolution of q field for the 1-layer straight coast case, with x_c = 100 km. From top left to bottom right, t = 50 days, t = 70 days, t = 100 days, t = 150 days, t = 200 days, t = 300 days. Only inflow and interior regions are shown. The gray-dashed line indicates the inflowing steady-state region.

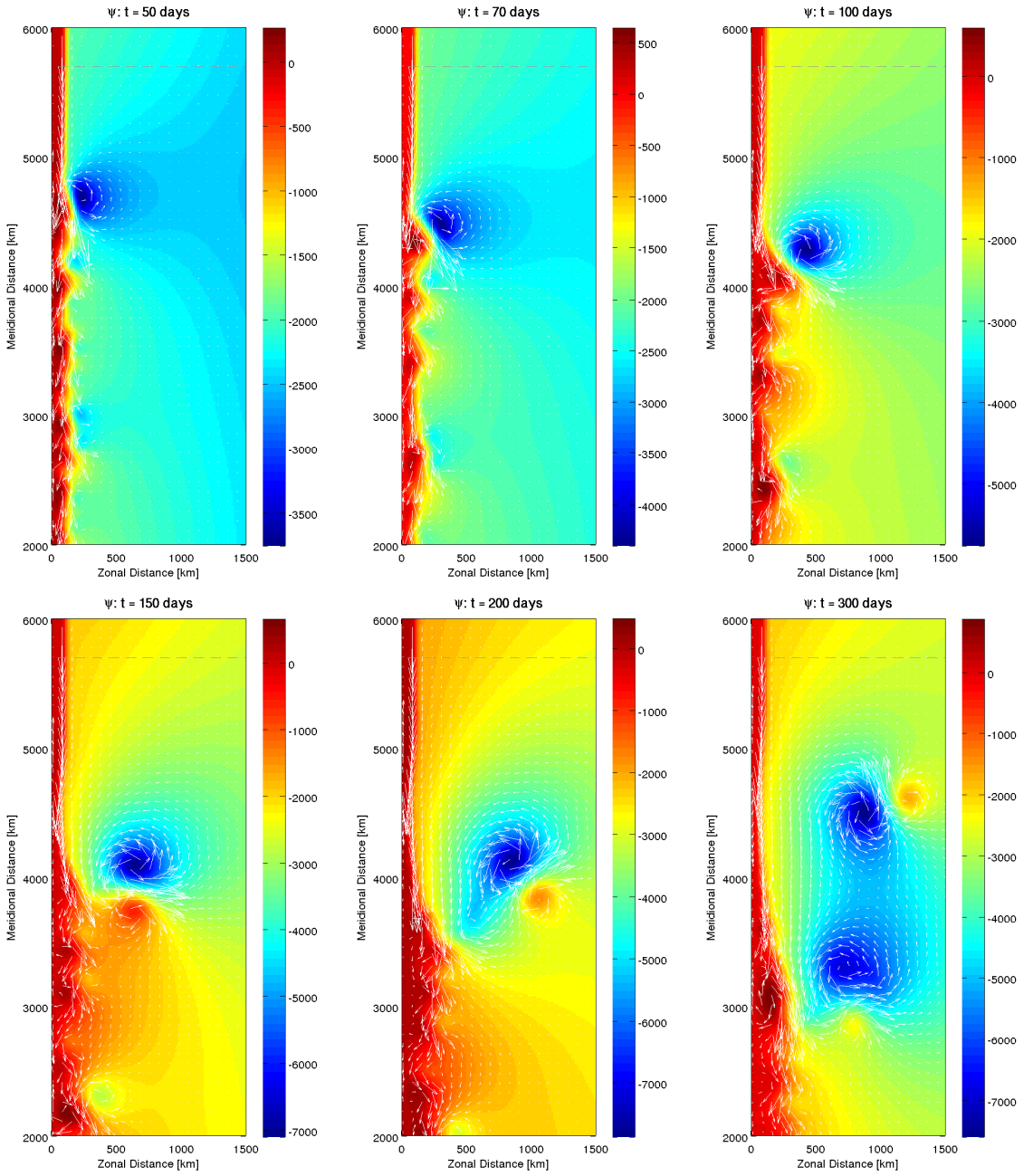

Figure 4.11: Time evolution of ψ field (color) over velocity (arrows) for the 1-layer straight coast case, with x_c = 100 km. From top left to bottom right, t = 50 days, t = 70 days, t = 100 days, t = 150 days, t = 200 days, t = 300 days. Only inflow and interior regions are shown. The gray-dashed line indicates the inflowing steady-state region.

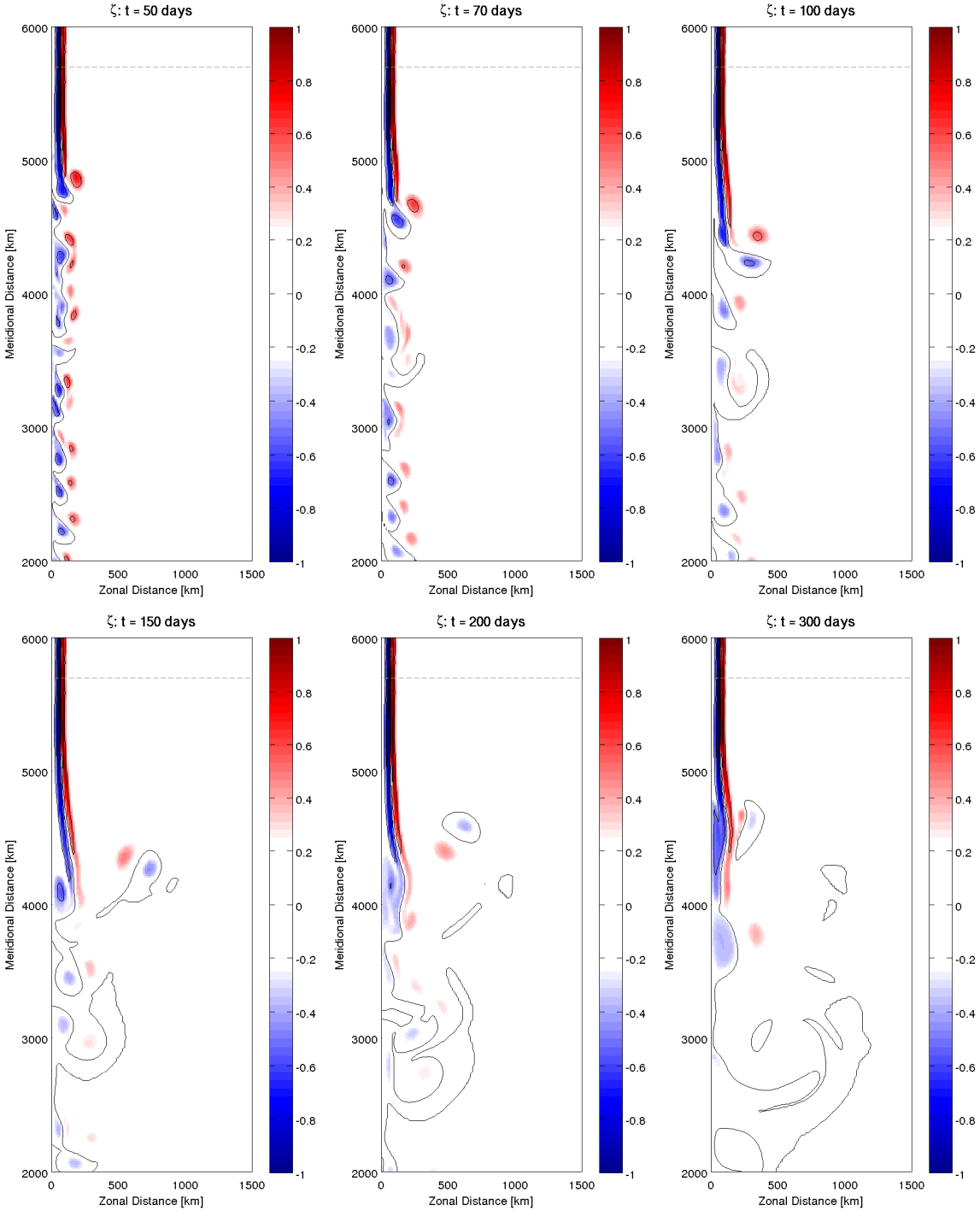

Figure 4.12: Time evolution of q field for the 1-layer straight coast case, with x_c = 60 km. From top left to bottom right, t = 50 days, t = 70 days, t = 100 days, t = 150 days, t = 200 days, t = 300 days. Only inflow and interior regions are shown. The gray-dashed line indicates the inflowing steady-state region.

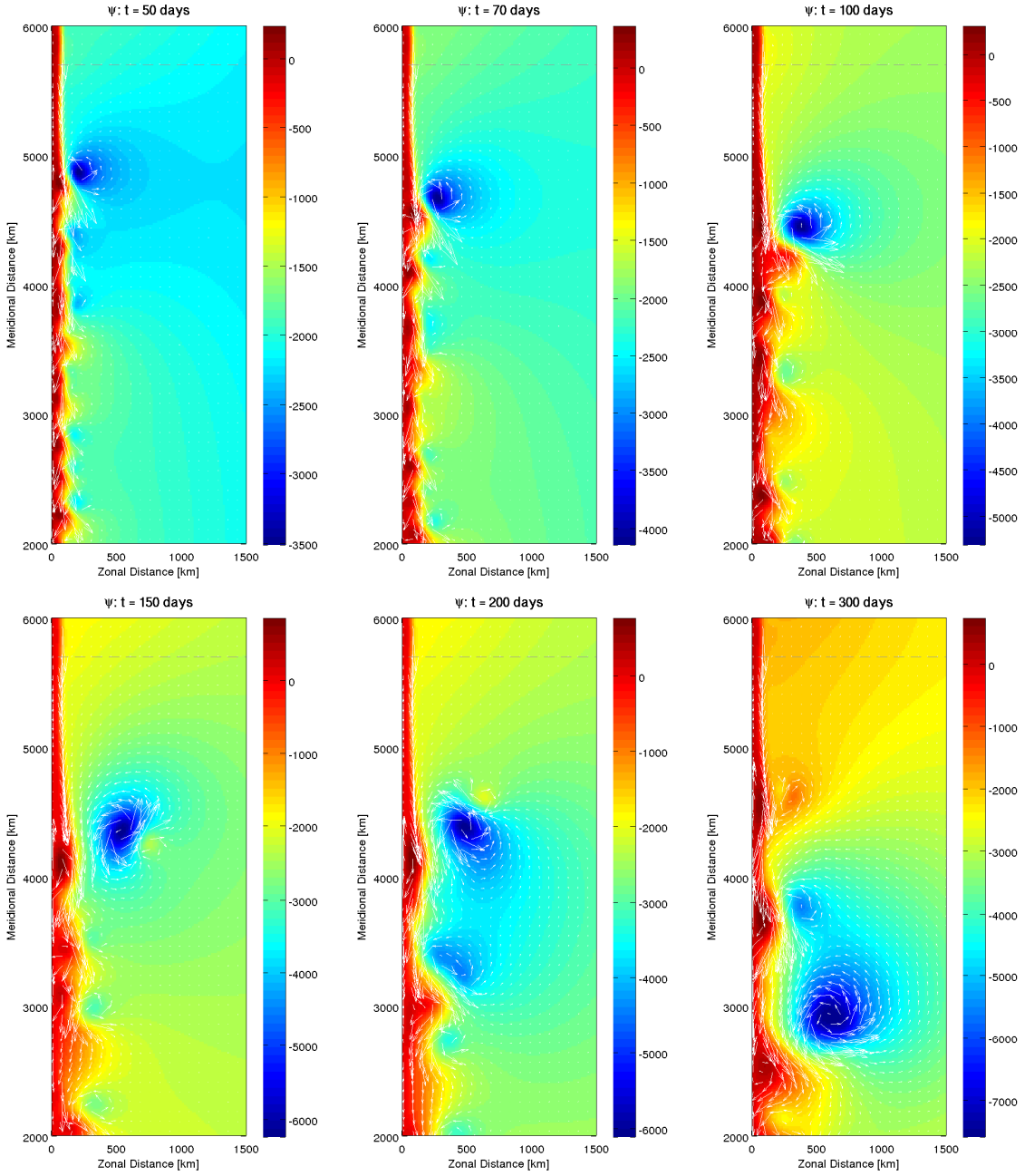

Figure 4.13: Time evolution of ψ field (color) over velocity (arrows) for the 1-layer straight coast case, with x_c = 60 km. From top left to bottom right, t = 50 days, t = 70 days, t = 100 days, t = 150 days, t = 200 days, t = 300 days. Only inflow and interior regions are shown. The gray-dashed line indicates the inflowing steady-state region.

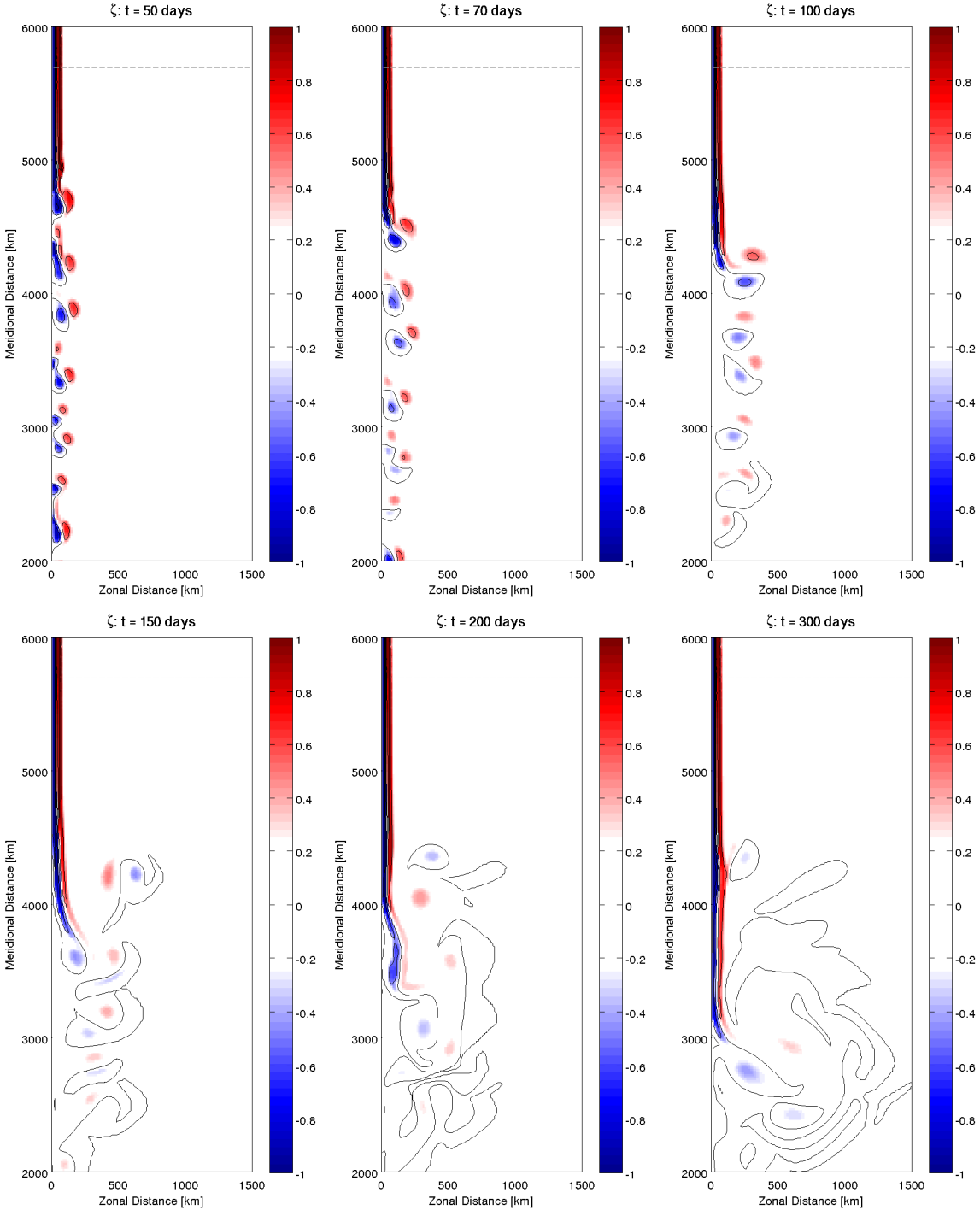

Figure 4.14: Time evolution of q field for the 1-layer straight coast case, with x_c = 30 km. From top left to bottom right, t = 50 days, t = 70 days, t = 100 days, t = 150 days, t = 200 days, t = 300 days. Only inflow and interior regions are shown. The gray-dashed line indicates the inflowing steady-state region.

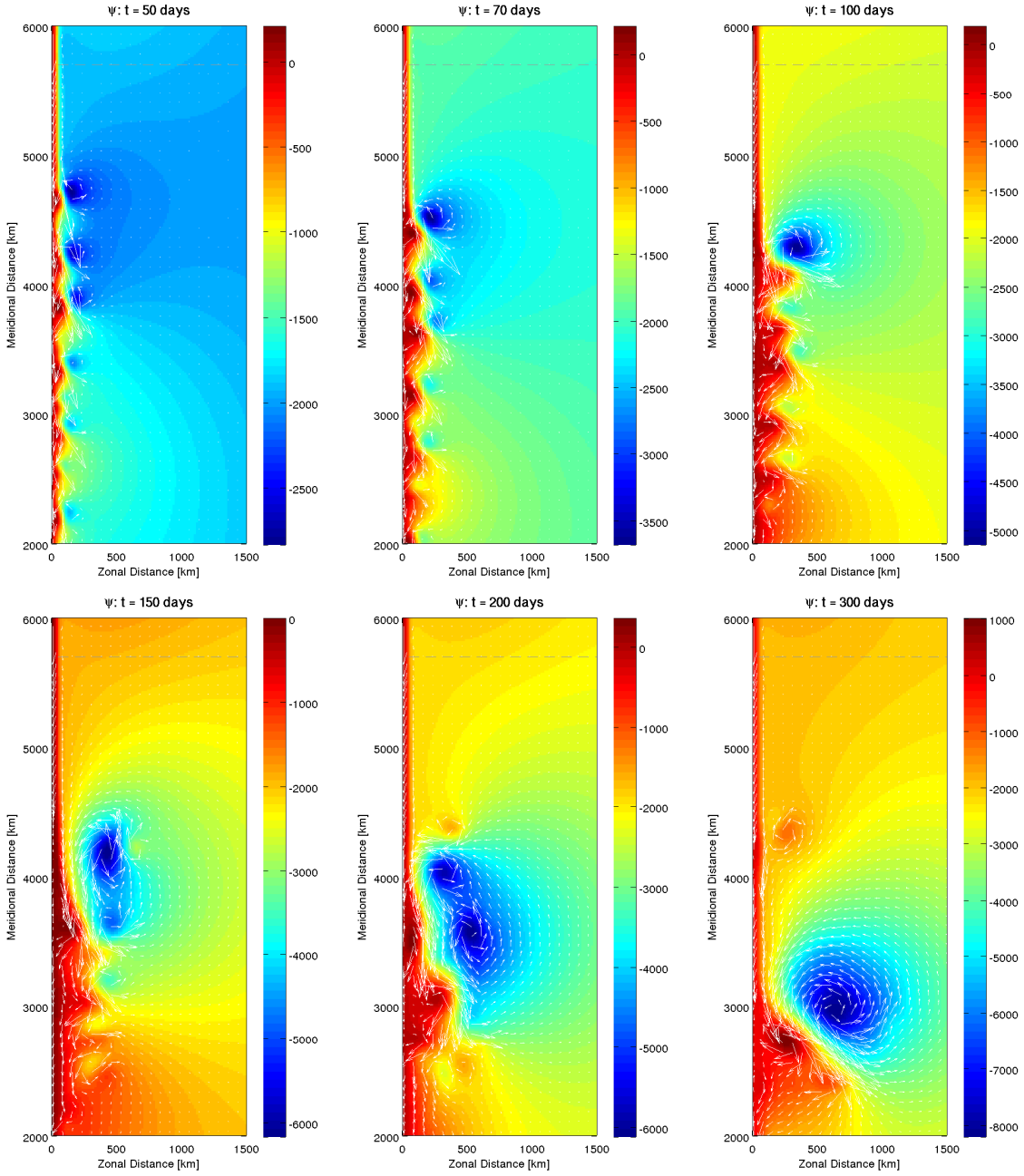

Figure 4.15: Time evolution of ψ field (color) over velocity (arrows) for the 1-layer straight coast case, with x_c = 30 km. From top left to bottom right, t = 50 days, t = 70 days, t = 100 days, t = 150 days, t = 200 days, t = 300 days. Only inflow and interior regions are shown. The gray-dashed line indicates the inflowing steady-state region.

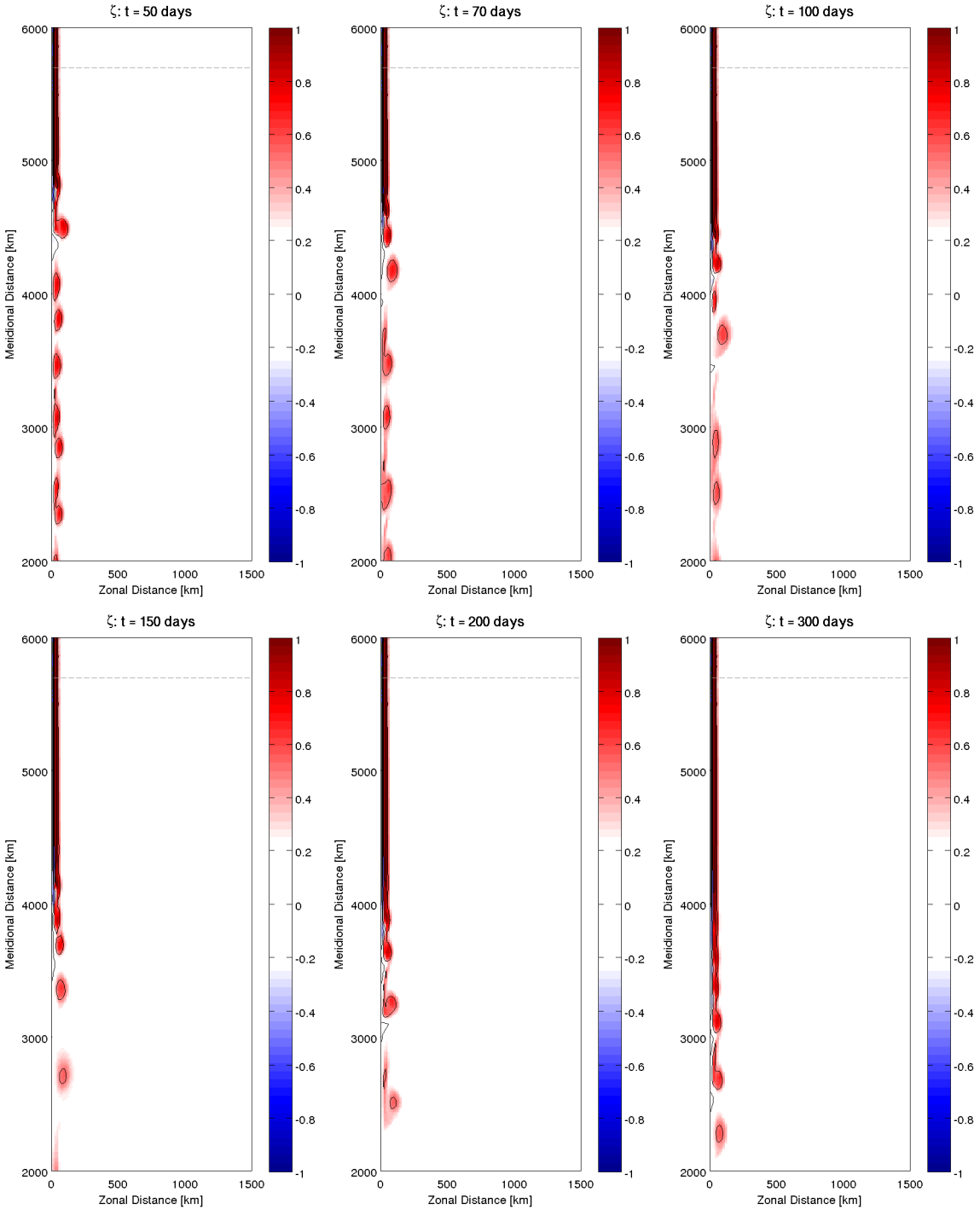

Figure 4.16: Time evolution of q field for the barotropic, straight western boundary case, with x_c = 10 km. From top left to bottom right, t = 50 days, t = 70 days, t = 100 days, t = 150 days, t = 200 days, t = 300 days. Only inflow and interior regions are shown. The gray-dashed line indicates the inflowing steady-state region.

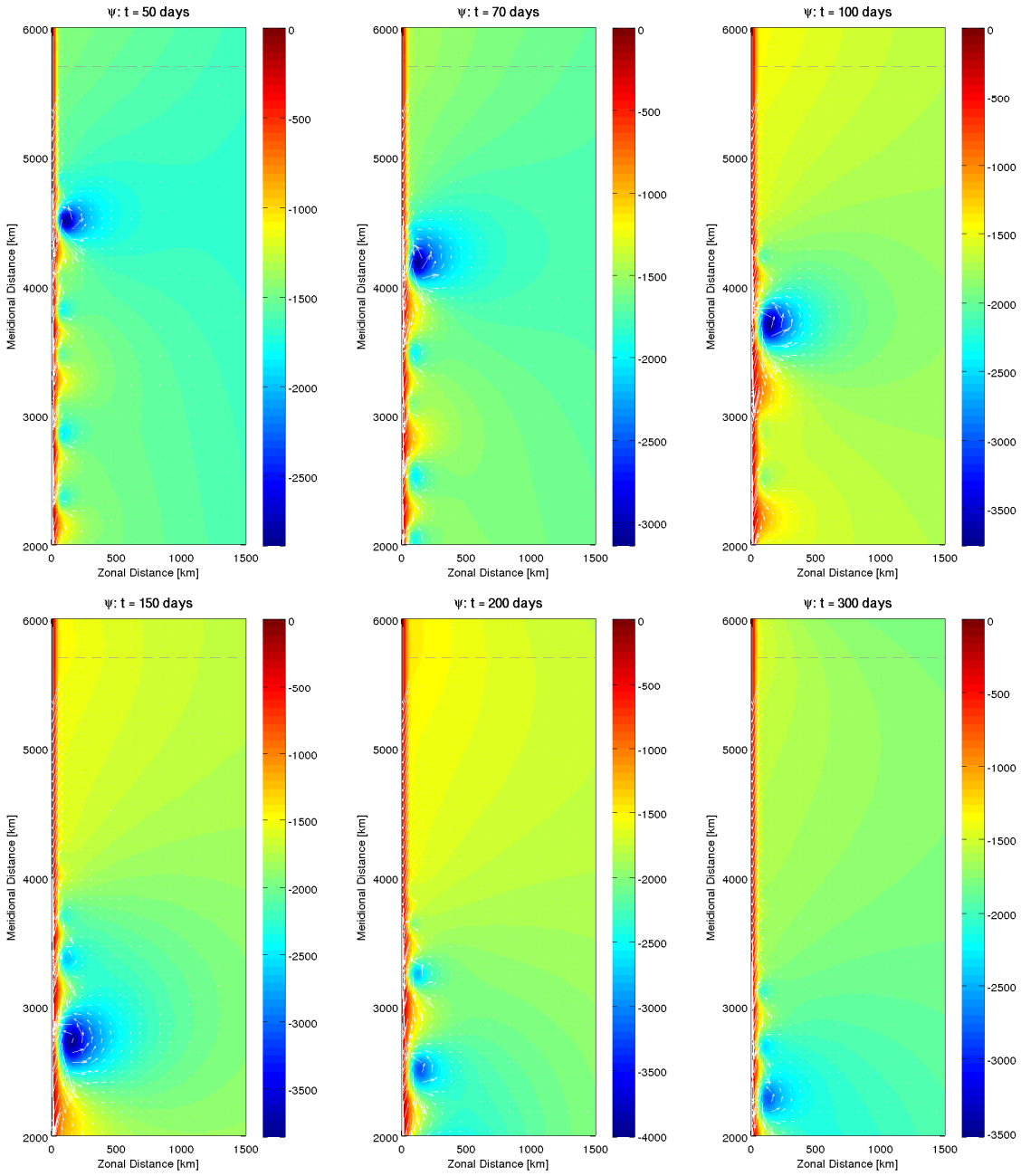

Figure 4.17: Time evolution of ψ field (color) over velocity (arrows) for the 1-layer straight coast case, with x_c = 10 km. From top left to bottom right, t = 50 days, t = 70 days, t = 100 days, t = 150 days, t = 200 days, t = 300 days. Only inflow and interior regions are shown. The gray-dashed line indicates the inflowing steady-state region.

and the correspondent curvature radius is $R = 1/K$. We computed K for the 200 m isobath curve from ETOPO 1 database in Cape Frio region and obtained an approximate R = 149 km close to the point where the coastline changes direction. We did the same to the idealized coastline profile of Equation 4.6 and obtained R = 150 km. Therefore, the idealized coastline used for the present scenario has a very similar (although smoothed) profile of the real one that is actually "felt" by the WBC (that's the reason why we used the 200 m isobath as reference). Still in Equation 4.6, the value of 300 was chosen to sets a realistic difference in the distance between the easternmost and the westernmost regions of Cape Frio area.

We performed a few tests in which we varied the value of the curvature radius, ranging between a smooth varying coastline to a steep one. The results showed us that the smoother the coastline variation is, the latter the jet starts getting unstable. We opted for fixing a given and appropriate value of curvature radius and perform tests in which we varied the jet profile, as we did in the previous section.

Therefore, the $sech^2$ jet (Equation 4.4) was run in a meridional channel that was set again to a 6000x3000 km size configuration. Such configuration was big enough so the boundaries did not have any influence on the dynamics of the interior, and the features that had appeared during the runs remained in the interior of the channel. The integration time was 600 days (about 2 year, double of the previous), so we could see the model reach an equilibrium state, that will be discussed ahead. As mentioned, we constructed several experiments in which we varied the distance of the jet core from the coast, which gave us different jet profiles. We selected the same 4 cases as the previous section: x_c = 100 km, x_c = 60 km, x_c = 30 km and x_c = 10 km. Table 4.3 summarizes these experiments, in which the values are correspondent to the inflowing steady-state jet. The parameters based on the BC characteristics are: v_o, x_c, δ (described in Equation 4.4) and $jetw$ (jet width). In all the cases we fixed δ as having the same value of the deformation radius computed for the BC in Chapter 2 ($R_d = 36$ km).

Figure 4.18 shows the initial velocity profiles at the inflow for each case. Figure 4.19 and 4.20 illustrates the initial q and ψ horizontal fields. In all the following representation of the horizontal fields, only the dynamical relevant part of the channel will be shown, e.g. the inflow and interior areas. For the curvy coast case, we did not per-

Table 4.3: Experiments run in the 1-layer barotropic QG model with curvy coastline.

Coast shape	v_o (m s^{-1})	x_c (km)	$jetw$ (km)	δ (km)
Curvy	-0.5	100	120	36
Curvy	-0.5	60	120	36
Curvy	-0.5	30	112	36
Curvy	-0.5	10	98	36

turbed the jet initially, since the change in coastline direction is enough to make the jet unstable, and this is the effect we want to isolate. Looking to these figures, one can see that the inflowing jet is directed southward. In each given x_c, the jet gets closer to the wall.

Figure 4.21 shows the Rayleigh condition we computed for each case, and Figure 4.22 shown the Fjørtoft one. In all the cases, $^{\partial q}/_{\partial x}$ and $(\bar{v} - v_o)^{\partial q}/_{\partial x}$ changes sign at least once in the cross-jet direction. However, as the jet gets far away from the coast, more sign changes occurs, which may indicates that the jet is getting more potentially unstable.

The time evolution of the 4 cases are shown in Figures 4.23 to 4.30. The x_c = 100 km case is when the jet is more unstable. The current is initially located attached to the western boundary. As soon as the jet encounters the coastline indentation, it "feels" the coastline absence and has room to develop instabilities. It initially forms a dipole, which sets the path for the trailing jet. As the jet tries to return to the western boundary, it presents a eddy-shedding mode. First an anticyclone (clockwise eddy) forms, and afterwards, a cyclone occurs at the lee of the indentation. An eddy-wall interaction occurs in the coastal side of the jet, while a recirculation starts in the interior side, which formed a large scale bipolar structure of about 1500 km in total diameter. The jet keeps detached from the coast until the end of the run and presents an eddy-shedding mode downstream. Typical length scales of these eddies were approximately 200 km, and the propagation of the features was approximately 8 km day^{-1}.

In x_c = 60 km case, the jet behavior was very similar. It also forms a dipole initially,

which sets the path for the trailing jet. As the jet gets close to the western boundary, this dipole grows and detaches from the jet and travels to the interior. At the same time, eddy-wall interaction occurs in the coastal side, forming a lee-eddy that also grows and propagates northward, reaching the jet upstream. This scenario characterized the formation of a large scale slow-propagation dipole. Typical length scales of these eddies were approximately 400 km, and the propagation of the features was approximately 7 km day^{-1}.

The x_c = 30 km case is more stable than the previous cases. Initially there is the formation of a dipole, that recirculates in the interior and has the anticyclonic part (that grows) bigger than the cyclonic part (which vanishes after some time). During this recirculation, it is noticeable the jet tries to return to the western boundary. After about 200 days, the jet is attached again to the wall, a lee-eddy forms and the recirculation remain quasi-stationary. Typical length scales of these eddies were approximately 300 km, and the propagation of the features was approximately 8 km day^{-1}.

In x_c = 10 km case, the jet is much more stable, meandering and forming less eddies. The anticyclonic ones are predominant, since there exists only the anticyclonic part of the jet in this case. Any eddy detaches from the main flow, and they propagate with the current southward and leave the domain throughout the southern boundary. The jet gets stable after 180 days. The propagation of the features along channel was approximately 10 km day^{-1} close to the indentation, but south of 4000 km, the propagation velocity increases to 25 km day^{-1}. The typical length scale of the eddies was approximately 150 km in diameter.

In all the four case, the model reached what we considered an equilibrium state by day 300. In x_c = 10 km, the jet presented a steady-state pattern (before 300 days), while in the others, it was observed the formation of large scale features, which presented a slow-propagating pattern. In both situation, we considered the dynamics as not relevant to our investigation anymore.

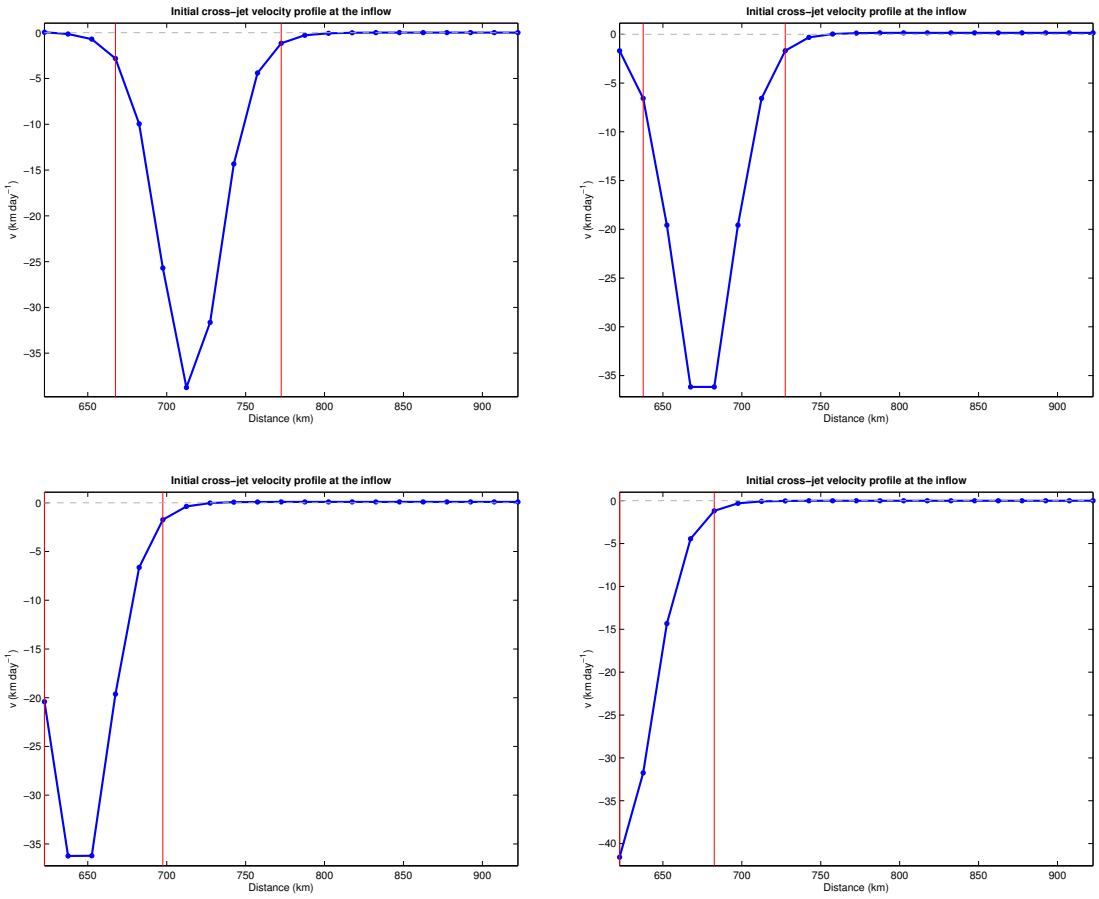

Figure 4.18: Initial velocity profile at the inflow for the 1-layer curvy coast case. The sequence of 4 profiles are correspondent to x_c = 100 km (top left), x_c = 60 km (top right), x_c = 30 km (bottom left) and x_c = 10 km (bottom right). Values are in km and day units, and 0.5 m s^{-1} = 43.2 km day^{-1}.

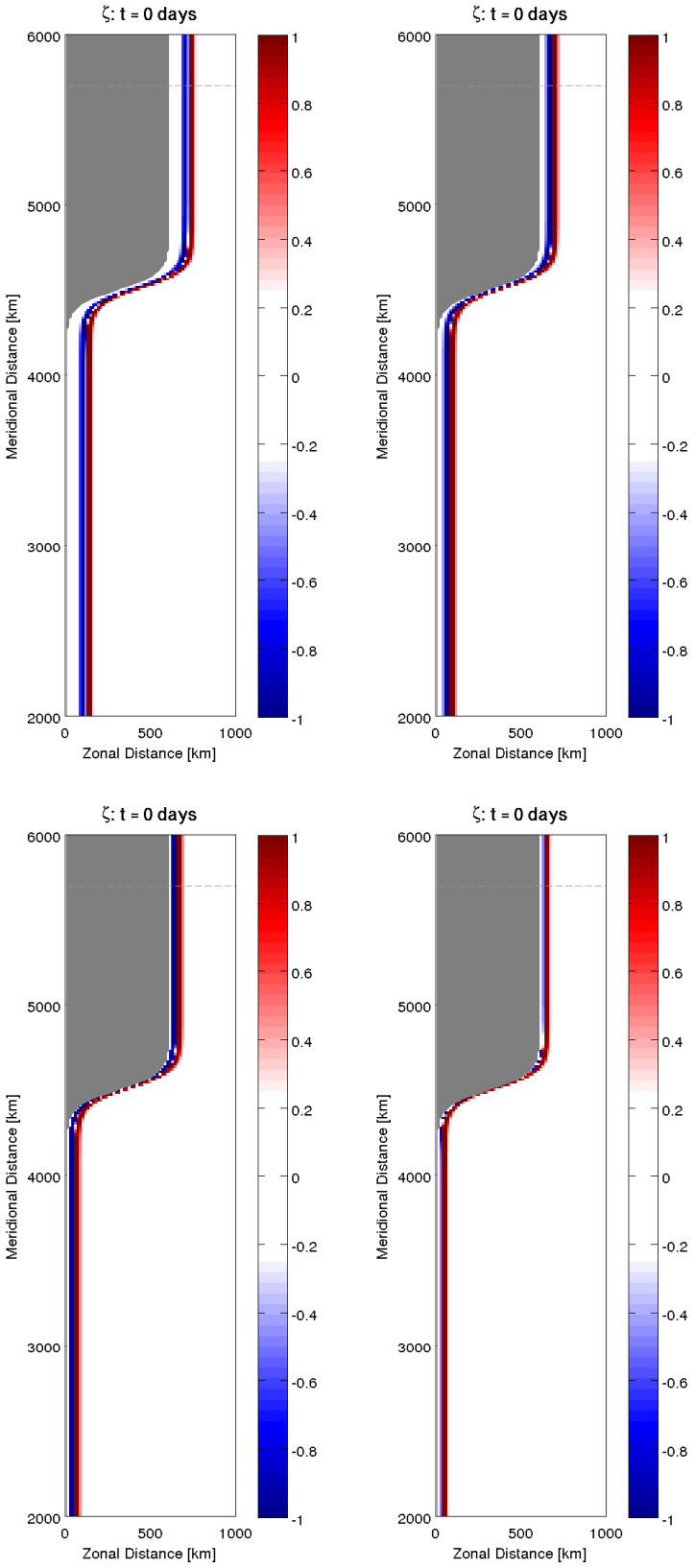

Figure 4.19: Initial q field for the 1-layer curvy coast case. Only inflow and interior regions are shown. The gray-dashed line indicates the inflowing steady-state region. The sequence of 4 profiles are correspondent to x_c = 100 km (top left), x_c = 60 km (top right), x_c = 30 km (bottom left) and x_c = 10 km (bottom right).

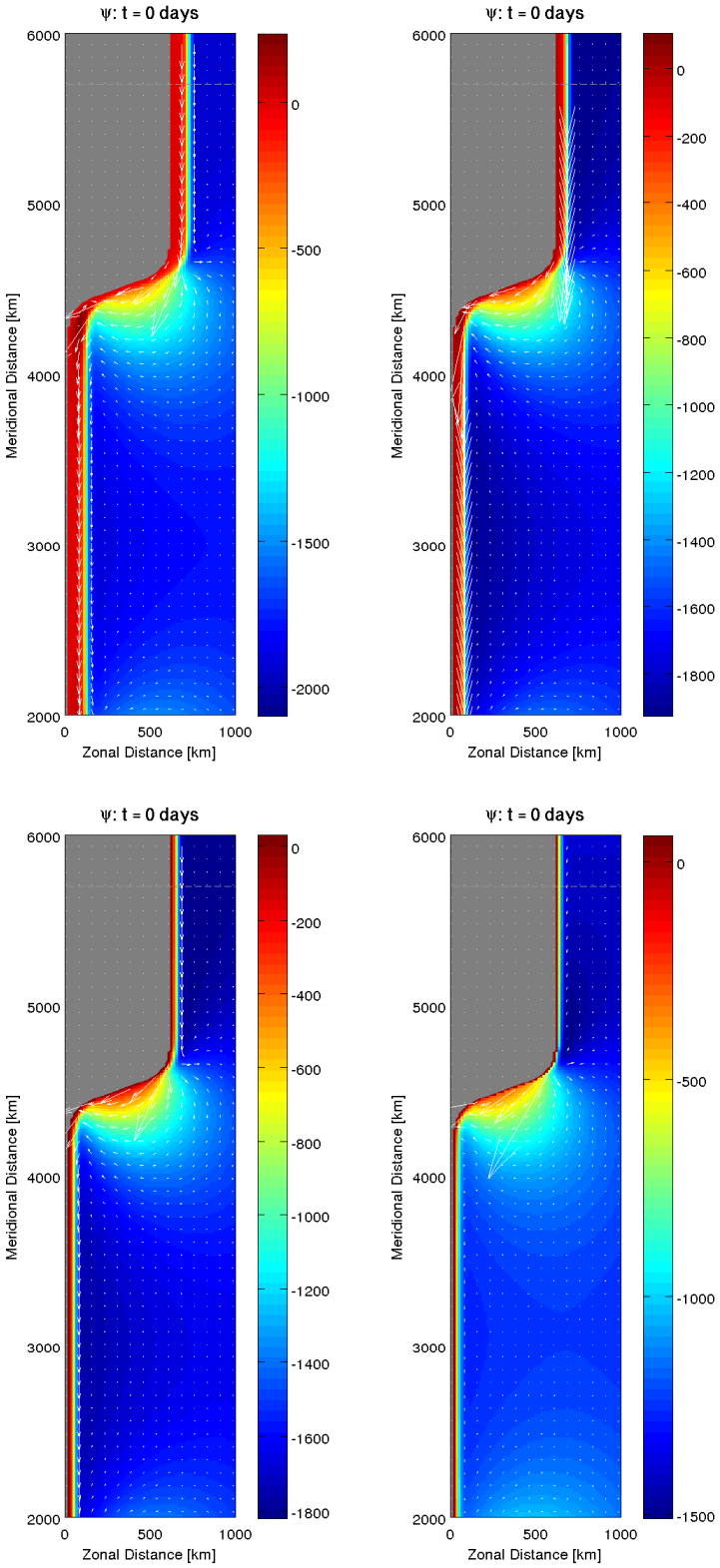

Figure 4.20: Initial ψ (color) and velocity (arrows) fields for the 1-layer curvy coast case. Only inflow and interior regions are shown. The gray-dashed line indicates the inflowing steady-state region. The sequence of 4 profiles are correspondent to x_c = 100 km (top left), x_c = 60 km (top right), x_c = 30 km (bottom left) and x_c = 10 km (bottom right).

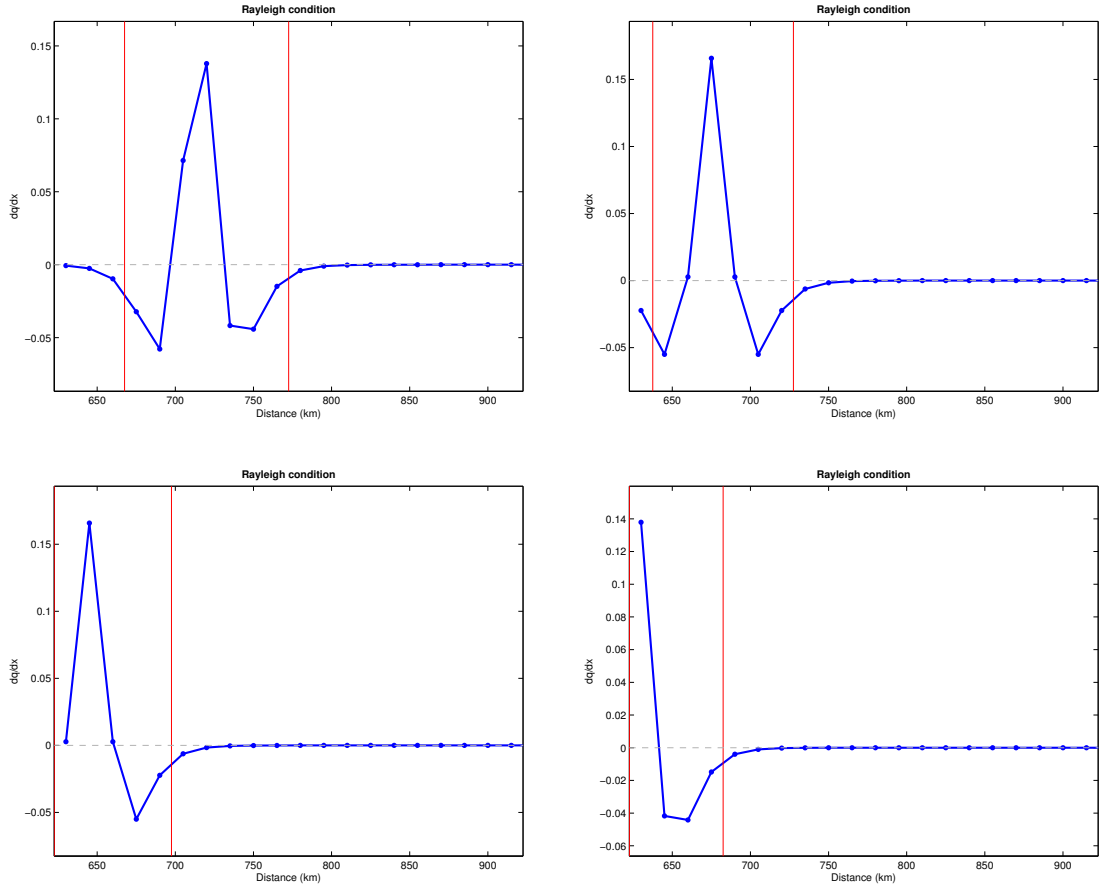

Figure 4.21: Necessary but not sufficient conditions for barotropic instability: the Rayleigh condition (dq/dx). The sequence of 4 profiles are correspondent to x_c = 100 km (top left), x_c = 60 km (top right), x_c = 30 km (bottom left) and x_c = 10 km (bottom right). Values are in km and day units.

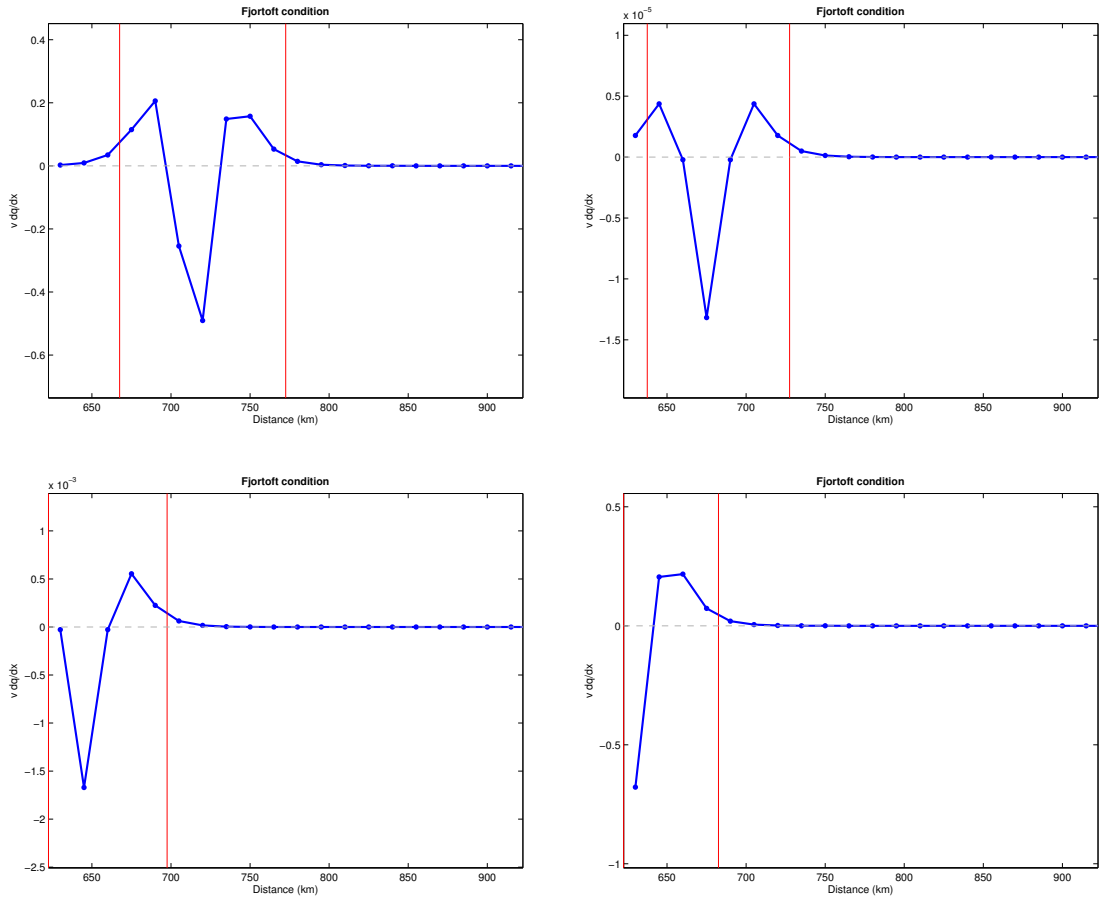

Figure 4.22: Necessary but not sufficient conditions for barotropic instability: the Fjørtoft condition ($(\bar{v} - v_o)^{dq}/_{dx}$). The sequence of 4 profiles are correspondent to x_c = 100 km (top left), x_c = 60 km (top right), x_c = 30 km (bottom left) and x_c = 10 km (bottom right). Values are in km and day units.

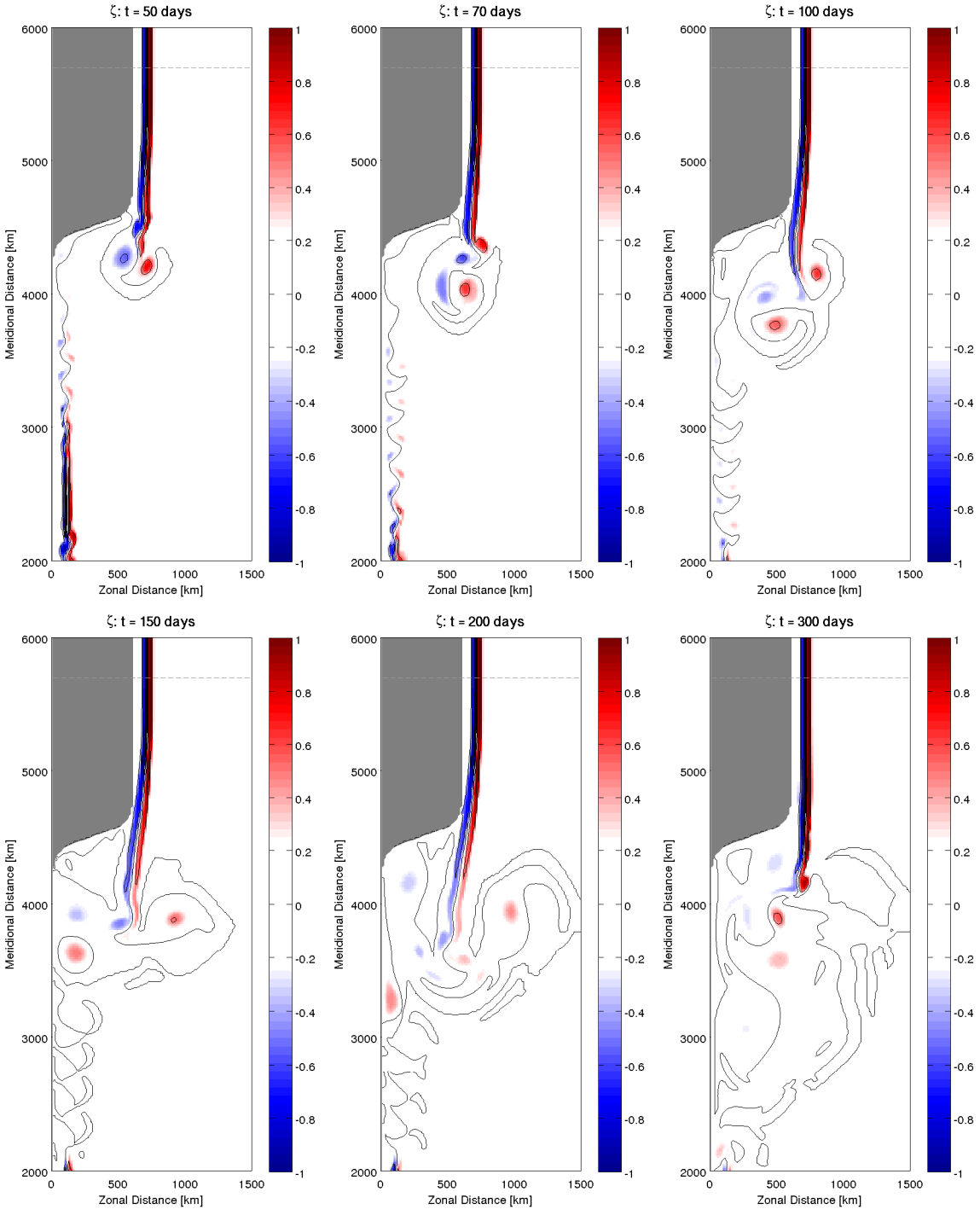

Figure 4.23: Time evolution of q field for the 1-layer curvy coast case, with x_c = 100 km. From top left to bottom right, t = 50 days, t = 70 days, t = 100 days, t = 150 days, t = 200 days, t = 300 days. Only inflow and interior regions are shown. The gray-dashed line indicates the inflowing steady-state region.

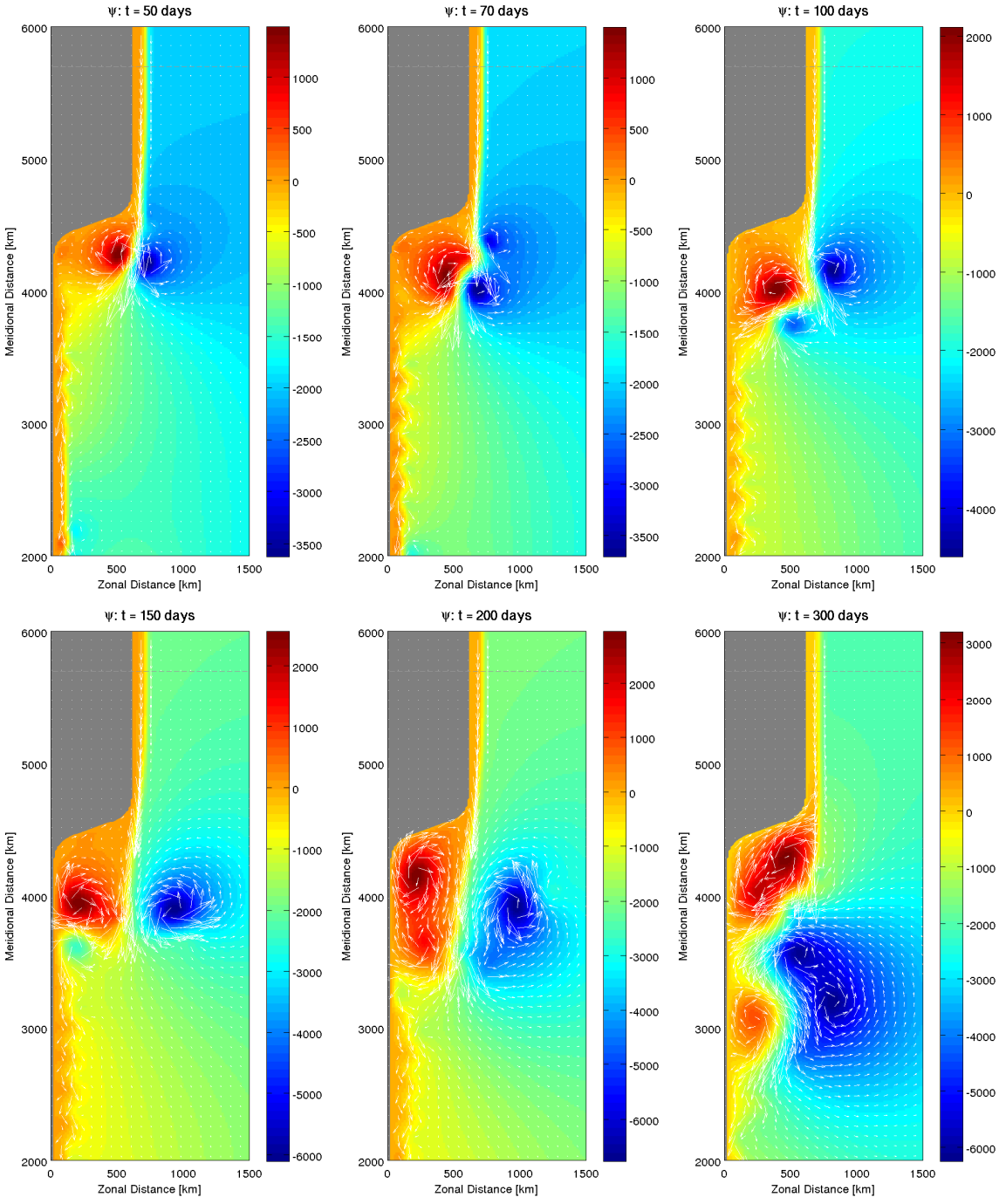

Figure 4.24: Time evolution of ψ field (color) over velocity (arrows) for the 1-layer curvy coast case, with x_c = 100 km. From top left to bottom right, t = 50 days, t = 70 days, t = 100 days, t = 150 days, t = 200 days, t = 300 days. Only inflow and interior regions are shown. The gray-dashed line indicates the inflowing steady-state region.

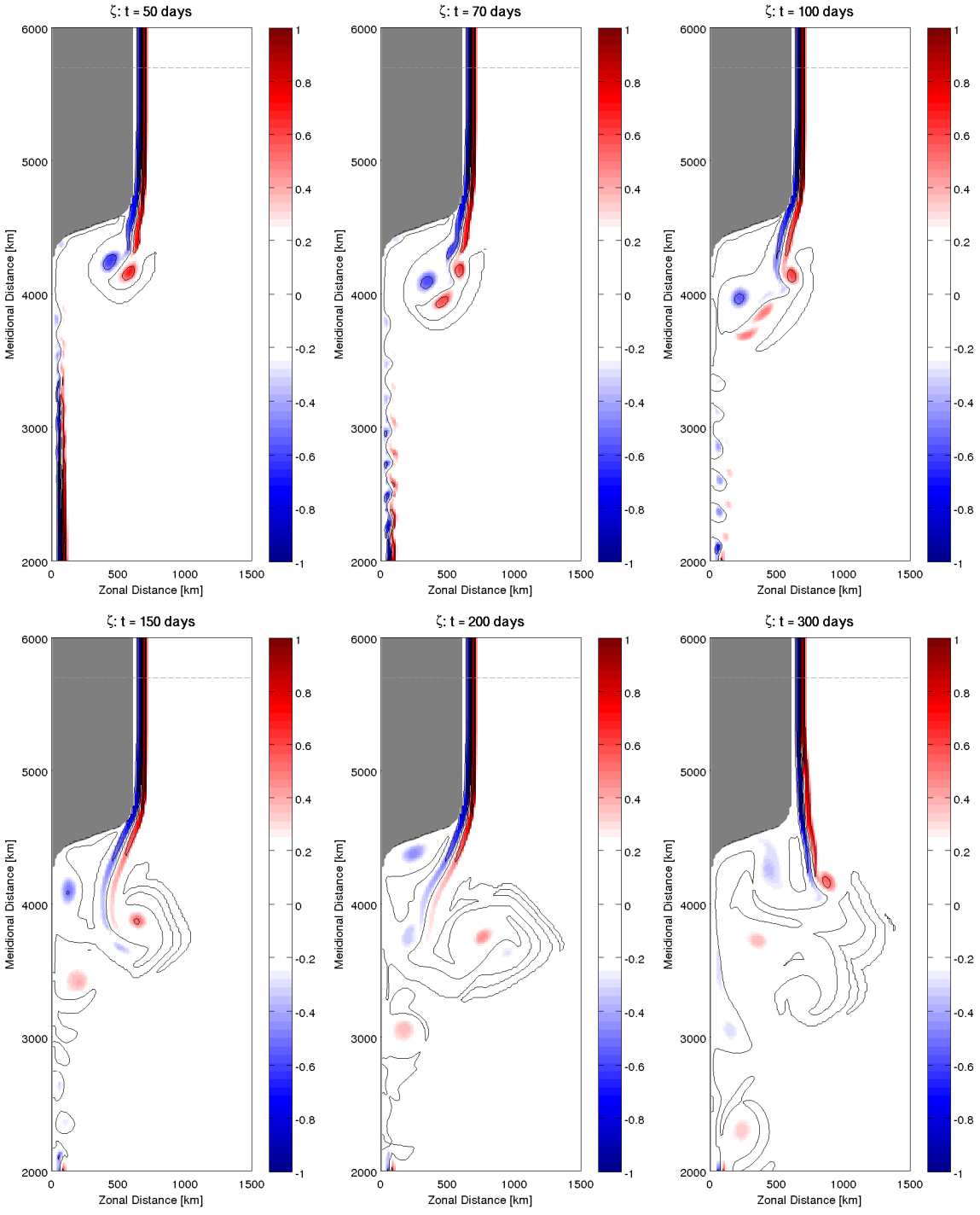

Figure 4.25: Time evolution of q field for the 1-layer curvy coast case, with x_c = 60 km. From top left to bottom right, t = 50 days, t = 70 days, t = 100 days, t = 150 days, t = 200 days, t = 300 days. Only inflow and interior regions are shown. The gray-dashed line indicates the inflowing steady-state region.

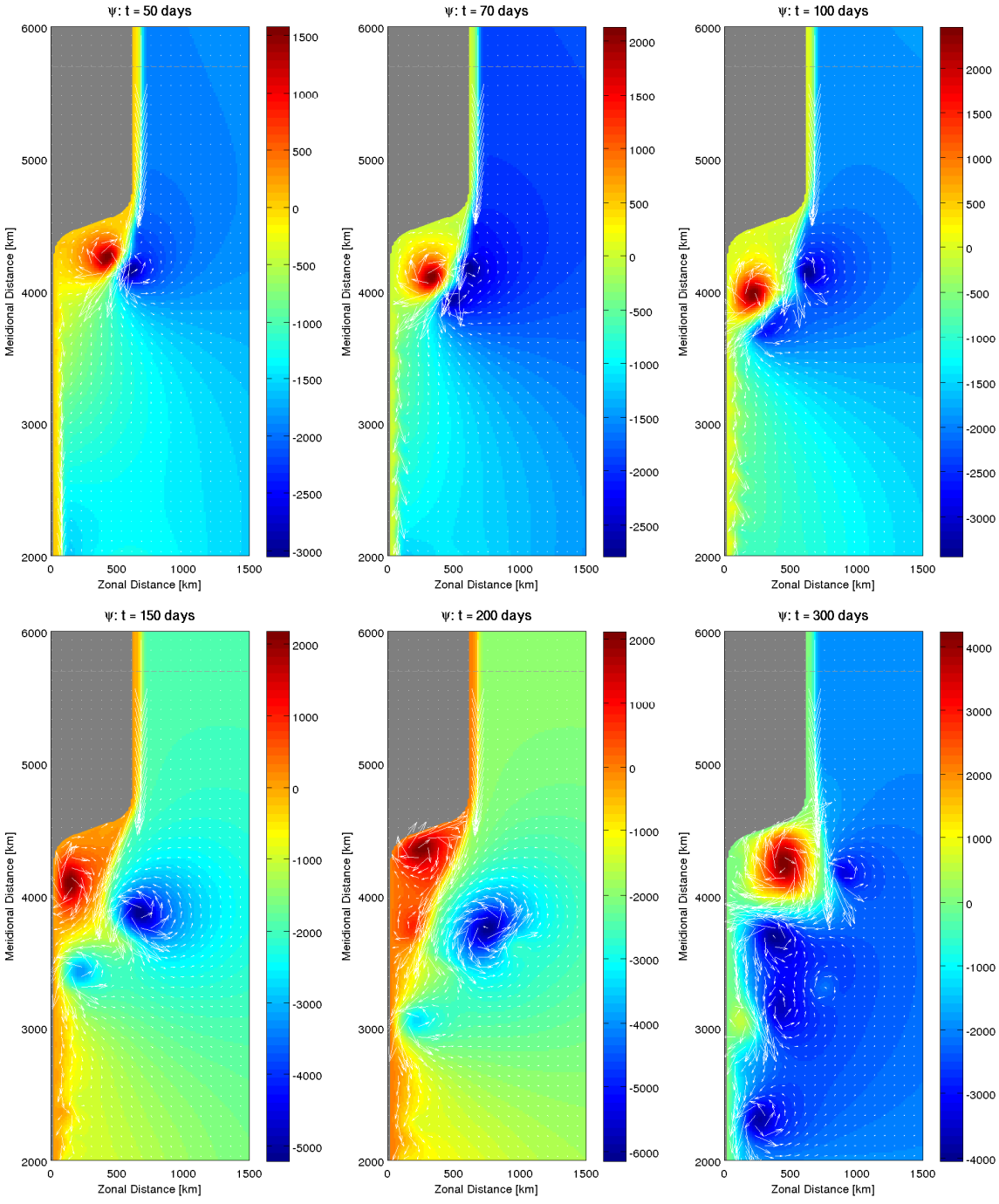

Figure 4.26: Time evolution of ψ field (color) over velocity (arrows) for the 1-layer curvy coast case, with x_c = 60 km. From top left to bottom right, t = 50 days, t = 70 days, t = 100 days, t = 150 days, t = 200 days, t = 300 days. Only inflow and interior regions are shown. The gray-dashed line indicates the inflowing steady-state region.

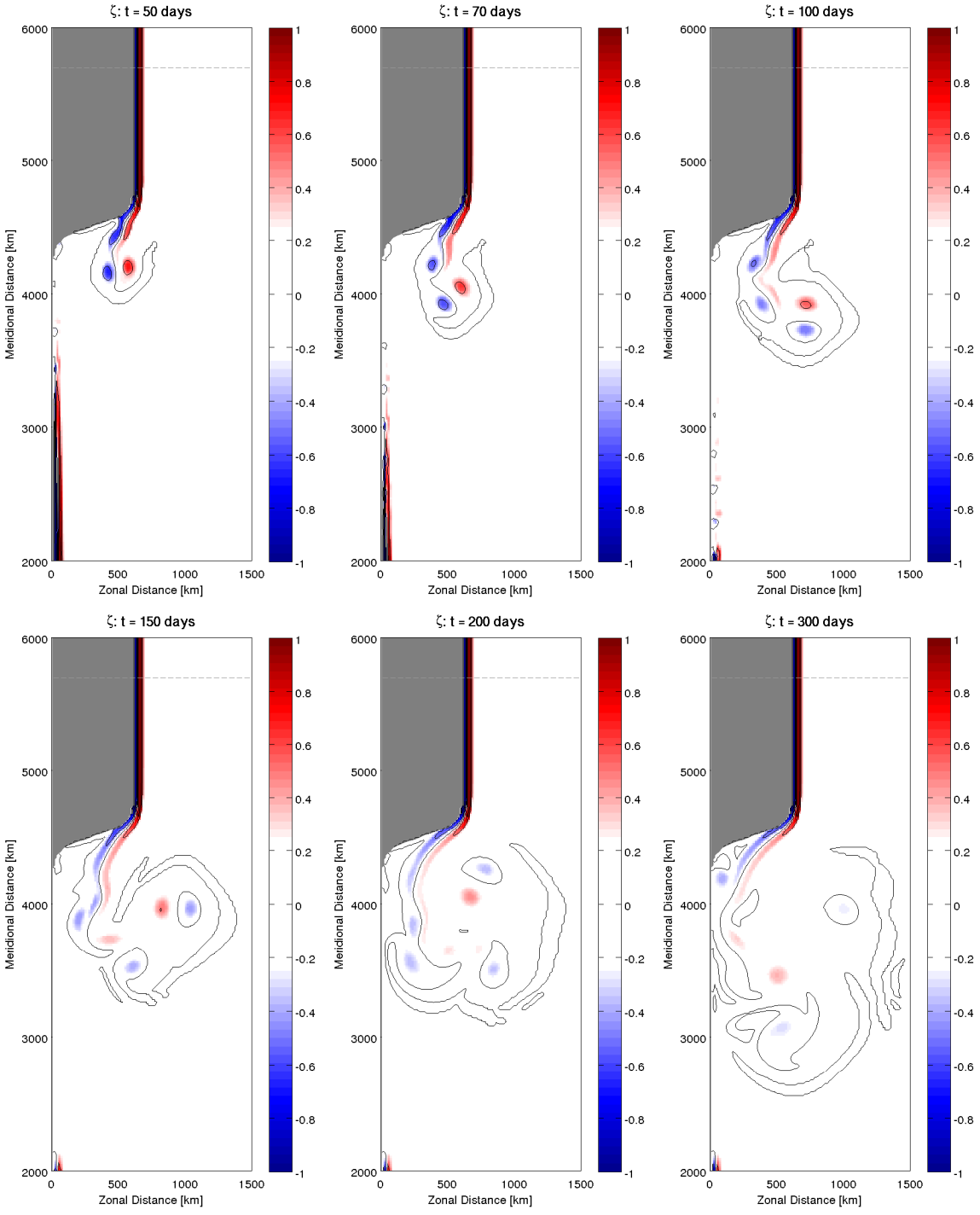

Figure 4.27: Time evolution of q field for the 1-layer curvy coast case, with x_c = 30 km. From top left to bottom right, t = 50 days, t = 70 days, t = 100 days, t = 150 days, t = 200 days, t = 300 days. Only inflow and interior regions are shown. The gray-dashed line indicates the inflowing steady-state region.

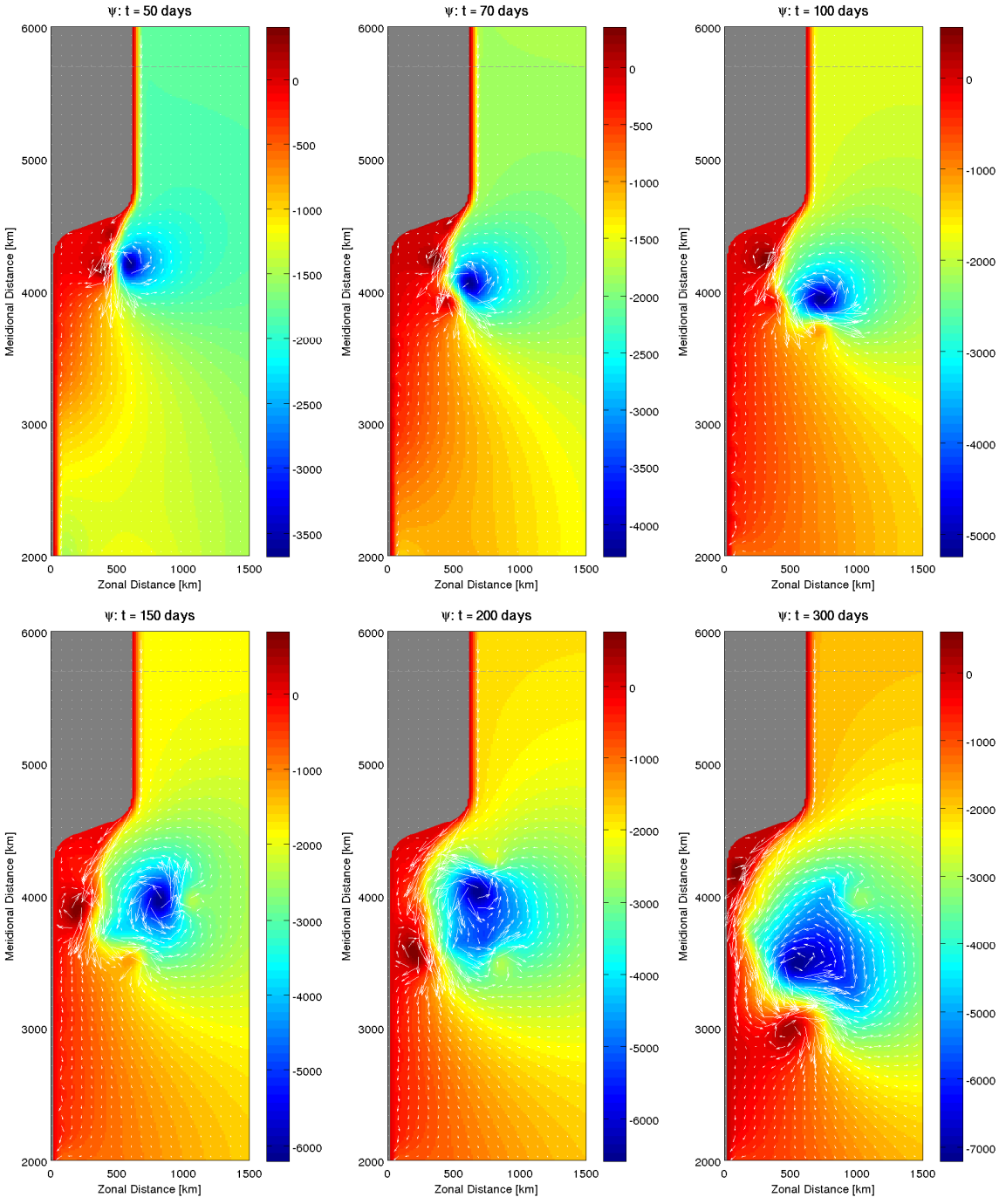

Figure 4.28: Time evolution of ψ field (color) over velocity (arrows) for the 1-layer curvy coast case, with x_c = 30 km. From top left to bottom right, t = 50 days, t = 70 days, t = 100 days, t = 150 days, t = 200 days, t = 300 days. Only inflow and interior regions are shown. The gray-dashed line indicates the inflowing steady-state region.

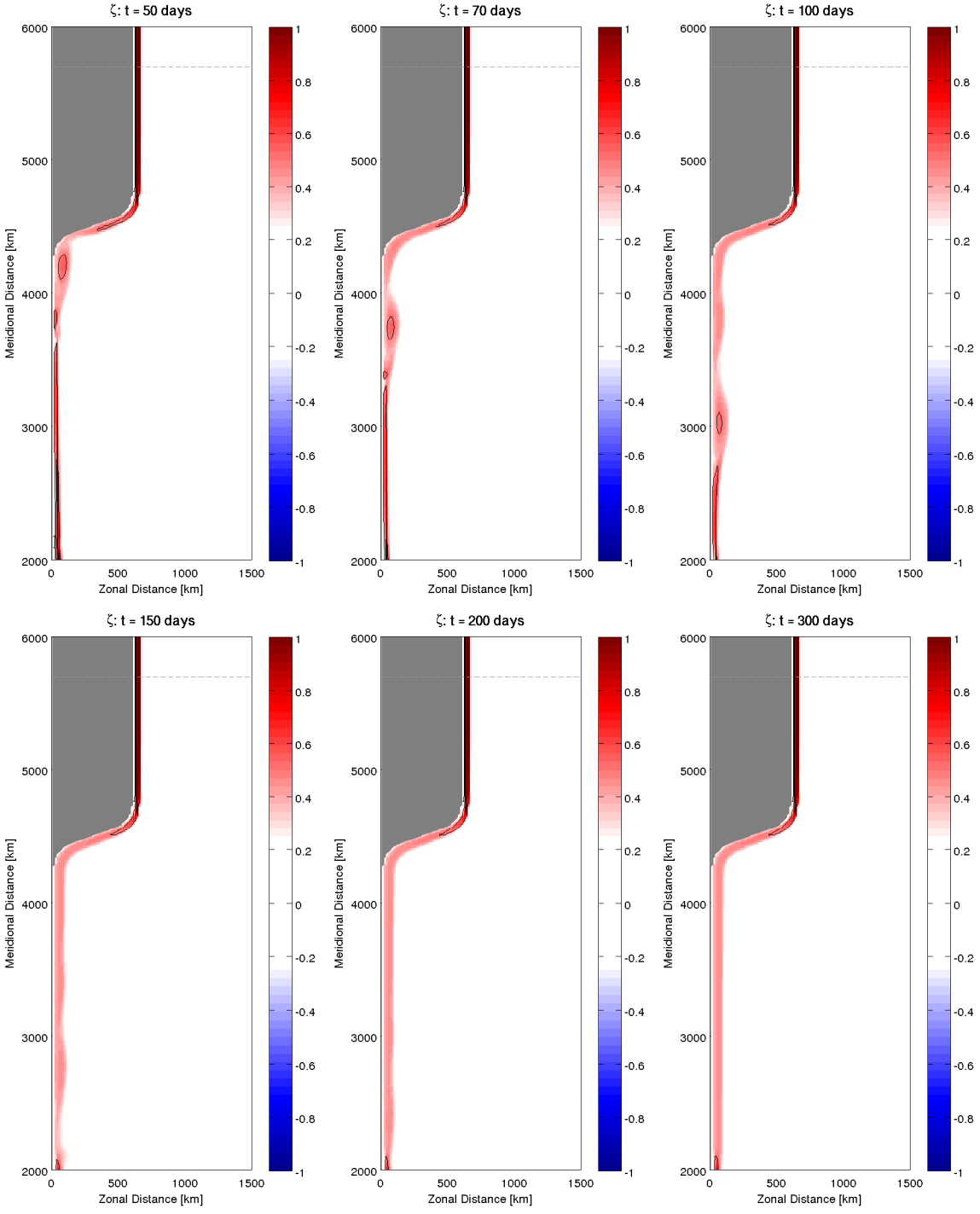

Figure 4.29: Time evolution of q field for the barotropic, curvy western boundary case, with x_c = 10 km. From top left to bottom right, t = 50 days, t = 70 days, t = 100 days, t = 150 days, t = 200 days, t = 300 days. Only inflow and interior regions are shown. The gray-dashed line indicates the inflowing steady-state region.

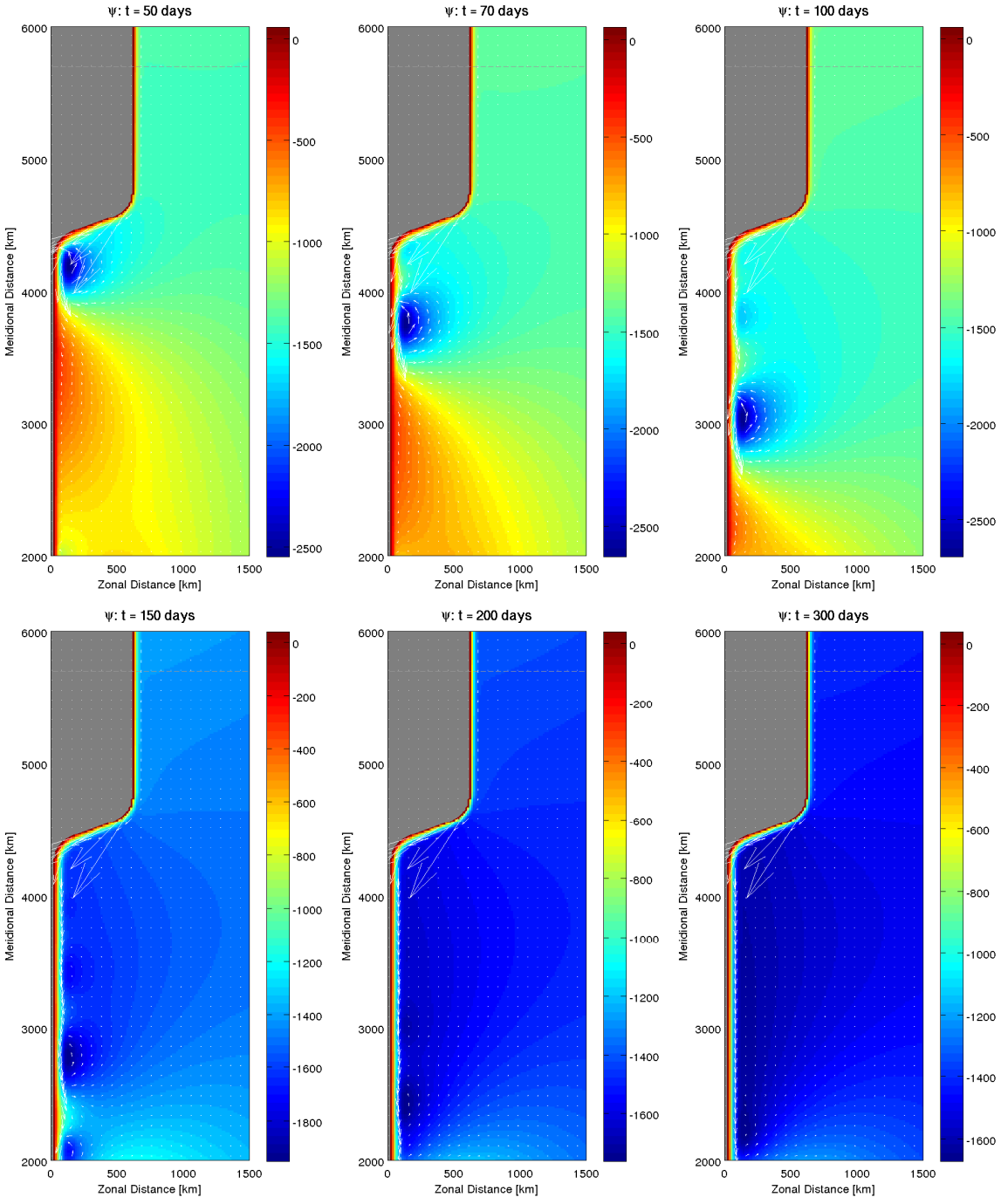

Figure 4.30: Time evolution of ψ field (color) over velocity (arrows) for the 1-layer curvy coast case, with x_c = 10 km. From top left to bottom right, t = 50 days, t = 70 days, t = 100 days, t = 150 days, t = 200 days, t = 300 days. Only inflow and interior regions are shown. The gray-dashed line indicates the inflowing steady-state region.

4.3 The equivalent-barotropic case

Here we evolved Equation 4.1 considering q of Equation 4.3, and such dynamical approximation is more in accordance with the BC scenario off Cape Frio region. We are still focusing on barotropic instabilities, and again the equivalent-barotropic approximation is very appropriate. The prescribed jet was the $sech^2$ one of Equation 4.4, calibrated with the BC characteristics obtained in Chapter 2. The study conducted for the $1^1/_2$-layer approximation consists only of the open domain case.

4.3.1 Open domain

Considering the same arguments presented in Section 4.2.1, we investigated a meridional BC-like jet in a $1^1/_2$-layer open domain model. The model consisted of a channel with size 6000x3000 km, and we run for 300 days, which means about 1 year. Here we tested one jet profile, such as in Section 4.2.1. Table 4.4 summarizes the $1^1/_2$-layer model experiment, in which the values are correspondent to the inflowing steady-state jet. The parameters based on the BC characteristics are: v_o, x_c, δ (described in Equation 4.4) and $jetw$ (jet width). Such as in the previous sections, we fixed δ as having the same value of the deformation radius computed for the BC in Chapter 2 ($R_d = 36$ km).

Table 4.4: Experiments run in the $1^1/_2$-layer open ocean QG model.

v_o (m s^{-1})	x_c (km)	$jetw$ (km)	δ (km)	R_d (km)
-0.5	0	200	36	36

Figure 4.31 (upper panel) shows the initial velocity profiles at the inflow for each case. Figure 4.32 illustrates the initial q and ψ horizontal fields. In all the following representation of the horizontal fields, only the dynamical relevant part of the channel will be shown, e.g. the inflow and interior areas. Here, the jet was initially perturbed, otherwise, without no source of instability, the jet would be totally stable in this configuration. The perturbation was the same used for the previous cases (a small noise). Looking to these figures, one can see that the inflowing jet is directed southward.

As we have done for the BC profile in Chapter 2 and in the previous section, we computed the Rayleigh and Fjørtoft conditions, that give us the necessary but not sufficient conditions for barotropic instabilities. In Rayleigh condition, $^{\partial q}/_{\partial x}$ should change signal at least once in the horizontal cross-jet direction. In Fjørtoft condition, a similar expression states a more robust condition, which is $(\bar{v} - v_o)^{\partial q}/_{\partial x}$, and also should change signal at least once in the horizontal cross-jet direction. Figure 4.31 center panel shows the Rayleigh condition we computed for each case, and Figure 4.31 lower panel shown the Fjørtoft one. In the present case, $^{\partial q}/_{\partial x}$ and $(\bar{v} - v_o)^{\partial q}/_{\partial x}$ changes sign at least once in the cross-jet direction.

The time evolution of the $1^1/_2$-layer case is shown in Figures 4.33 to 4.36. Here both time and length scales differ considerable from the barotropic case. The first difference was in the integration time period. We run this case for 600 days (double of the barotropic cases), since the jet started presenting variations much latter. However, even at advanced days, the jet was much more stable than the barotropic cases. It showed a meandering pattern, but any eddy developed, since we could not see any arrow closing in circles in the velocity fields. The propagation was typically around 6 km day^{-1} southward. The typical wavelength of the propagating meanders was of 200 km during the entire run.

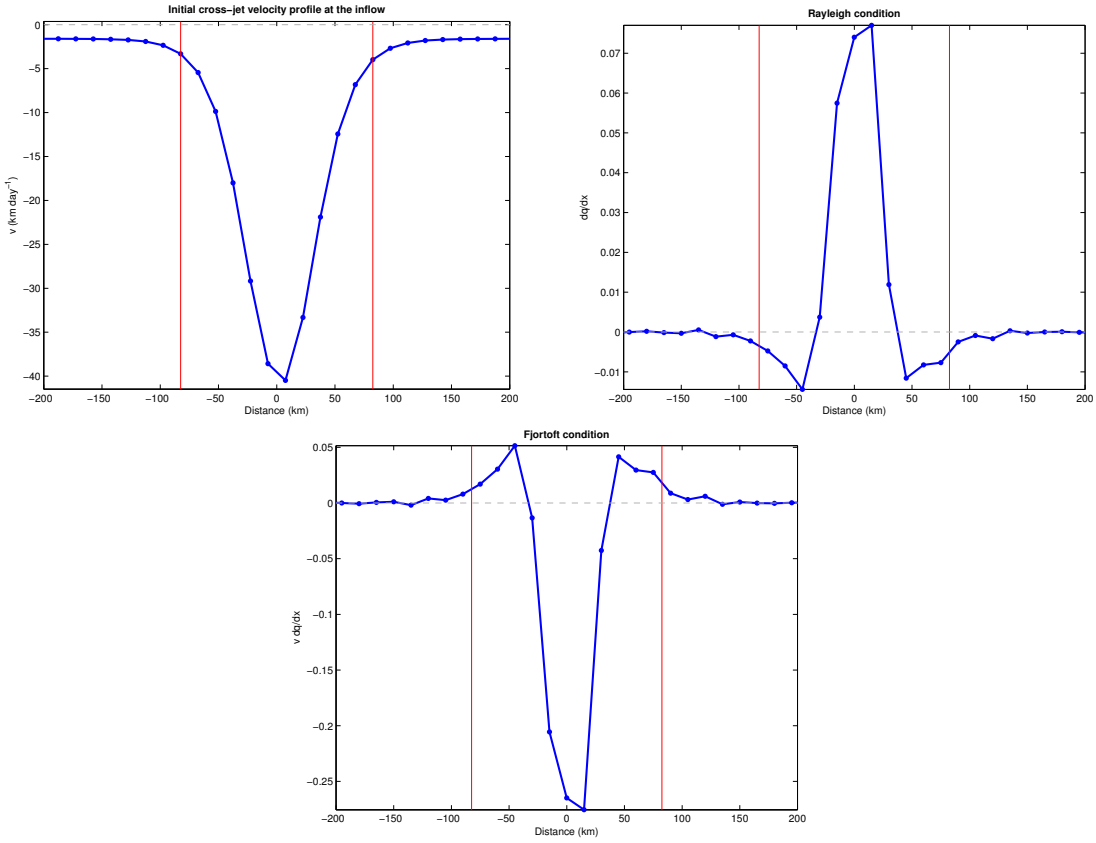

Figure 4.31: Top panel: initial velocity profile at the inflow for the $1^1/_2$-layer open domain case. Top right panel: the Rayleigh necessary condition for barotropic instability ($^{dq}/_{dx}$). Lower panel: Fjørtoft necessary condition for barotropic instability ($(\bar{v} - v_o)^{dq}/_{dx}$). Values are in km and day units, and 0.5 m s^{-1} = 43.2 km day^{-1}.

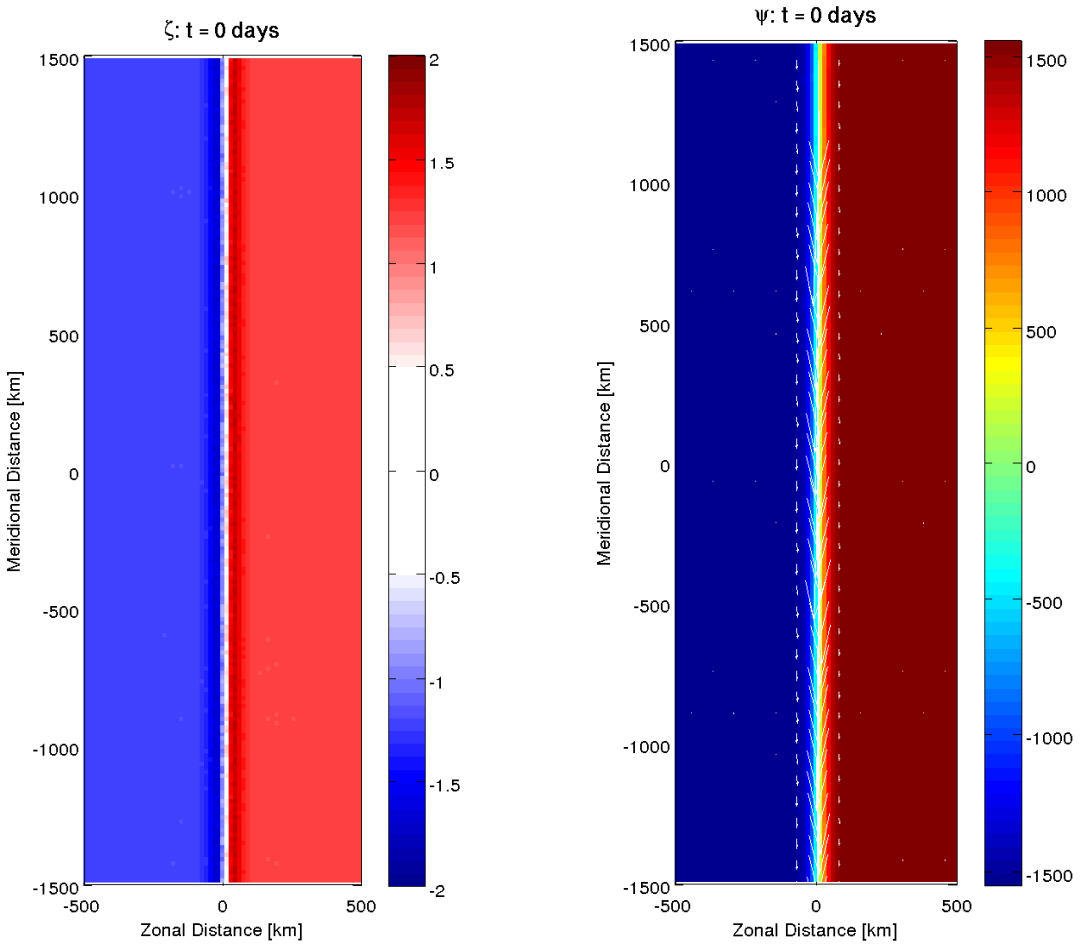

Figure 4.32: Initial fields for the $1\frac{1}{2}$-layer open domain case. Only interior region is shown. Left panel: q field. Right panel: ψ (color) and velocity (arrows) fields.

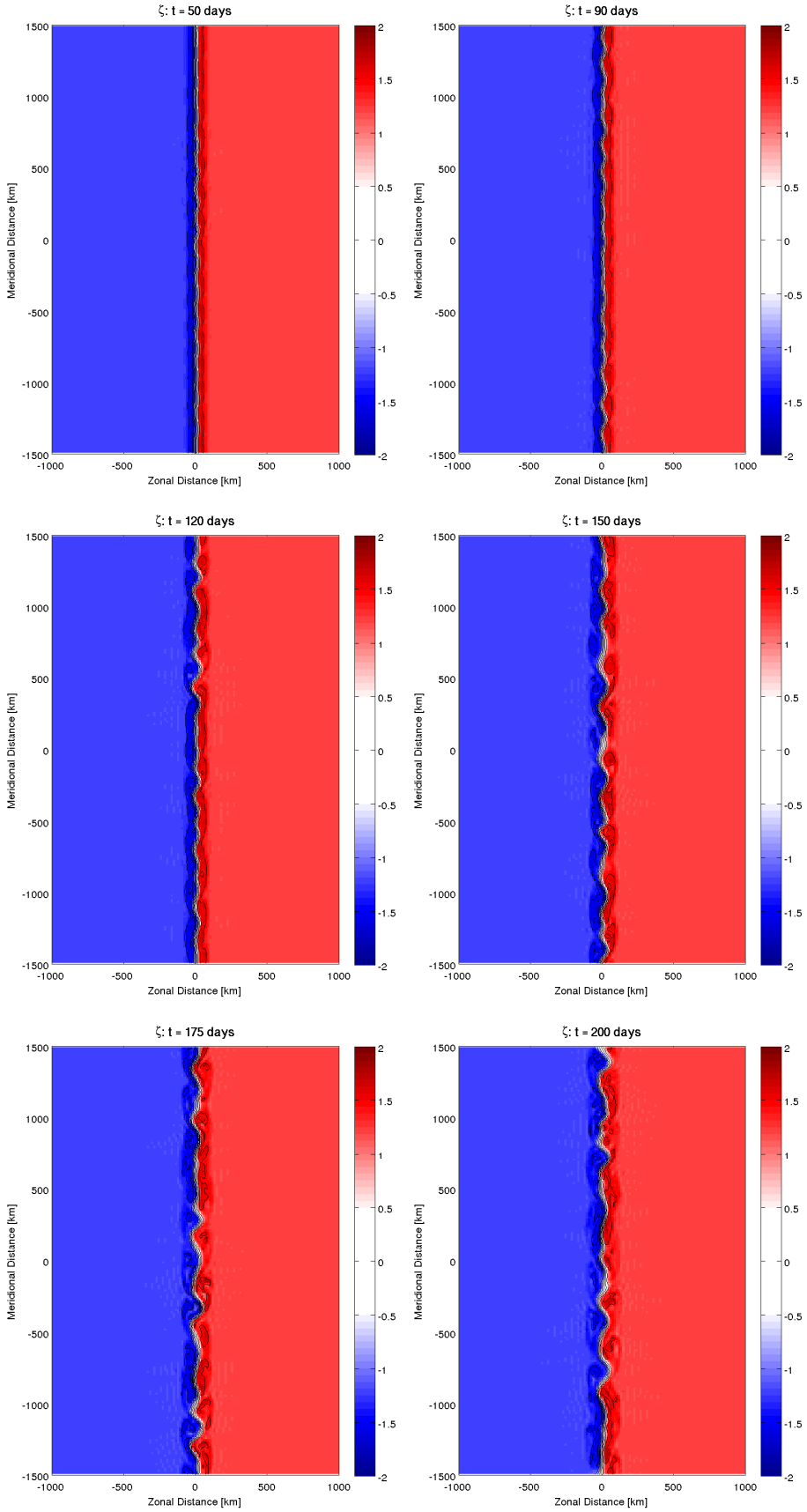

Figure 4.33: Time evolution of q field for the $1\frac{1}{2}$-layer open domain case. Only interior region is shown. From top left to bottom right, t = 50 days, t = 90 days, t = 120 days, t = 150 days, t = 175 days, t = 200 days.

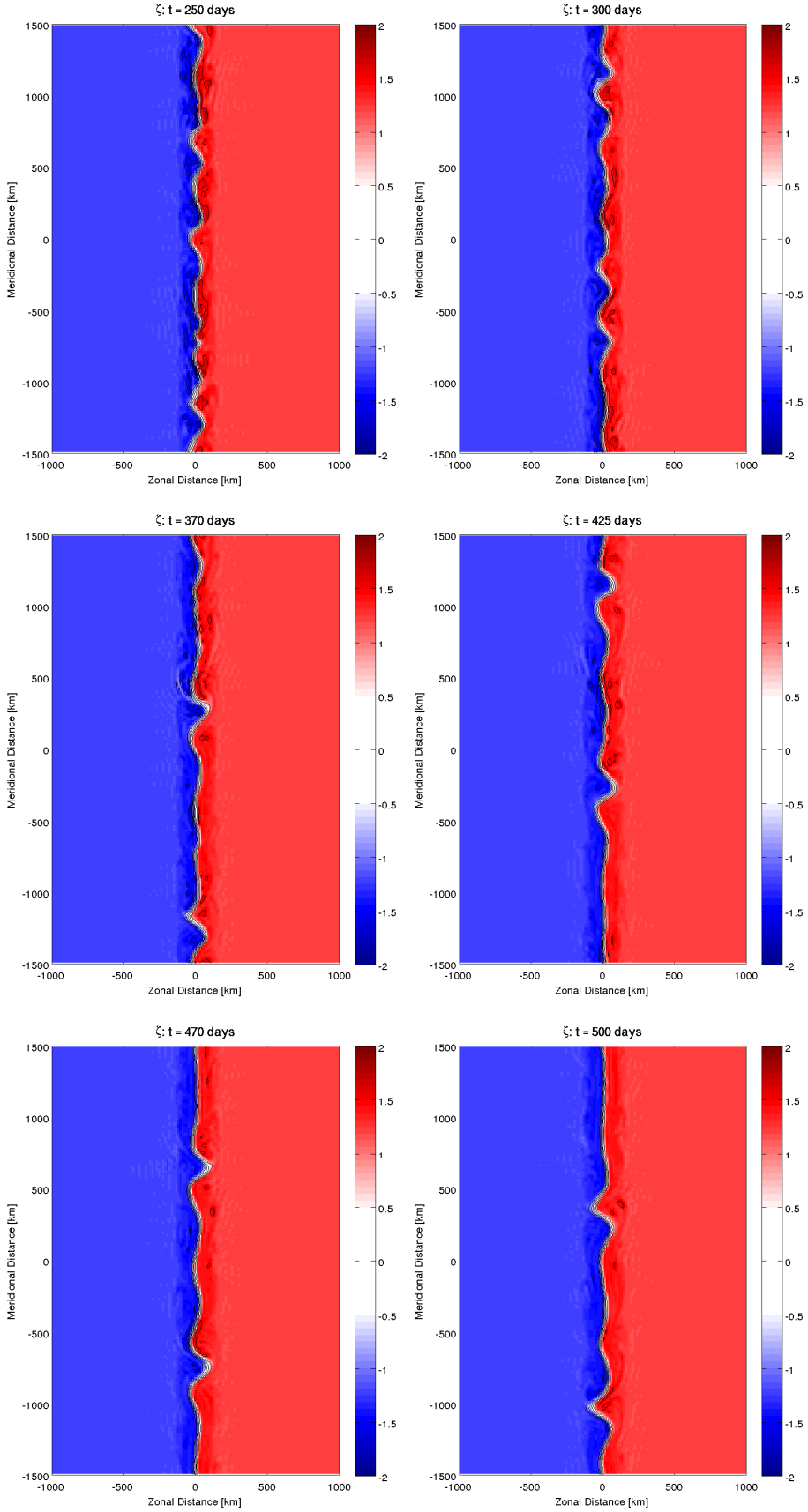

Figure 4.34: Time evolution of q field for the $1\frac{1}{2}$-layer open domain case. Only interior region is shown. From top left to bottom right, t = 250 days, t = 300 days, t = 370 days, t = 425 days, t = 470 days, t = 500 days.

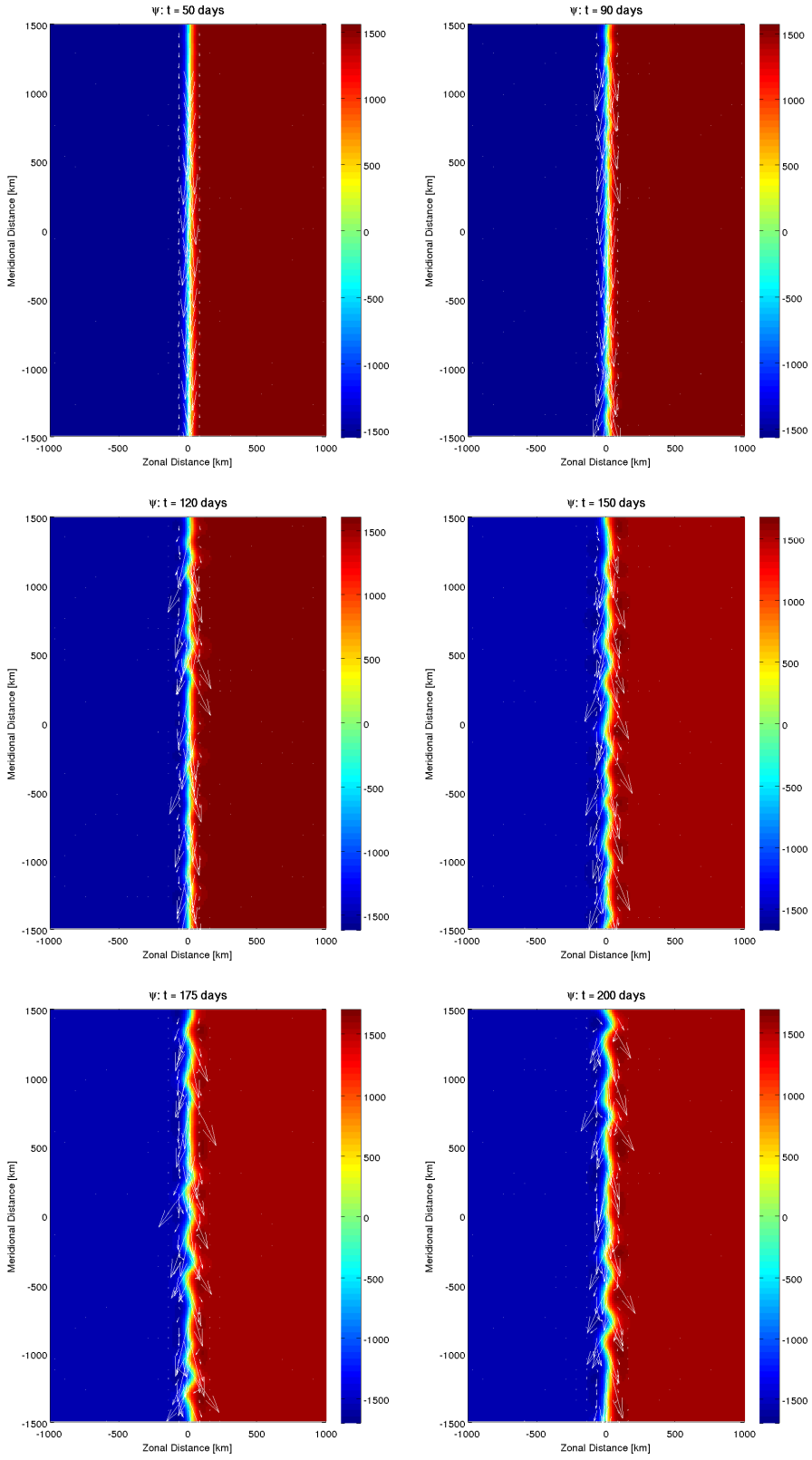

Figure 4.35: Time evolution of ψ field (color) over velocity (arrows) for the $1^1/_2$-layer open domain case. Only interior region is shown. From top left to bottom right, t = 50 days, t = 90 days, t = 120 days, t = 150 days, t = 175 days, t = 200 days.

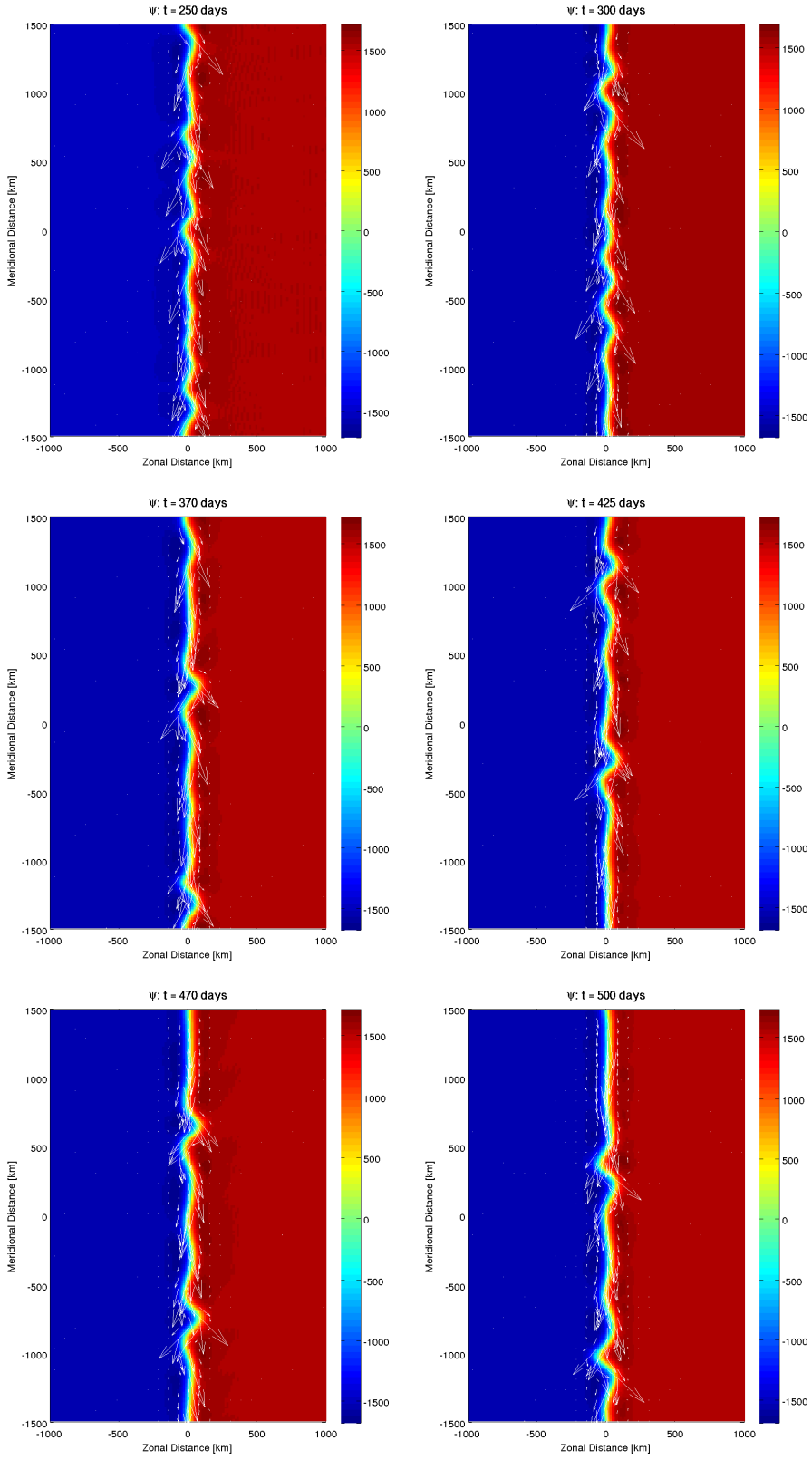

Figure 4.36: Time evolution of ψ field (color) over velocity (arrows) for the $1^1/_2$-layer open domain case. Only interior region is shown. From top left to bottom right, t = 250 days, t = 300 days, t = 370 days, t = 425 days, t = 470 days, t = 500 days.

4.4 Summary and Discussion

In the present chapter, we used a QG numerical model to study the downstream evolution of a potentially barotropically unstable jet. We aimed to investigate and construct a theoretical understanding of the interaction of a southward flowing jet with the lateral boundary, and this jet was prescribed based on the BC kinematic characteristics of the observed current presented in Chapter 4. In order to understand the behavior of the jet, we selected three different scenarios. The first was the open ocean domain, where we evolved a free inertial jet over the interior of the open ocean. It was our intent to disregard the effect of the coastline in order the analyze the simplest scenario. Although dynamically simpler, we considered this case relevant and appropriate to study the BC dynamics, since the BC, after passing by Cape Frio, actually encounters open waters. *Waterman & Jayne* [2011] considered the same idea in a theoretical study of the downstream evolution of an idealized Kuroshio current after the separation from the western boundary. The second scenario was a meridional channel domain with a rectilinear western boundary. The effect of the presence of a wall was included and the jet was imposed flowing attached to it. The third one consisted of a meridional channel domain with a curvilinear western boundary. The jet was also imposed attached along the wall initially, and the western boundary was construct to resemble the Cape Frio region coastline profile. For the three scenarios, we used the barotropic approximation, and the equivalent-barotropic was applied only in the open ocean domain case.

The barotropic cases gave us a baseline regarding the interaction of a jet in the simplest QG approximation. In open waters, the jet was initially perturbed (a noise perturbation along the entire PV field), otherwise the inflowing steady-state jet would not present variation, since no perturbations were imposed along the domain (such as topographic or lateral variations). In this case, the jet developed a sequence of opposing sign eddies along the channel, results very similar to the scenario presented by *Bell & Pratt* [1992], in what they called a "vortex street". The eddies presented the same length scale of the jet horizontal extension and propagated southward, leaving the domain by the southern boundary.

In the straight coast scenario, we presented four cases. In each one, we changed the distance of the jet core from the coast, which means we varied the parameter x_c

of Equation 4.4. The change in the jet core position generated different jet profiles. The low x_c case (x_c = 10 km) presented a lower jet width and the horizontal shear was restricted to the oceanic side. With the increasing of x_c, the jet had a bigger horizontal width and more horizontal shear was gradually added in the coastal side of the jet. Consequently, as we increased x_c, the jet seemed to be more unstable, and more inflexion points in the Rayleigh and Fjørtoft criteria were seen. Although we had tested many values of x_c, here we considered relevant to present four cases: x_c = 10 km, x_c = 30 km, x_c = 60 km, x_c = 100 km. We also imposed an initial perturbation along the jet, and allowed the flow to respond to it. Besides x_c = 10 km case, the jet generate bipolar features downstream as paired eddies that propagated southward, so barotropic instabilities actually occurred. A dipole detached from the jet and recirculated in the interior. Eddy-wall interaction as an "image effect" was observed in x_c = 100 km case, and for values higher than 100 km, the jet presented strong eddy-wall interaction and a more "chaotic" behavior. Therefore, x_c = 100 km was approximately the upper limit that separates a weak perturbed continuous flow regime from a highly unstable regime, not in accordance with typical WBC flows. The x_c = 10 km case presented a very stable behavior. A weak meandering pattern was observed, where the anticyclones were more prominent. One anticyclonic eddy was formed, but it traveled with the jet and left the domain through the southern boundary.

Comparing the open ocean domain with the straight coast channel, the main difference was the formation of a recirculating dipole, generated upstream, close to the jet inflow. The horizontal shear in both sides of the current is clearly important for the generation of vortex dipoles and the vortex street patterns observed, and these are scenarios comparable with the BC in southeast area of the Brazilian continental margin.

In the curvy coastline scenario, we tested the same four x_c values and allowed the jet to interact with a variant coastline, which was idealistic constructed to resemble the real one off Cape Frio region. No perturbations were imposed initially, since we intended to isolate the effect of the coast variation. Such perturbation was sufficient to make the jet unstable in all the four cases. Initially, a dipole was formed close to the indentation area and set the path for the trailing jet. In general, the trailing jet developed a cyclone, which located at the lee of the coastline indentation at least for

some time. The initial dipole recirculated and was absorbed latter by the flow. The higher values of x_c presented eddy-wall interaction at some point in the run and the x_c = 100 km case limited the weak perturbed continuous flow regime from a highly unstable regime, where nonlinearities dominate the dynamics.. As the jet core got closer to the wall, it was clearer the tendency of returning to the western boundary. Comparing the curvy coastline with the straight coastline scenario, similar behaviors were observed. Dipoles were formed initially, and a meandering pattern composed by eddies of opposing sign was observed downstream. In the x_c = 10 km cases, the jet presented similar behavior as well, where we had a very stable flow that formed one anticyclone that propagated southward and left the domain. It was also noticed that in both cases, as the jet got closer to the wall, it became more stable, and it started generating features latter.

In the $1^1/_2$-layer case, we have presented one case, which was a initially perturbed jet in a open ocean domain. The jet started developing perturbations much latter than the 1-layer one, and a meandering pattern was observed, resembling a southward-propagating wave with wavelength of 200 km and 6 km day^{-1} of phase velocity. Although we could set up the $1^1/_2$-layer approximation only for the open domain scenario, it seems the relatively weak stratification effect can produce differences in the flow. Comparing the two open ocean domain cases, the length scales of the features were very similar, but the time scales differed, where the 1-layer case had approximately the double of the propagation velocity of the $1^1/_2$-layer case. *Flierl* [1999] applied an hybrid model (with piecewise constant potential vorticity in the upper layer and a deep layer initially at rest) and a contour dynamics model and demonstrated that, the barotropic mode plays a fundamental role in the long-wave dynamics. For f plane jets, it leads to unstable waves whereas the n$^1/_2$-layer models have stable waves. Ring formation appears to occur via an initial stage of baroclinic growth - a "heton" mechanism whereby opposite-signed upper and lower layer PV anomalies propel each other away from the jet axis. At latter stages, the equivalent-barotropic dynamics acts to pinch off the eddy. Comparing his results with the ones we obtained here, we did have a more stable jet in the open ocean $1^1/_2$-layer case, where a stable wave pattern was obtained. Additionally, they showed the importance of the baroclinic effect in generating eddies,

so we imagine that this approximation would promote the development of eddies in our idealized scenarios. The equivalent-barotropic study certainly must be better explored, in the sense of including this approximation in a channel and considering a curvy coastline. Moreover, from the preliminary results we obtained here, it seems the model parameters and scales applied did not work as good as for the barotropic approximation, since no eddies grew. Probably, the baroclinic approximation excite unstable wavelengths that are different from the barotropic one, and our model configuration could not allow these wavelengths to manifest. In other words, we need to study what the ideal scales are when configuring a baroclinic jet, even in its simplest approximation.

The results obtained in x_c = 100 km and x_c = 60 km for the curvy coastline deserves special attention. The initial vortex dipole evolved to a scenario of southward-propagating opposing signs eddies located upstream, at least during some periods of the runs. Such dipole also seemed to trigger instabilities downstream, translated in a southward-propagating wave pattern. This specific situations resembled the observed pictures we presented in Chapter 1 for the BC off Cape Frio and southeast Brazilian coast, illustrated again in Figure 4.38. It seems the indentation triggers the formation of a vortex-dipole, which besides setting the path for the trailing jet, made it unstable and favorable to develop new eddies right upstream. The dipole eventually detached from the jet, but the current remained unstable and evolved to a scenario of opposing signs eddies. We have selected four snapshots to illustrate this description, and they can be seen in Figure 4.37. It is important to point out that the comparison is merely qualitative. The scales of the observed features in Figure 4.38 are much smaller than the scales we obtained in the runs, and it is expected since the purely barotropic scales are greater. *Verron et al.* [1991] mentioned that studies that had investigated the dynamics of a flow past a cape under the homogeneous rotating QG framework obtained, in general, eddies forming at the apex, either propagating downstream as isolated eddies or combining to form larger scale eddies. In the snapshots of Figure 4.37, right panels, we also obtained this combination of eddies that formed larger features, although here we have an indentation instead of a cape. After day 300, the eddies combined to form growing slow-propagating large scale features until the end of the run. Still in *Verron*

et al. [1991], they also investigated the evolution of a eastward zonal flow past a cape under the homogeneous (barotropic) QG framework, and tested different cases where they varied the Reynolds number Re. This parameter compares the strength of the jet with the friction intensity, and is defined as $Re = {}^{UL}/_{\nu}$ (U and L are the typical velocity and length scales of the jet, and ν is the fluid turbulent viscosity). Re appears in the nondimensional PV equation when considering the importance of lateral friction. They obtained attached lee anticyclones (clockwise rotation since they were considering northern hemisphere) at the rear face of the cape at low Reynolds number (strong friction), and for high Reynolds number (weak friction), attached eddies were formed and shed periodically from the cape. Here we have not tried experiments with the inclusion of the lateral friction term, but the comparison with that study is relevant since here we also dealt with a barotropic QG numerical model. In our results, after the jet passed by the indentation, it tended to form also a clockwise motion. If we rotate our reference framework to be equivalent to them, the inflowing jet past the coastline perturbation demonstrated similar behavior. Here, an eddy-shedding mode was also observed after the flow passed the indentation, but only in the case where the jet was closer to the wall. In *Verron et al.* [1991], this mode was obtained with high Re (e.g. weak friction), and here we considered a frictionless ocean. Anyways, as we shifted the jet core offshore, lee eddies started to appear, and we had periods that these eddies were steady for a considerable time. In our case, the horizontal shear strength at the coastal side of the jet seems to be comparable to the consideration of lateral friction. A weak or absent shear (such as in x_c = 10 km and x_c = 30 km) is equivalent to a weak friction, and the jet tends to a eddy-shedding regime. In the other hand, a strong shear (such as in x_c = 60 km and x_c = 100 km) is equivalent to a stronger friction, and the lee eddy regime is favored.

Although the effect of vertical shear may play an important role on the dynamics of the BC off southeast Brazil, and the $1{}^1/_2$- or 2-layer approximation would be more realistic in terms of dynamical simplifications, the barotropic approximation presented interesting results already. Barotropic instabilities do generate bipolar features when the jet presents horizontal shear. Moreover, an eddy-shedding mode is observed after the dipole formation, at least during an specific period of the integration time. The

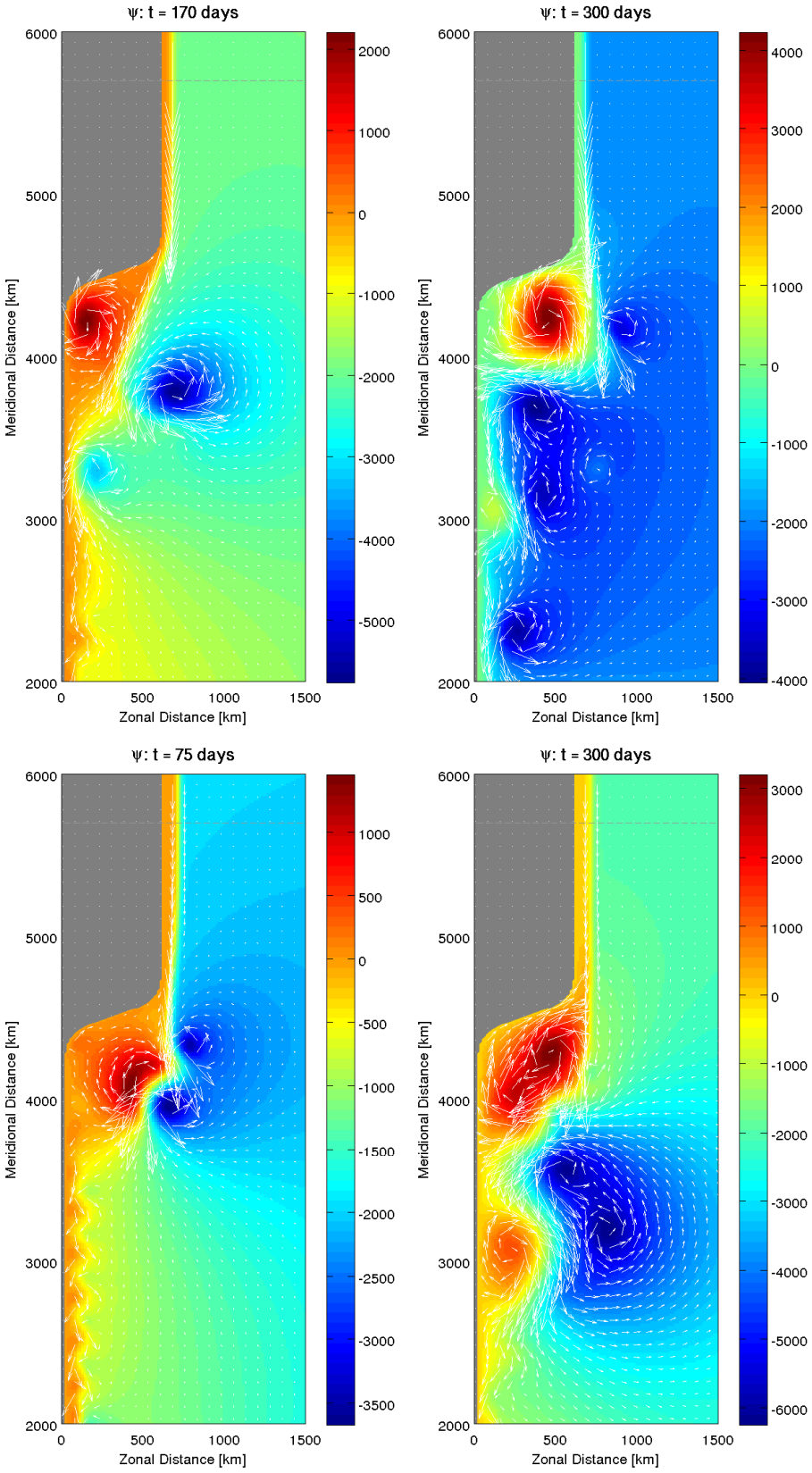

Figure 4.37: Snapshots of the velocity field over the ψ field for the curvy coastline barotropic case. Top panels: x_c = 60 km at t = 60 days (left) and t = 300 days (right). Bottom panels: x_c = 100 km at t = 75 days (left) and t = 300 days (right).

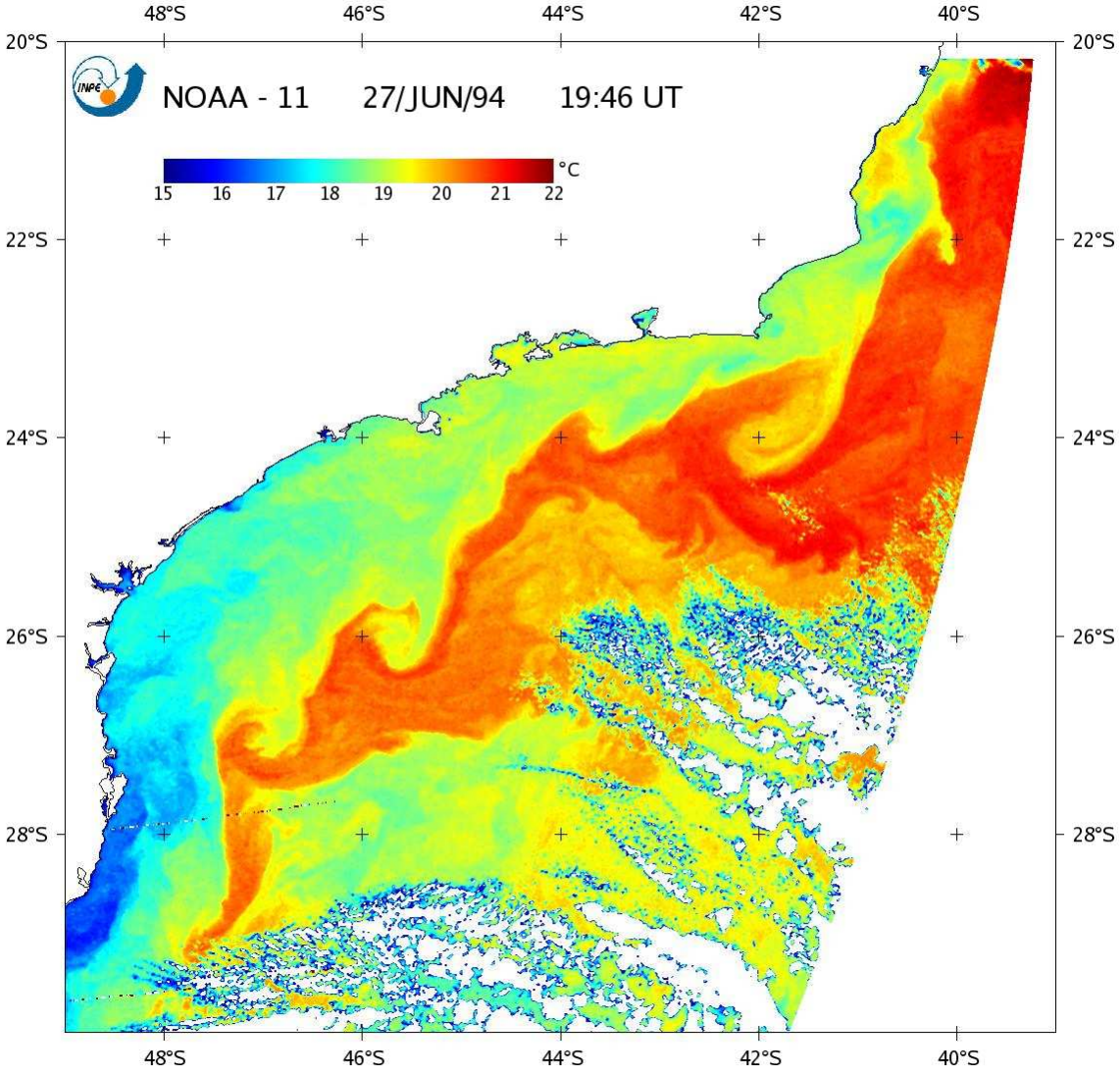

Figure 4.38: An AVHRR image from 27 June 1994, illustrating the southwestward propagating meanders associated to the BC flow. The bluish-green colors are associated with the cooler- and fresher-Coastal Water on the shelf and the reddish colors mark the presence of the warmer- and saltier-Tropical Water. From: *Mattos* [2006].

shear in the coastal side is essential to allow all the process described above to happen. In all the four cases of the curvy coastline case, it was observed that anticyclonic eddies were formed more frequently than cyclones. We mentioned the possible importance of the horizontal shear, in which the oceanic side was always present and it was favorable to the formation of anticyclones. However, *Verron et al.* [1991] pointed out that in rotating case such as the one they investigated, it was observed asymmetry in terms of occurrence and form in cyclones and anticyclones. The cyclonic eddies were smaller and shed slower than the anticyclonic eddies.

A similar study in terms of dynamical approximation was conducted by *Munday & Marshall* [2005]. In their investigation, the problem of western boundary current separation is investigated using a barotropic vorticity model. Specifically, a boundary current flowing poleward along a boundary containing a cape is considered. The meridional gradient of the Coriolis parameter (the β effect), the strength of dissipation (represented by the Reynolds number Re), and the geometry of the cape are varied. They found that (i) all instances of flow separation are coincident with the presence of a flow deceleration; (ii) an increase in the strength of the beta effect is able to suppress flow separation; and (iii) increasing coastline curvature can overcome the suppressive beta effect and induce separation. They cited that a change in direction of the coastline can decelerate a boundary current and induce its flow separation. Although we are not testing a cape shape in our western boundary, some accelerations/deceleration process might have occurred in our results. Anyways, they obtained that an increase in curvature promotes flow separation, while small curvatures results in an fully attached flow regime. Although not showed here, we performed a few tests in which we varied the coastline curvature, and we also obtained the *Munday & Marshall* [2005] pattern. Small curvature results in high curvature radius, which results in a smoother coastline profile. Hence, it exerts less perturbation in the flow. The smoother the coastline (e.g., close to a straight coast), the less unstable is the jet. These results regarding coastline curvature corroborate the investigation of *Stern & Whitehead* [1990]. These authors performed an evaluation of variations in coastline curvature, but the shape was very similar to our case, e.g., an indentation where the coastline changes direction. They used the barotropic approximation with no viscous forcing neither variation of plane-

tary vorticity. They obtained a critical value of the angle of change that separated two different regimes. A high obtuse angle (small curvature) promotes an eddy attached regime where the flow tends to pass by the cape attached to the wall or shedding eddies that propagate downstream. Those eddies were cyclonic in their experiments (counter-clockwise because f was positive), just like in our results of attached regime. A low angle (high curvature) makes the jet to separate from the coast and a mushroom-like structure is formed, setting the path for the trailing jet. Their results also indicate that perturbations in the coastline can induce the jet to form bipolar features in a homogeneous ocean through barotropic instabilities. The dipole formation case also presented a recirculating pattern, and this was obtained in our results.

Generally speaking, in the 1-layer cases, barotropic instabilities generated bipolar features. The presence of a simple rectilinear coastline made the dipole to detach from the jet, but in the curvy coast the jet had room to interact with open water when it separates from the indentation. The bipolar features, although apparently very intense, did not make the jet discontinuous, and this fact made possible the formation of eddies in the downstream region. Stratification may play an important role in determining the type of regime a jet presents when interacting with the coastal variations, whether it is eddy-shedding, eddy-attached and so on. For instance, *Magaldi et al.* [2008] and *Castelao & Barth* [2006] investigated the role of stratification in idealized scenarios of a flow past a cape using a primitive equation numerical model and could obtain distinct regimes. *Magaldi et al.* [2008] designed a fully idealized experiment where a steady jet impinges on an obstacle (triangular cape) in a rotating and linearly stratified environment. They kept the small Rossby number constant and did sensitivity runs varying the Burger Number (Bu),

$$Bu = \left(\frac{R_d}{D}\right)^2, \tag{4.8}$$

which measures the ratio between baroclinic deformation radius (R_d) and the length scale of the obstacle (D). In their experiment of a zonal homogeneous flow (Bu = 0), they obtained the generation of small anticyclones in the stripe over slope topography that propagated downstream. For low Bu, e.g., $Bu < 0.1$ (weak stratification), a fully attached regime is established, and the jet flows smoothly over the cape. For interme-

diate Bu, e.g., $0.1 < Bu < 1$, fluid parcels flow more around the obstacle than over it. Flow separation occurs and small tip eddies start to shed. The increasing of Bu shifts the system from a eddy-attached regime (where eddies are formed behind the cape and shed downstream) to a lee eddy regime (where small lee eddies are formed and grow behind the cape). For high Bu, e.g., $Bu > 1$, (strong stratification), tip eddies merge to form larger eddies in the lee of the cape. Our results are comparable with the regime of $Bu = 0$ obtained by the authors, where they obtained the generation of small anticyclones propagating downstream. The authors mentioned that the presence of stratification, even if very weak, changes the dynamics considerably.

The discussion above took us to obtain some conclusion. The strength of the jet horizontal shear determines the regime the flow is going to present. More specifically, the shear at the coastal side of the jet is key to obtain changes in the unstable jet behavior. The absence of shear in the coastal side makes the jet more stable and an eddy attached or fully attached flow regimes are promoted. As we increase the coastal shear, the tendency of jet separation also increases, and we obtain two concomitants scenarios: formation of vortex-dipoles and the latter establishment of larger scales lee eddies followed downstream by other eddies.

It is important to point out that, given the model configuration and initial conditions, we are only allowing the formation of meanders and eddies due to barotropic instability. Hence, the physical process we had isolated here was the horizontal shear. Rossby waves and other large scale waves are being filtered here, since the parameter β = 0 (we are using the f plane) and we are not considering a sloping bottom (the bottom is flat). So, we are absolutely not forcing the model with topographic Rossby waves, although this was one of the processes suggested by *Silveira et al.* [2000] when he compares the BC scenario off southeast Brazilian coast with the GS warm outbreaks. The appearance of topographic Rossby waves would be possible if the model could have at least one region shallower than a second one. The planetary Rossby waves needs the variation of f to appear, and this effect would be effective only in a zonal jet.

The effect of friction due to the presence of a solid boundary is being ignored here, although several studies consider this process in determining the formation of vortical structures and shedding regimes. Another aspect considered to play important role

on the formation of such features is accelerations and decelerations in the flow, which can be promoted by solid barriers such as capes. Our coastline profile does not have a barrier effect in the jet, so we think this effect is unlikely to be happening here.

It seems the barotropic approximation requires different temporal and spatial scales if compared to the approximations that consider the stratification. In our study, the barotropic scenario comparable to past studies such as *Verron et al.* [1991] (weak friction) and *Magaldi et al.* [2008] (homogeneous ocean) was with $x_c = 10$ km. It seems that using the same jet (fixed Ro) for both homogeneous and stratified scenarios results in having a more stable scenario in the equivalent-barotropic case. This is probably due to the fact that the baroclinic scales excite unstable waves with wavelengths very different from the barotropic approximation, and the configuration applied in the QG model could not allow these scales to manifest. So the "more stable" results actually indicated the equivalent-barotropic approximation needs adjustments to allow the baroclinic scales to excite appropriated unstable waves.

Finally, it is important to highlight that our goals number 4 presented in Section 1.2 were accomplished in the present chapter, e.g we examined the interaction of a barotropically unstable meridional jet and a western boundary in idealized configurations relevant to BC jet system, in particular the role of lateral boundary variations in making the jet unstable and able to generate eddies and dipoles. The perturbation as a varying boundary is sufficient to excite the formation of barotropic dipoles, and the presence of the lateral boundary can make these dipoles to detach from the jet, e.g. they not necessarily keep associated to the current main axis all the time. In the next chapter, we will try to address the stratification effect still ignoring the presence and interaction with the IWBC.

Chapter 5

The primitive equations numerical model

This chapter aims to investigate the BC dipoles dynamics in a more complex framework in terms of dynamical simplification. Here we added to a primitive numerical model the technique know as Feature-Oriented Regional Modeling System (FORMS). The idea is to create the initial conditions of the numerical model through the construction of parametric features that were done based on previous observations of the study area. Therefore, our parametric feature consisted of a jet along the western boundary which presented the same kinematic characteristics of the BC. Therefore, we implemented the Regional Ocean Modeling System (ROMS) in an idealized scenario, where there is only a BC-like jet (potentially barotropically unstable) flowing along the Brazilian coast. Here, the more complex oceanic scenario is composed by real topography and a density field background (necessary for the ROMS initial conditions). The FORMS methodology and its implementation in ROMS will be presented in the next section.

5.1 Methodology

According to *Gangopadhyay & Robinson* [2002], each oceanic region, however unique in their individual behavior, consists of a number of *generic* or *common* characteristic synoptic circulation structures. These synoptic entities or *features*, when put together in

a particular region, interact and evolve to generate the combined circulation variability due to different regional set-up of multi-scale processes, bathymetry, boundaries and forcing due to winds and buoyancy. This approach, called feature-oriented regional modeling system (FORMS) [*Gangopadhyay & Robinson*, 2002], consists of empirically/analytically creating initial and/or boundary conditions for momentum/tracers for primitive equation model simulations. The technique is widely used for atmospheric and ocean nowcasting and forecasting [*Robinson et al.*, 1988, 1989; *Spall & Robinson*, 1990; *Fox et al.*, 1992; *Hurlburt et al.*, 1992; *Cummings et al.*, 1997; *Gangopadhyay et al.*, 1997; *Robinson & Glen*, 1999; *Gangopadhyay et al.*, 2003; *Calado et al.*, 2008, 2010], but it is also applicable for feature-oriented process studies, as we aim here.

According to the methodology developed by *Gangopadhyay & Robinson* [2002], when the typical characteristics of the features from previous observations or studies are known, we can parameterize them and use as input for different process studies numerical experiments and study their dynamical processes. The empirical-analytical design formulation of the three-dimensional velocity and water mass structures of a feature is called the *feature model* (FM).

We use this technique to analytically create the time-averaged smooth BC flow off southeast Brazilian coast. We ignored the presence of IWBC (as we did in Chapters 3 and 4) since we still don't want to incorporate the effect of a strong vertical shear in the system, although some shear does exists along the BC flow. Then our FM is represented by a BC-like jet, which is required to meet observation-based kinematic characteristics (obtained in Chapter 2) and mass conservation criteria. This field is then interpolated to a numerical model grid with the best available bathymetry, and allowed to evolve for one year. This period is typically a minimum time spawn to see the development of mesoscale variability. The 3D field construction will be detailed in the next section.

5.1.1 Formulation of the idealized system

Velocity FMs can be designed through two main approaches [*Lozano et al.*, 1996]: forward approach and backward approach. The forward approach consists of parameterizing the shape of T and S surfaces that composes the baroclinic pressure gradients that are in geostrophic balance with the velocity structures of interest. In this case, the

associated velocity field may be computed by the primitive equation model or beforehand. In the backward approach, the exact aimed velocity structure is parameterized and the tracers are computed afterwards through a variety of methods [*Gangopadhyay & Robinson*, 2002]. In this work, both velocity and tracers are considered as the initial field to the primitive equation ocean model. Generally, the choice of either approach is based on the available source of observations. Availability of direct velocity measurements favors the backward approach; and availability of tracers observations favors the forward approach. The velocity-based backward approach is also more suitable for current or front-dominated regions. In the present process-study work, the backward approach is employed.

In stage 1 of the FM backward approach, a quasi-meridional jet (which represents the BC flow) is parameterized. Since we are using real topography data (ETOPO1 data base), the jet along the western boundary is not fully meridionally-oriented. In stage 2, geostrophically balanced potential temperature (T) and salinity (S) fields are computed from the FM 3D velocity field. The last stage consists in computing the remaining prognostic variables required by the numerical model as initial conditions, which are the depth-averaged velocity field and the sea surface height (SSH). The application of each one of these stages is detailed in the following paragraphs.

Starting with stage 1, the orientation of the system defined within the study area is a natural coordinate frame of reference, where x is the cross-stream axis, y is the along stream axis and z is the vertical axis. The y axis is roughly parallel to the isobath of 200 m, which represents the interface between the coastal and the deep oceans. For the BC-like jet construction, we considered the jet core always at surface. Now we aim to model a jet that is surface-intensified and keeps the same transport at the inflow and outflow regions. So, BC horizontal cross-jet structure is parametrized by Equation 5.1 as

$$v_h = v_c \ \ sech^2\left(\frac{x - x_c}{\delta}\right), \tag{5.1}$$

which describes the same Bickley jet used in Chapter 4, with a constant amplitude defined by v_c. For the cross-stream structure, a constant width proportional to δ is

adopted, and x_c defines the position where the jet core occurs. This position x_c is also considered constant to keep the system at a fixed distance from the shelf break, roughly following the local topography. Hereinafter, the subscript c refers to *core*, which is where the maximum velocity of the jet occurs at a given y location.

For the BC vertical structure, we incorporate the variation in z through a Gaussian variation as

$$v_z = v_c \ \ exp\left[-\frac{(z-z_c)^2}{2\delta_b^2}\right], \ \ at \ \ z < 0. \tag{5.2}$$

where the parameter δ_b refers to the vertical length of the Gaussian decay, proportional to the jet vertical extension.

The graphical representation of all the relevant FM parameters are presented in by Figure 5.1. The choice of the parameters was based in the observational data presented in Chapter 2, so realistic jet positions, width, thickness, maximum velocities and transports were aimed. The current transport was computed analytically by integrating Equation 5.1 from $-\infty$ to ∞, which results in the simple expression

$$\mathcal{T} = v_c \, \delta(\delta_t + \delta_b). \tag{5.3}$$

Stage 2 consists in computing T and S fields by inverting the thermal wind relation and using a linearized version of the equation of state, as in *Schmidt et al.* [2007] and *Fernandes* [2007]. We use local climatological T, S and potential density (ρ) regional averaged vertical profiles to keep water masses and stratification within a realistic range. The first step to obtain T and S is to compute ρ, from the thermal wind equation

$$f_0 \frac{\partial v}{\partial z} = -\frac{g}{\bar{\rho}} \frac{\partial \rho}{\partial x}, \tag{5.4}$$

where f is the Coriolis parameter, v is interpreted as the along-shelf velocity and $\bar{\rho}$ is the reference density (1027 kg m^{-3}, from climatology). Integrating Eq. 5.4 in respect to x, we get an expression to ρ, which is

$$\rho(x,z) = \rho(0,z) - \frac{f_0 \bar{\rho}}{g} \int_0^L \frac{\partial v}{\partial z} dx, \tag{5.5}$$

where $\rho(0, z)$ is a mean density profile (also obtained from climatology) at the initial location of the transect and L is the length of the transect. Figure 5.2 show the resulting σ_θ fields computed from Figure 5.1 velocity fields. Figures 5.3 and 5.4 show how the resulting system sets horizontally, after computing all the transects in the study area domain. Therefore, the adopted parameters for the velocity-based BC FM system were: x_c = 160 km, δ = 36 km, z_c = 0 m, $\delta_b/2$ = 300 m and v_c = 70 cm s^{-1}. The resulting transport was T = 5 Sv.

The $T - S$ fields, which are actually required for the primitive equation model as initial and boundary conditions, are computed through

$$\rho(x, z) = \bar{\rho}[1 + \bar{\beta}S_0(z) - \bar{\alpha}T(x, z)], \tag{5.6}$$

which is a bi-dimensional linearized equation of state used by *Fernandes* [2007]. Mean haline contraction coefficient is represented by $\bar{\beta}$ (8.0 $\times$ 10^{-4}), $\bar{\alpha}$ is the mean thermal expansion coefficient (2.2 $\times$ 10^{-4} $^\circ C^{-1}$) and S_0 is a mean S profile computed from climatology. Temperature is then computed by re-arranging Equation 5.6 as

$$T(x, z) = \frac{\frac{-\rho}{\bar{\rho}} + 1 + \bar{\beta}S_0(z)}{\bar{\alpha}}, \tag{5.7}$$

and salinity is obtained following *Fernandes* [2007] by Equation 5.8,

$$S(x, z) = S_0(z) - 10^{-2}T(x, z). \tag{5.8}$$

Finally, in stage 3, to complete the prognostic variables required by the numerical model, depth-averaged flow and SSH are computed. In that case, SSH is simply computed through

$$SSH = \frac{\Delta\Phi}{g}, \tag{5.9}$$

where the geopotential anomaly ($\Delta\Phi$) is obtained through S and T using 1200 m as level of no motion.

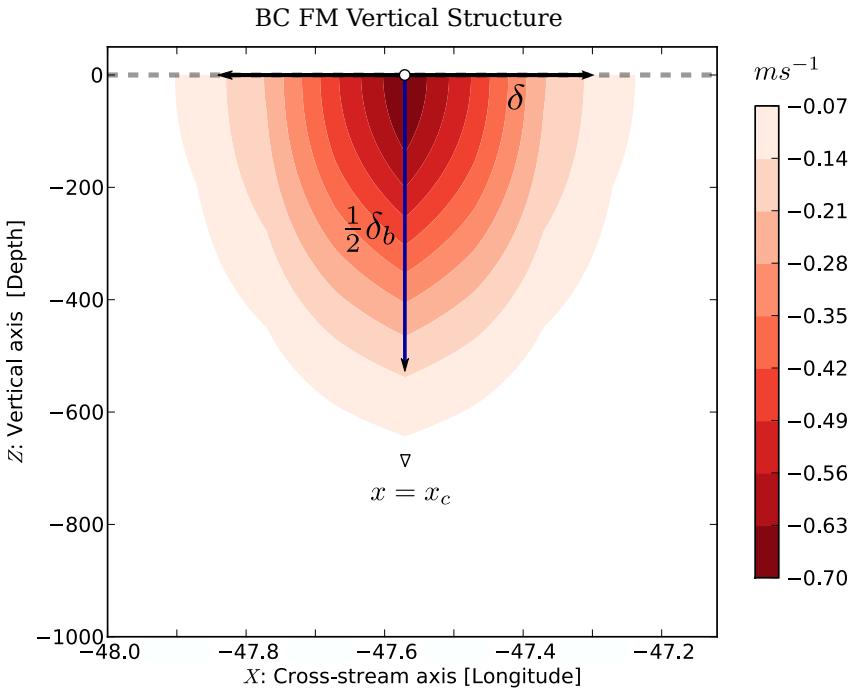

Figure 5.1: Graphical representation of the cross-jet vertical velocity distribution, which was the same along the domain. This section represents the velocity-based stage 1 of the FM system configuration.

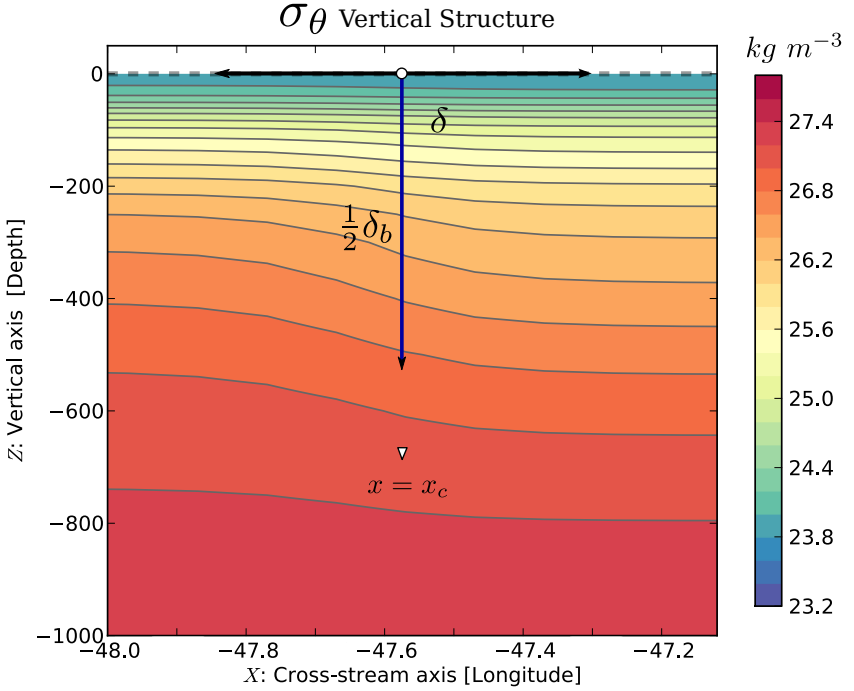

Figure 5.2: Cross-sectional geostrophically balanced σ_θ distributions, which was the same along the domain.

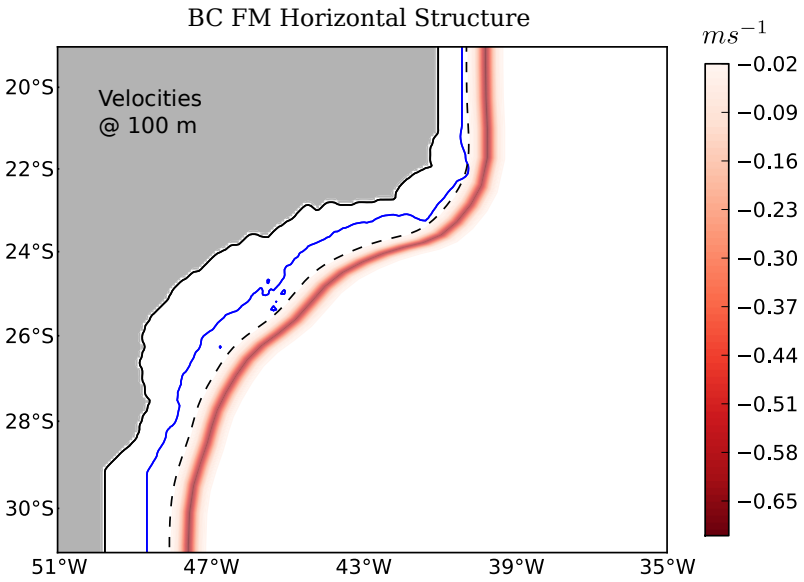

Figure 5.3: Along-shelf velocity horizontal map for surface. The blue contour represents depths shallower than 100 m and the dashed line is the smoothed shallow- deep ocean interface that serves as origin for the FM transects, and was based on the 200 m reference level.

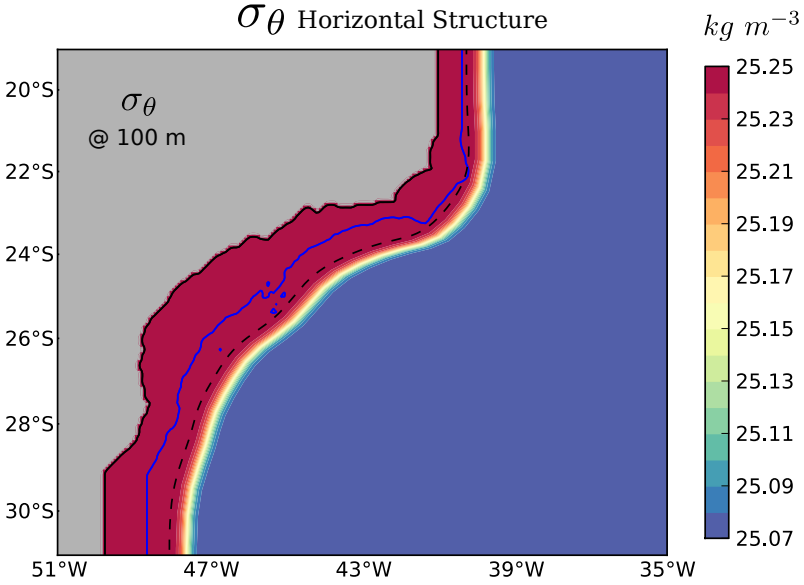

Figure 5.4: Horizontal σ_θ map for surface. The blue contour represents depths shallower than 100 m and the dashed line is the smoothed shallow-deep ocean front that serves as origin for the FM transects, and was based on the 200 m reference level.

5.1.2 Model implementation

The primitive equation model chosen for this study is the Regional Ocean Modeling System (ROMS) [*Shchepetkin & McWillians*, 2005]. ROMS has curvilinear horizontal coordinate system and terrain-following in the vertical. The model domain for our area has a 1/24° resolution with 220 x 210 grid points, comprising the area 14°S to 35°S and 54°W to 32°W, as in Figure 5.5. The total number of vertical levels is 20. For the topography configuration, ETOPO1 is truncated in 1500 m and than interpolated to the grid, minimizing pressure gradient errors by restricting the bathymetry gradients under an r-factor of 0.2 [*Haidvogel et al.*, 2000]. Additionally, the inflow and outflow regions were configured to have a meridionally rectilinear orientation, and only the area comprised by 22°S to 29°S kept the real topographic variation (Figure 5.5). In this sense, we intended to configure an steady-state inflowing jet and introduce the topographic perturbation only in the region of interest, which was Cape Frio and Cape São Tomé areas, similarly to the approach used in Chapter 4.

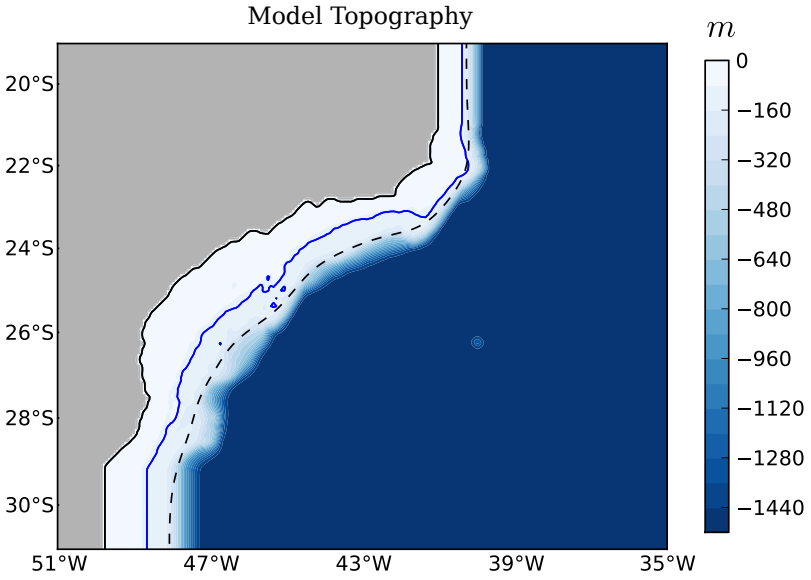

Figure 5.5: Numerical model grid and bathymetric configuration based on ETOPO 1 real topography truncated in 1500 m. The blue contour represents depths shallower than 100 m and the dashed line is the smoothed shallow- deep ocean interface that serves as origin for the FM transects. Note the idealized meridionally rectilinear continental margin in the inflow and outflow regions.

Vertical mixing of momentum and tracers is done by the k-profile turbulent closure model by *Large et al.* [1994]. Harmonic horizontal mixing and diffusivity are used both with 5 m^2s^{-1} coefficients in the interior of the domain and a mild sponge layer of six grid points is applied at the open boundaries (N, S, E), linearly increasing the viscosity up to 50 m^2s^{-1}. At the three open boundaries, we follow *Peliz et al.* [2003] approach by keeping the FM fields nearly steady through the use of strong relaxation in a layer of six grid points. Nudging time scales vary from 6 to 1 day from the interior to the boundary. In order to avoid reflections of the flow, additional active/passive conditions were also used at the boundaries [*Marchesiello et al.*, 2001], with strong inflow time scale of 1 day.

In the experiment, the FM field is interpolated to ROMS grid with its bathymetry setup. No other forcing are imposed, so all the dynamics are consequence of one year evolution of the initial field interacting with itself and the topography.

5.2 Results

Before we start the description of our ROMS experiment results, we would like to highlight some characteristics of the initial jet, and compare them with the parameters we used for the jets in Chapter 4. The jet core position here was more offshore. In the QG experiments, the higher value of this parameter was x_c = 100 km. Here, we used x_c = 160 km for a more appropriate fit of the jet with the real topography. We have to remember that the real topography presents a slope region. Therefore, the higher value allowed that the prescribed jet could be configured to have the vertical extension with no interference from the shallower regions of the slope. Moreover, the parameter δ, which defines the jet width, was the same as the QG experiments (δ = 36 km), which corresponds to the value of the Rossby deformation radius R_d in the region. The parameters that define the vertical structure of the jet were not necessary in the QG experiments, since we were using the approximation of homogeneous ocean there.

Figure 5.6 illustrates the velocity vertical section at the inflow region (20 °S) correspondent to the first day of run. One can see the jet nicely adjusted to the topographic configuration, where the coastal border is close to the continental shelf break. The core

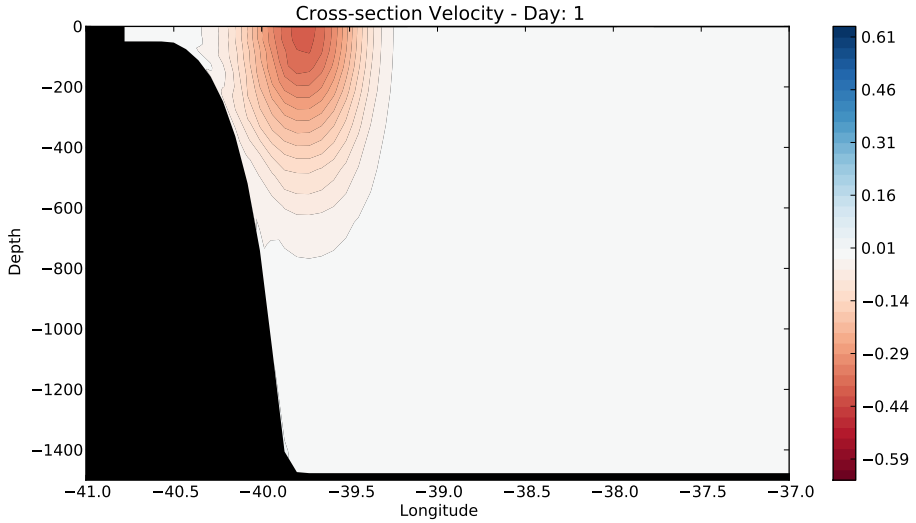

Figure 5.6: Vertical velocity section at the inflow region for the first day of simulation.

is centered in approximately 39.7°W and has a velocity of about -0.45 m s^{-1}. The jet horizontal extension is about 110 km, while the vertical extension is 700 m of depth. In order to assure the initial jet is potentially barotropically unstable, we tested the Rayleigh and Fjørtoft conditions (discussed in Chapter 2). To do so, firstly we obtained the velocity cross-jet profile correspondent to Figure 5.6 at the surface ($z = 0$). Such profile is illustrated in Figure 5.7 (upper panel). The PV profile is illustrated in 5.7 (lower panel). The Rayleigh and Fjørtoft profiles obtained from the velocity profile are both represented in Figure 5.8 (upper and lower panels respectively).

The results obtained in the ROMS experiment are shown in Figures 5.9 and 5.10, where we chose a sequence of 12 snapshots representative of 31 days of run. In the plots, we are showing only the area we are focusing in (which comprises the region of real topographic variation). The idealized inflow and outflow regions are partially showed with the intention of giving a better visualization of the inflowing jet.

During the 31 days period, we could see the jet interacting with the changes in topography. The BC jet is initially following the continental margin and we start to see meandering by day 9. In days 12 to 15, around the parallel of 23°S, the jet seems to tend to form a cyclonic eddy or meander in its coastal side and an anticyclonic eddy is formed in its oceanic side. This apparently indicates the tendency of dipole generation. This instability seems to have had origin due to the change in the 200 m isobath

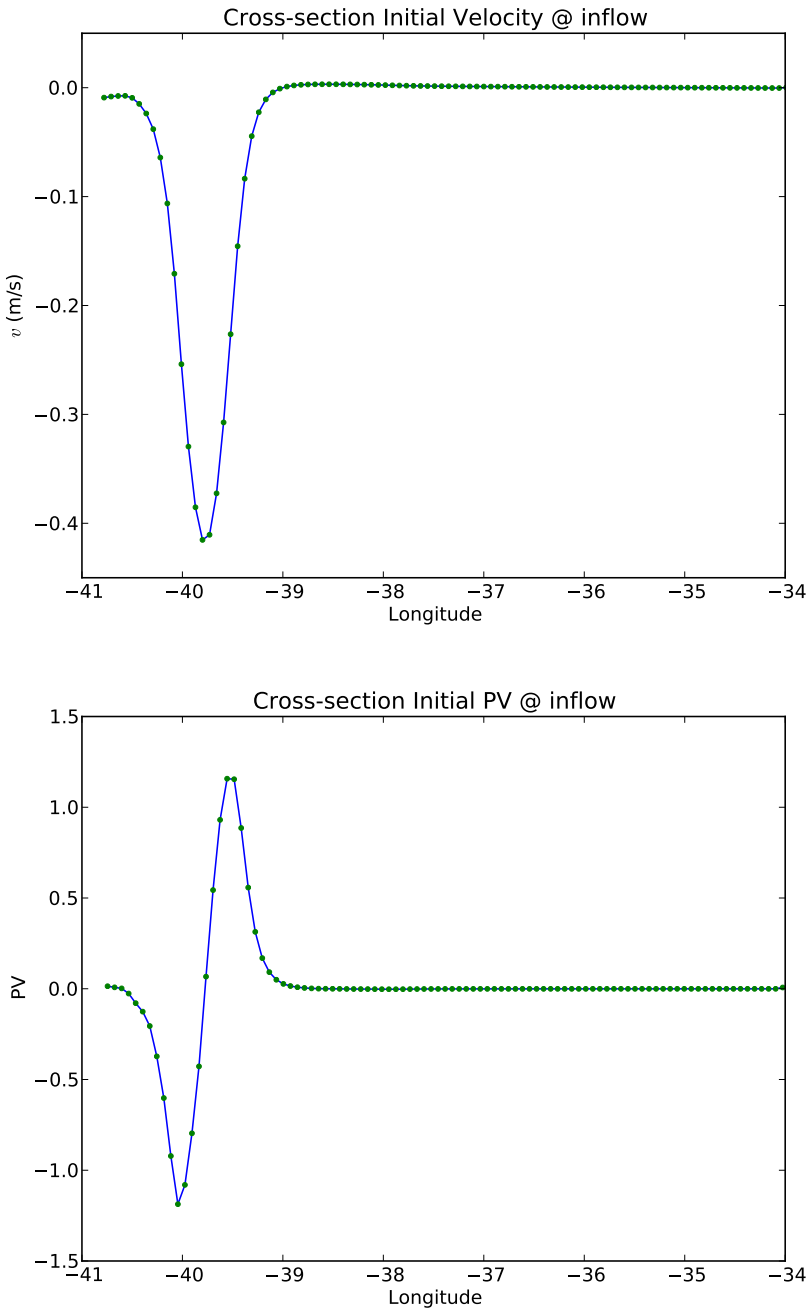

Figure 5.7: Cross-jet velocity (upper panel) and PV (lower panel) profiles at the inflow region and at surface.

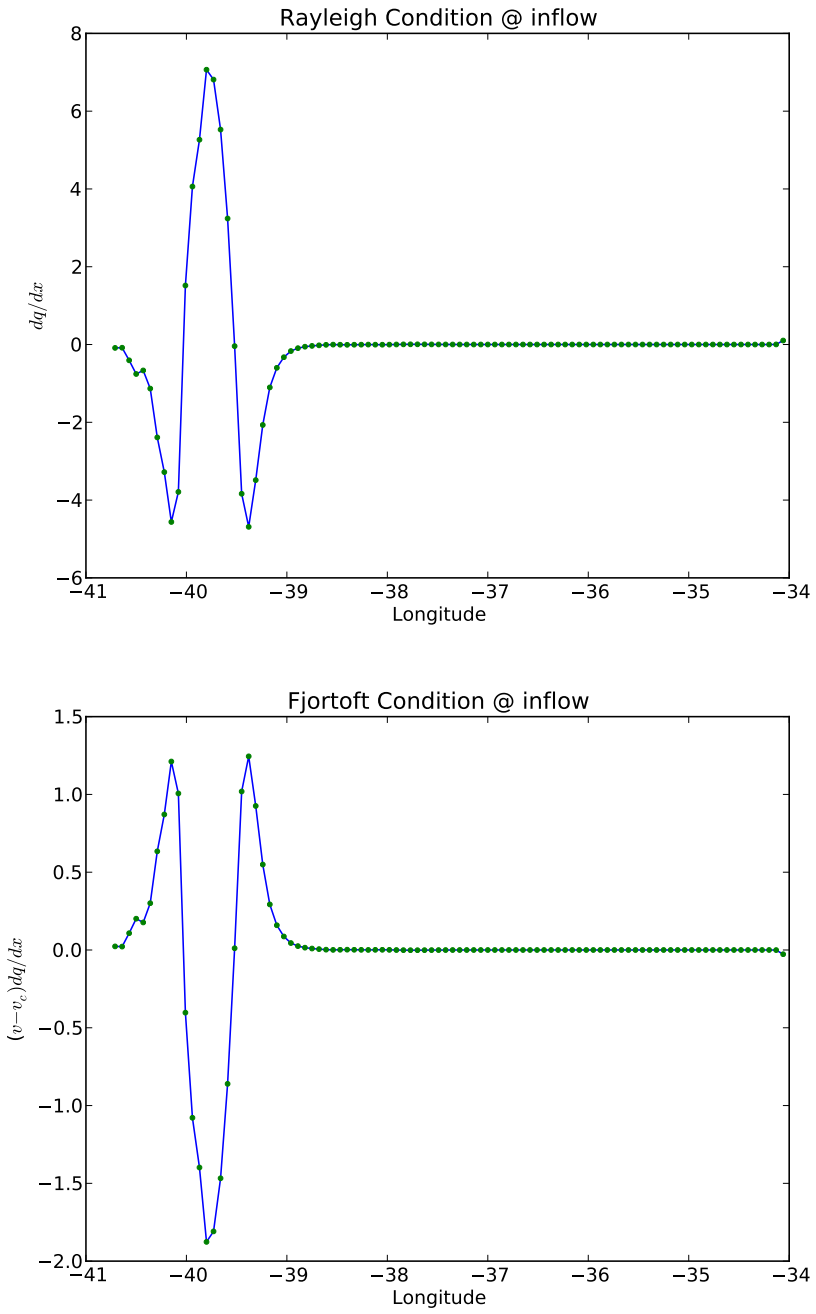

Figure 5.8: Rayleigh (upper panel) and Fjørtoft (lower panel) conditions for barotropic instability computed for the initial inflowing jet.

profile, represented by Cape Frio indentation. At the same time, we can see the meanders intensifying in the downstream region of the area (around 27°S). After day 17, the bipolar feature in Cape Frio developed, started presenting growth and intensified. The process can be seen in days 17 to 31. During this period, the jet started presenting some instabilities right off Cape São Tomé (parallel of 22°S), and it started forming an anticyclonic eddy. This eddy also presented growth and extended meridionally, forcing the jet upstream. By day 27, the Cape São Tomé anticyclone and Cape Frio dipole are formed and established, and two anticyclonic eddies appeared downstream, centered in 27°S and 29°S. The Cape Frio vortex-dipole presented a weak propagation downstream, where the anticyclonic side developed more and presented higher dimensions than the cyclonic one. The horizontal dimensions of the final features were about 200 km.

In order to have more insight in the formation of the bipolar structure we speculated in the previous paragraph, we looked to the vertical velocity section in day 30, where we obtained a zonal slice of the field centered in 24°S. Figure 5.11 illustrates such vertical section. It is possible to see the BC current (represented by the negative velocity values) associated with positive velocities in both sides of its flow. The jet core shifted offshore, and now it is centered in 42°W. This indicates the jet had some separation from the coast probably due to the change in coastline orientation. Moreover, this configuration seem to be favorable to the formation of a yet incipient dipole.

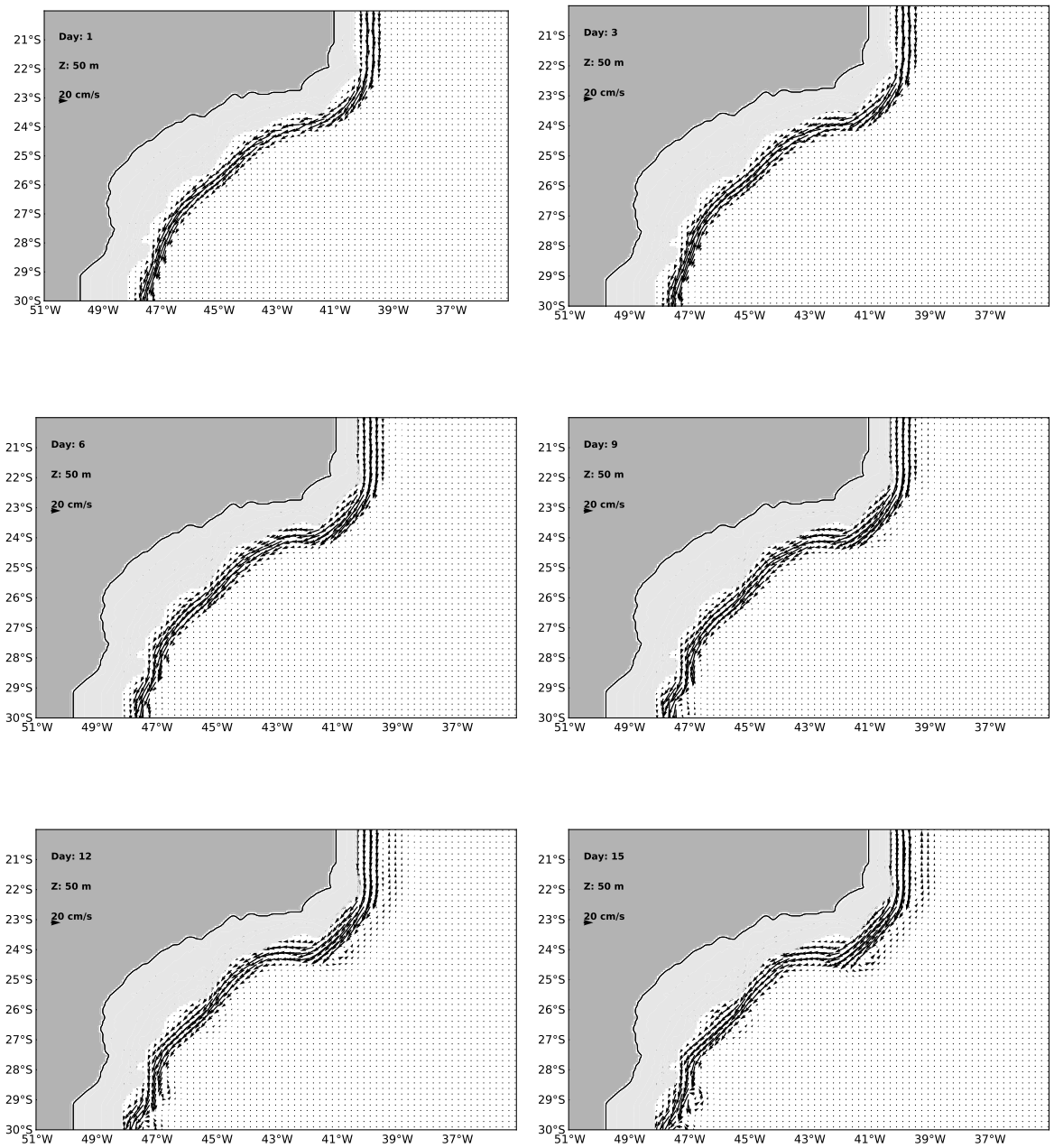

Figure 5.9: Synoptic velocity fields at 50 m for the ROMS experiment. Correspondent time indicated in each plot, as well as the vectors scales. From top left to bottom right, day 1 to day 15. The light gray mask represents depths shallower than 100 m. The dark gray mask represents the continent.

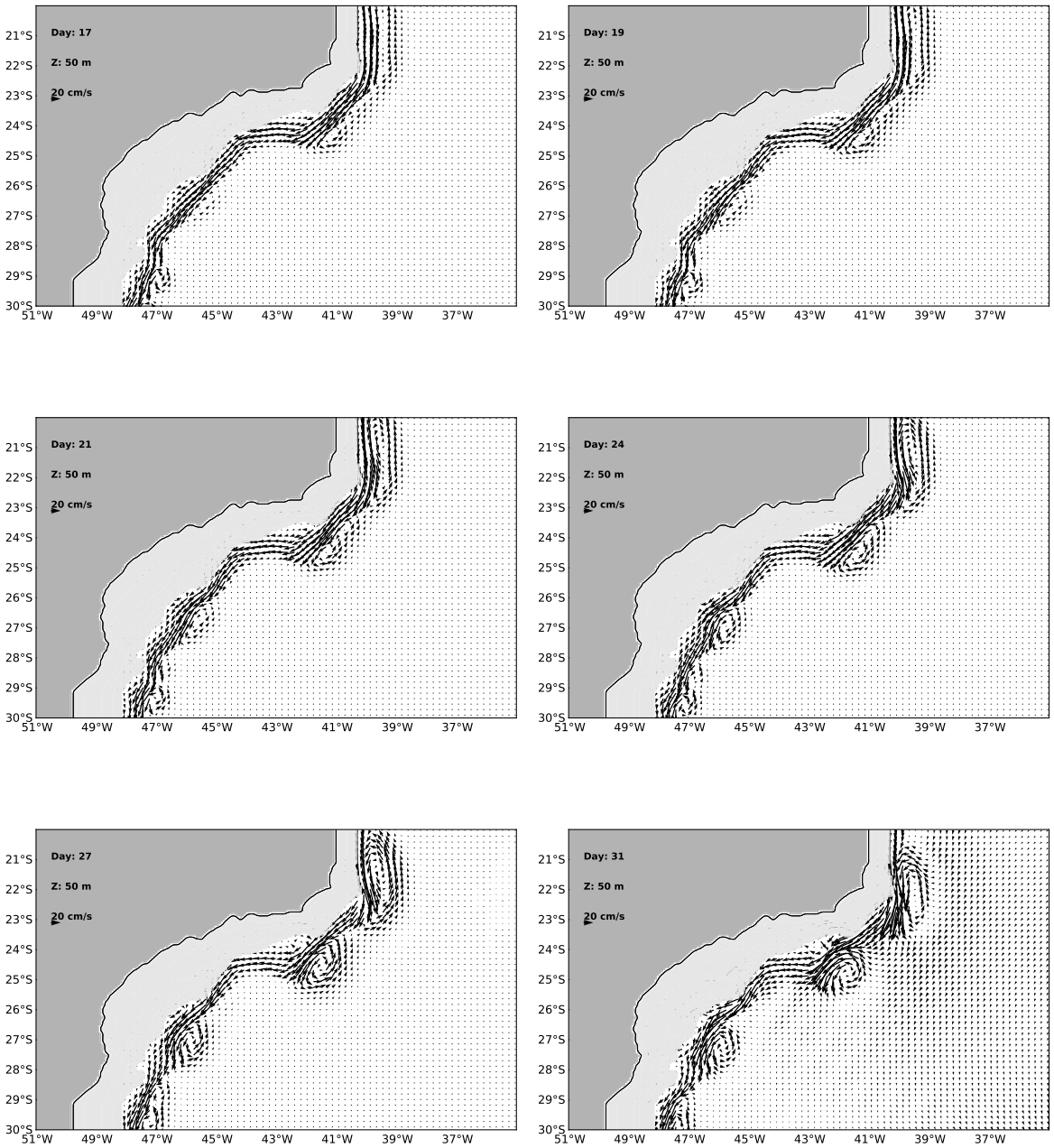

Figure 5.10: Synoptic velocity fields at 50 m for the ROMS experiment. Correspondent time indicated in each plot, as well as the vectors scales. From top left to bottom right, day 17 to day 31. The light gray mask represents depths shallower than 100 m. The dark gray mask represents the continent.

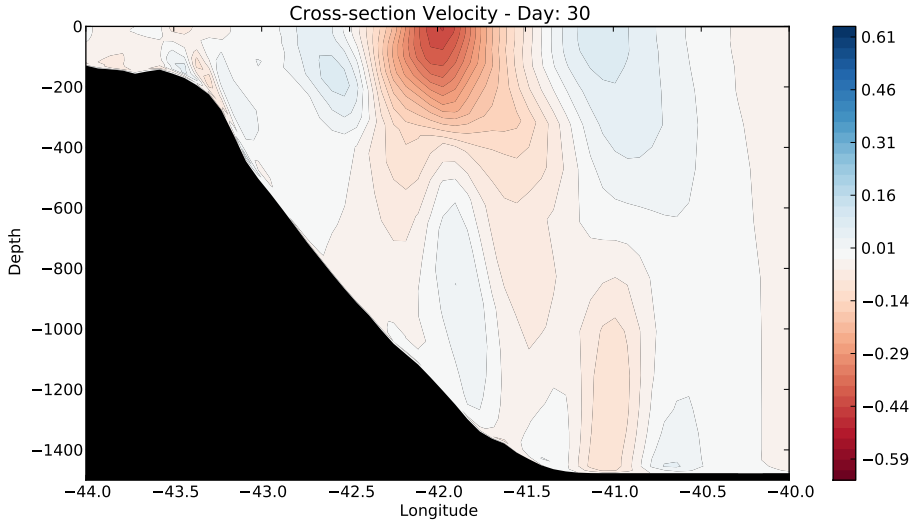

Figure 5.11: Vertical section of the along-shore velocity centered in 24°S after 30 days of simulation.

5.3 Summary and Discussion

In the present chapter our intention was to add more dynamical complexity to our physical system through the implementation of a primitive equation numerical model, where we used ROMS. As we did in Chapter 4, we prescribed a BC-like jet using the technique known as Feature-Oriented Regional Modeling System (FORMS). The jet was potentially barotropically unstable due to horizontal shear, and a weak vertical shear had to be included in order to reproduce a realistic BC. Two important characteristics were introduced here: real topography and stratification effect. Here, the ocean is continuously stratified, and, although only one jet was prescribed along the domain (we ignored the IWBC jet), a weak vertical shear is present, which means baroclinic instability may occur concomitantly with barotropic instability. The real topography not only incorporates changes in coastline orientation, but also includes the slope.

Within the set of parameters relevant to the BC characteristics and applied here, it is clear the jet showed perturbations located where there is changes in coastline orientation. It seems we obtained the formation of a bipolar feature right off Cape Frio, since the feature was depicted in the vertical velocity section of Figure 5.11. Such structure presented (in day 31) about 200 km of diameter and had the same length scale and position obtained by *Pereira* [2009]. Figure 5.12 illustrated a zoom of the right lower

panel of Figure 5.10, so the reader can have a better looking into the feature scales.

Downstream of the dipole, a wave-like pattern is present and some anticyclones were formed. This scenario resembles the one obtained by *Campos et al.* [1996] and depicted in our simulation of Chapter 3, e.g. the formation of a dipole upstream and a sequence of eddies downstream. Here we cannot say we obtained a sequence of several eddies, but we speculate this results could evolve to a similar scenario afterwards.

Trying to have some insights of the dynamics of our simulation, we used the QG framework and evaluated the BC-like flow in terms of this approximation. Firstly, we computed the Rossby number according to Equation **??**, where

$$Ro = \frac{\left(\frac{\partial v}{\partial x} - \frac{\partial u}{\partial y}\right)}{|f_0|}, \tag{5.10}$$

for the BC jet at the inflow. We obtained Ro = 0.2, which indicates the system can be explained by the QG approximation. Going further in our dynamical analyses, we followed once again *Magaldi et al.* [2008], as we did in Chapter 4. So we evaluated the coastline curvature and compared with the jet deformation radius, according to Equation 4.8, and obtained Bu = 8.20. This calculation was conducted for the initial jet. As discussed by *Magaldi et al.* [2008], they obtained a pattern, where for low Bu, e.g., $Bu < 0.1$ (weak stratification), a fully attached regime is established, and the jet flows smoothly over the cape. For intermediate Bu, e.g., $0.1 < Bu < 1$, fluid parcels flow more around the obstacle than over it. Flow separation occurs and small tip eddies start to shed. The increasing of Bu shifts the system from a eddy-attached regime (where eddies are formed behind the cape and shed downstream) to a lee eddy regime (where small lee eddies are formed and grow behind the cape). For high Bu, e.g., $Bu > 1$, (strong stratification), tip eddies merge to form larger eddies in the lee of the cape. In our results, we could see indeed the formation of tip eddies in coastline inflexion points, which is in accordance with the pattern obtained by the above authors, although we used a different coastline shape. The computed Bu indicates, according to the authors, we have a strong stratification system. We know that both rotation and stratification are actually important in Cape Frio region. However, we must have in mind we are using an idealized system here, where we do not have the presence of the IWBC. Nevertheless, we could not see the evaluation of the structures after 31 days,

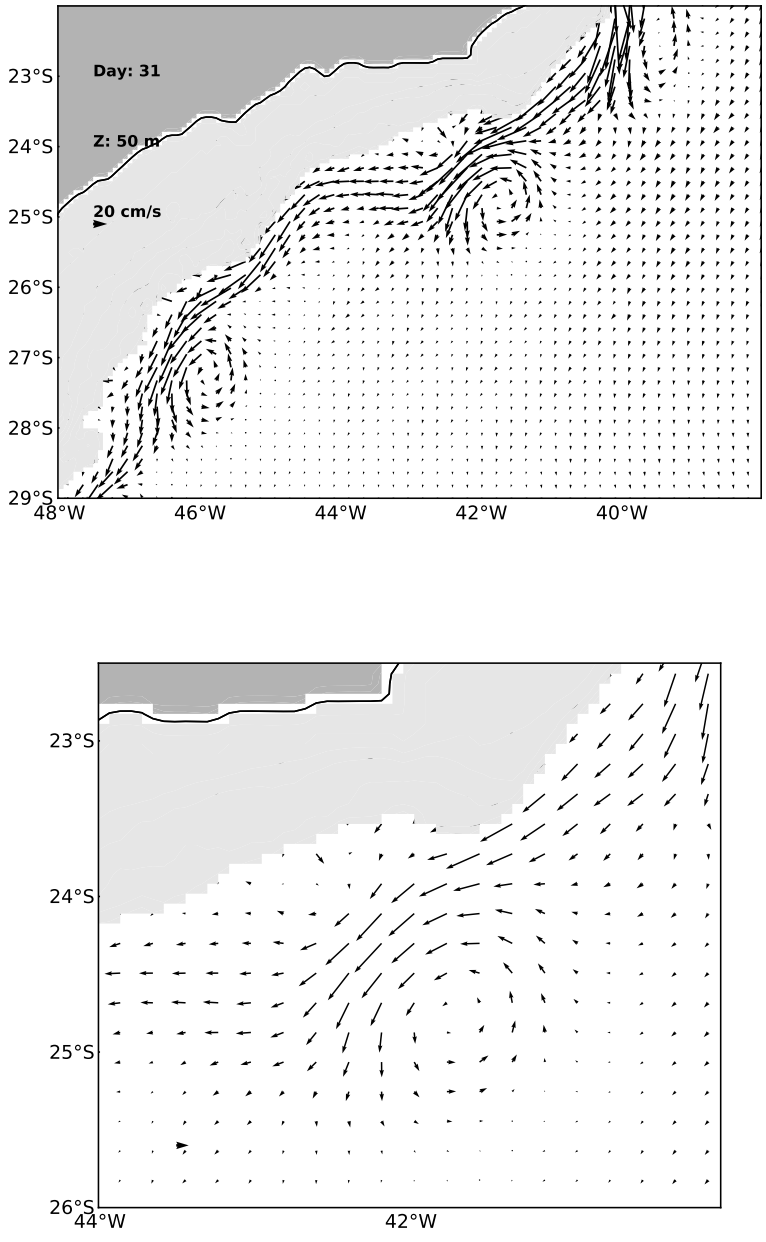

Figure 5.12: Synoptic velocity field at 50 m in day 31, both zooming in the dipole area.

and how the propagation would be given.

We cited, in Chapter 4, the study of *Stern & Whitehead* [1990], where they evaluated the role of variations in coastline curvature in the behavior of a jet passing around an indentation similar to Cape Frio scenario. According to the pattern obtained by the authors, an abrupt angle would favor separation of the jet from the boundary, and a mushroom-like structure would form and set the path for the trailing jet. In the other hand, a smoother angle (they discussed the critical angle) would favor an attached jet that eventually would form eddies. The scenario obtained here resembles this second regime obtained by these authors, since we could not see separation in any moment.

Finally, it is important to highlight that our goals number 5 presented in Section 1.2 were accomplished in the present chapter, e.g we examined the interaction of a barotropically unstable meridional jet and the western boundary in a realistic topography scenario. We saw the formation of features that seemed to be triggered by lateral boundary perturbations (or variations). A bipolar feature was incipiently formed off Cape Frio indentation. However, due to the short-run conducted here, and could not see propagation and possible detachment of these structures and their interaction with the current.

Chapter 6

Conclusions

In this final chapter we present a brief overview of the study conducted here, compare important points obtained from each model results, point out unresolved important issues and suggest future work.

In summary, we presented observational evidences of the formation of vortex dipole structures along the Brazilian continental margin south of Cape Frio (23°S). Information from the literature and a mere inspection of series of AVHRR images revealed the formation of paired eddies with opposite vorticity signs in each side of the BC nearby the Cape. Downstream, a staggered series of smaller cyclones and anticyclones were found forming what was called a vortex street by *Pratt et al.* [1991]. Additionally, the images also depicted different phenomena not yet reported for the BC: typical instability wave trains within Santos Bight (23°S-28°S). These trains seem to be very similar to those described for the Gulf Stream by *Xue & Mellor* [1993], upstream of the Charleston Bump.

The kernel of this dissertation is, then, to unravel the dynamics of the vortex dipole and vortex street formation phenomena. In order to address the issue, we stated two working hypotheses: (1) barotropic instability is the driving mechanism for the formation of dipoles and instability wave trains, and (2) changes in coastline orientation can promote perturbations in the BC jet which trigger those instabilities. We tested the two hypotheses through the formulation, implementation and application of a suite of three idealized models. We progressively added dynamical complexity to first isolate the instability mechanism and, later in document, to explore the role of lateral bound-

ary changes in the flow. The first of these models dealt with an idealized southward-flowing, barotropically unstable jet in a QG contour dynamics model (Chapter 3); the second model consisted of exploring a continuous potential vorticity QG full numerical model of a jet flowing adjacent to western boundary that could be either meridional or curvy (Chapter 4). The first two models employed an equivalent-barotropic and barotropic vertical structure, respectively. The third model employed consisted of a primitive equation numerical model (Chapter 5), through which we relaxed the layer approximation constraint of the former two, as well as the QG approximation. We performed simulations allowing the examination of a realistically shaped baroclinic jet flowing over a realistic continental margin.

In Chapter 3, we formulated a piecewise-constant PV, contour dynamics model that resembled both *Pratt et al.* [1991] and *Schmidt* [2004], but considered three contours (or three PV fronts) and the presence of the western boundary. The choice of the three fronts is due to the fact that such configuration is the minimal PV structure to support a vortex dipole structure to be formed in each side of the boundary jet. We also did not opt for a convention span of the CD model parameter. Instead, we attempted to do a match using one of the few scarce observations of the BC jet not meandering, and hence, assumed to be possibly closer to a (yet unknown) steady state. In the experiments conducted, we could reproduce the formation of paired eddies upstream (dipole) and a sequence of opposing-sign eddies downstream, which already resembled the observational evidences presented in Chapter 1. Therefore, we verified that barotropic instability can indeed generate bipolar vortical features in jets with a PV configuration similar to that of the Brazil Current.

In Chapter 4, we relaxed the piecewise constant PV field constraint of the CD method, and advanced the methodology regarding the PV field characteristics. The experiments employing a barotropic jet possessing a continuous PV structure produced richer dynamics occurring in the model domain. We could observe not only that barotropic instability can generate bipolar structures, but also that the change in the coastline orientation can indeed trigger perturbations in the boundary current. By changing the PV structure of the jet as well as the coastline configuration we were not only able to simulate the dipole/vortex street formation but also the instability wave

trains.

In Chapter 5, we implemented the ROMS model using feature models [*Gangopadhyay et al.*, 2003] as initial conditions. However, the feature models employed in our study were built to resemble the linear instability properties of the jets from Chapter 3. We used real topography of the study area and, therefore, added more dynamical complexity to our physical system. Again, we could see that both barotropic instability and topographic variations can induce the formation of bipolar structures. Even this more complex scenario kept the pattern of the two previous chapters regarding formation of structures. The dipole formed satisfactorily reproduced the velocity structure obtained by *Pereira* [2009] for the DEPROAS V cruise. Hence, our hypotheses were affirmatively verified for the present work.

Theory involving dynamics of current separation may be related to the scenario of a curvy coastline studied here. For instance, *Marshall & Tansley* [2001], *Castelao & Barth* [2006], *Stern & Whitehead* [1990] tried to find parameter that could limit regimes of flow separation and flow attachment. *Doglioli et al.* [2004] mentioned that eddy generation is connected to the ubiquitous phenomenon of current separation occurring in flows in presence of obstacles. However, as a general consensus, *Cessi & Ierley* [1993] mentioned that viscous shear instability is proposed as a primary mechanism for generating time-dependent eddies at western boundary. Because of the complex nonlinear nature of the phenomenon, a quantitative prediction of eddy characteristics as a function of environmental parameters is hard to achieve. Many different mechanisms, characterized by different non-dimensional parameters, play an important role, including bottom friction processes, vertical and horizontal mixing, and stratification [*Doglioli et al.*, 2004]. In this sense, *Flierl* [1999] showed that baroclinic processes play a significant role in the growth of meanders, while upper-layer interactions drive the final pinch-off of eddies.

Here we isolated the effect of the horizontal velocity shear, and consequently PV structure, to address the role of barotropic instability being the driving mechanism for the vortex dipole formation, as well as the vortex street and the instability wave trains. The topographic changes provide sites for perturbing the jet and letting the phenomena to develop. Certainly, other factors (such as the mentioned above) may play important role in the formation of eddies and dipoles, and may determine differ-

ent regimes.

As future work, we suggest the inclusion of the vertical shear effect in order to see the response of the jet regarding dipole formation and its downstream evolution. To complement our study, it would be important to evaluate other dynamical aspects of the results, such as trying to fit solutions for the results obtained (Rossby wave solutions, pulse-train solutions and so on). Particularly, using topographic Rossby wave forcing would be interesting to compare to the processes of warm outbreaks in the GS. The inclusion of the β effect should give important changes in the results. Moreover, simulations of the interaction of the jet with a cyclone could give important dynamical insights regarding the BC interacting with the Cape Frio eddies. And simulations of the interaction of the jet with an anticyclone could be carried assuming the anticyclones of Agulhas rings reach the western boundary of the South Atlantic and also interact with the BC.

Bibliography

Bell, G. I. & L. J. Pratt, 1992: The Interaction of an Eddy with an Unstable Jet. *J. Phys. Oceanogr.*, *22*, 1229–1244.

Berloff, P. & J. McWilliams, 1999: Quasigeostrophic Dynamics of the Western Boundary Current. *J. Phys. Oceanogr.*, *29*, 2607–2634.

Böebel, O., R. E. Davis, M. Ollitraut, R. G. Peterson, P. L. Richard, C. Schmid, & W. Zenk, 1999: The intermediate depth circulation of the Western South Atlantic. *Geophys. Res. Lett.*, *26(21)*, 3329–3332.

Bouchut, F., B. Ribstein, & V. Zeitlin, 2011: Inertial, barotropic, and baroclinic instabilities of the Bickley jet in two-layer rotating shallow water model. *Physics of Fluids*, *23(126601)*, 1–22.

Calado, L., 2001: Dinâmica da formação dos meandros e vórtices da Corrente do Brasil ao largo do sudeste brasileiro. Dissertação de Mestrado, Universidade de São Paulo, São Paulo, 95 pp.

Calado, L., A. Gangopadhyay, & I. Silveira, 2008: Feature-oriented regional modeling and simulations (FORMS) for the western South Atlantic: Southeastern Brazil region. *25(1-2)*, 48–64.

Calado, L., A. Gangopadhyay, & I. C. A. Silveira, 2006: A parametric model for the Brazil Current meanders and eddies off southeastern Brazil. *Geophys. Res. Lett.*, *33*, LI2602.

Calado, L., I. C. A. Silveira, A. Gangopadhyay, & B. M. Castro, 2010: Eddy-induced upwelling off Cape São Tomé (22°S, Brazil). *Continental Shelf Res.*, *30*, 1181–1188.

Campos, E. D. J., D. Velhote, & I. C. A. Silveira, 2000: Shelf break upwelling driven by Brazil Current cyclonic meanders. *Geophys. Res. Lett.*, *27(6)*, 751–754.

Campos, E. J. D., J. E. Gonçalves, & Y. Ikeda, 1995: Water mass structure and geostrophic circulation in the South Brazil Bight - summer of 1991. *J. Geophys. Res.*, *100(C9)*, 18.537–18.550.

Campos, E. J. D., Y. Ikeda, B. M. Castro, S. A. Gaeta, J. Lorenzzetti, & M. Stevenson, 1996: Experiment Studies Circulation in the Western South Atlantic. *Eos Transaction*, *77(27)*, 253 – 259.

Castelao, R. M. & J. A. Barth, 2006: The Relative Importance of Wind Strength and Along-Shelf Bathymetric Variations on the Separation of a Coastal Upwelling Jet. *J. Phys. Oceanogr.*, *36*, 412–425.

Cessi, P. & G. R. Ierley, 1993: Nonlinear disturbances of western boundary currents. *J. Phys. Oceanogr.*, *23*, 1727–1735.

Cummings, J., C. Szczechowski, & M. Carnes, 1997: Global and regional ocean thermal analysis systems. *Mar. Technol. Soc J.*, *31(6375)*.

Cunningham, P., 2000: Coherent Vortices in the Extratropical Upper Troposphere: A Dynamical Interpretation of Jet Streaks. Tese de Doutorado, University at Albany, State University of New York, New York, USA, 162p pp.

Doglioli, A. M., A. Griffa, & M. G. Magaldi, 2004: Numerical study of a coastal current on a steep slope in presence of a cape: The case of the Promontorio di Portofino. *J. Geophys. Res.*, *109(C12033)*, 1–19.

Fernandes, F. P. A., 2007: Modelos Teóicos Paraméricos do Sistema Corrente do Brasil. Dissertação de Mestrado, Universidade de São Paulo, São Paulo, 66 pp.

Flierl, G. R., 1999: Thin jet and contour dynamics models of Gulf Stream meandering. *Dyn. Atmos. Oceans*, *29(2-4)*, 189–215.

Fofonoff, N. P., 1981: Evolution of Physical Oceanography, capítulo The Gulf Stream System, pp 504 – 548. MIT Press.

Fox, D., M. Carnes, & J. Mitchell, 1992: Characterizing major frontal systems, a now-cast/forecast system for Northwest Atlantic. *5(1)*, 49–53.

Gangopadhyay, A. & A. Robinson, 2002: Feature-oriented regional modeling of oceanic fronts. *Dyn. Atmos. Oceans*, *36(1-3)*, 201–232.

Gangopadhyay, A., A. Robinson, & H. Arango, 1997: Circulation and dynamics of the western North Atlantic. I: Multiscale feature models. *J. Atmos. Oc. Tech.*, *14(6)*, 1314–1332.

Gangopadhyay, A., A. Robinson, P. Haley, W. Leslie, C. Lozano, J. Bisagni, & Z. Yu, 2003: Feature oriented regional modeling and simulation in the Gulf of Maine and Georges Bank. *Continental Shelf Res.*, *23(3-4)*, 317–353.

Garfield, N., 1990: The Brazil Current at subtropical latitudes. Tese de Doutorado, University of Rhode Island, Rhode Island, 121 pp.

Haidvogel, D., H. Arango, K. Hedström, A. Beckmann, P. Malanotte-Rizzoli, & A. Shchepetkin, 2000: Model evaluation experiments in the North Atlantic basin: simulations in nonlinear terrain-following coordinates. *Dyn. Atmos. Oceans*, *32(3-4)*, 239–281.

Hurlburt, H., A. Wallcraft, S. J. W., P. Hogan, & E. Metzger, 1992: Dynamics of the Kuroshio/Oyashio current system using eddy-resolving models of the North Pacific ocean. *J. Geophys. Res.*, *101(C1)*, 941–976.

Jayne, S. R. & N. G. Hogg, 1999: On Recirculation Forced by an Unstable Jet. *Notes and Corresp.*, *29*, 2711–2718.

Jayne, S. R., N. G. Hogg, & P. Malanotte-Rizzoli, 1996: Recirculation Gyres Forced by a Beta-Plane Jet. *J. Phys. Oceanogr.*, *26*, 492–504.

Large, W., J. McWilliams, & S. Doney, 1994: Oceanic vertical mixing: A review and a model with a nonlocal boundary layer parameterization. *Rev. Geophys.*, *32(4)*, 363–403.

Leal Silva, C. A. C., 2000: Dinâmica da separação de correntes de contorno oeste barotropicamente instáveis. Dissertação de Mestrado, Universidade de São Paulo, São Paulo, 104 pp.

Lima, J. A. M., 1997: Oceanic circulation on the Brazil Current shelf break and slope at 22°S. Tese de Doutorado, University of New South Wales, New South Wales, 144 pp.

Lipps, F. B., 1963: Stability of jets in a divergent barotropic fluid. *J. Atmos. Sci.*, *20*, 120–129.

Lozano, C. J., A. R. Robinson, H. G. Arango, A. Gangopadhyay, Q. Sloan, P. J. H. Jr., L. A. Anderson, & W. G. Leslie, 1996: An interdisciplinary ocean prediction system: Assimilation strategies ana structured data models. In P. Malanotte-Rizzoli, editor, Modern Approaches to Data Assimilation in Ocean Modeling, volume 61 de *Elsevier Oceanography Series*. Elsevier, 413–452.

Magaldi, M., T. Özgökmen, A. Griffa, E. Chassignet, M. Iskandarani, & H. Peters, 2008: *25*, 65–82.

Mallier, R. & A. M. J. Davis, 1999: Nonlinear Evolution of Singular Disturbances to the Bickley Jet. *S. in Appl. Math.*, *103*, 149–181.

Mano, M., A. M. Paiva, A. R. T. Jr., & A. L. G. A. Coutinho, 2009: Energy flux to a cyclonic eddy off Cabo Frio, Brazil. *J. Phys. Oceanogr.*, *39*, 2999–3010.

Marchesiello, P., J. C. McWilliams, & A. Shchepetkin, 2001: Open boundary conditions for long-term integration of regional oceanic models. *3(1-2)*, 1 – 20.

Marshall, D. P. & C. E. Tansley, 2001: An Implicit Formula for Boundary Current Separation. *J. Phys. Oceanogr.*, *31*, 1633–1638.

Mascarenhas, A. S. J., L. B. Miranda, & N. J. Rock, 1971: Ed. John D. Costlow Jr. (Org), Fertility of the Sea, capítulo A study of oceanographic conditions in the region of Cabo Frio., pp 285 – 308. Gordon and Breach Sciences Publishers, New York, 1 edição.

Mattos, R. A., 2006: Feições de meso e grande escalas da Corrente do Brasil ao largo do sudeste brasileiro. Dissertação de Mestrado, Universidade de São Paulo, São Paulo, 126 pp.

Meacham, S. P., 1991: Meander evolution on piecewise-uniform, quasi-geostrophic jets. *J. Phys. Oceanogr.*, *21(8)*, 1139–1170.

Munday, D. R. & D. P. Marshall, 2005: On the Separation of a Barotropic Western Boundary Current from a Cape. *J. Phys. Oceanogr.*, *35*, 1726–1743.

Mémery, L., M. Arhan, X. A. Alvarez-Salgado, M.-J. Messia, H. Mercier, C. G. Castro, & A. F. Rios, 2000: The water masses along the western boundary of the south and equatorial Atlantic. *Prog. Oceanogr.*, *47(1)*, 69–98.

Olson, D. B., G. P. Podesta, R. H. Evans, & O. B. Brown, 1988: Temporal variations in the separation of Brazil and Malvinas currents. *Deep-Sea Res.*, *35(12)*, 1971–1990.

Pedlosky, J., 1987: *Geophysical Fluid Dynamics*. Springer, New York, 728 pp.

Peliz, A., J. Dubert, D. B. Haidvogel, & B. Le Cann, 2003: Generation and unstable evolution of a density-driven Eastern Poleward Current: The Iberian Poleward Current. *J. Geophys. Res.*, *108(C8)*, 3268.

Pereira, D. P. C., 2009: Instabilidade barotrópica dos dipolos vorticais da Corrente do Brasil. Dissertação de Mestrado, Universidade de São Paulo, São Paulo, 101 pp.

Polvani, L. M., N. J. Zabusky, & G. R. Flierl, 1988: Applications of contour dynamics to two layer quasi-geostrophic flows. *Fluid Dyn. Res.*, *3*, 422–424.

Polvani, L. M., N. J. Zabusky, & G. R. Flierl, 1989: Two-layer geostrophic vortex dynamics. Part 1. Upper-layer v-states and merger. *J. Fluid. Mech.*, *205*, 215–242.

Pratt, L. J., J. Earles, P. Cornillon, & J. F. Cayula, 1991: The nolinear behavior of varicose disturbances in a simple-model of the Gulf Stream. *Deep-Sea Res.*, *38*, S591–S622.

Pratt, L. J. & M. E. Stern, 1986: Dynamics of potential vorticity fronts and eddy detachment. *J. Phys. Oceanogr.*, *16(6)*, 1101–1120.

Pullin, D. I., 1992: Contour Dynamics method. *Annu. Rev. Fluid. Mech.*, *24*, 89–115.

Robinson, A. & S. Glen, 1999: Adaptive sampling for ocean forecasting. *Nav. Res. Rev.*, *51(2)*, 28–38.

Robinson, A., M. Spall, & N. Pinardi, 1988: Gulf Stream simulations and the dynamics of ring and meander processes. *J. Phys. Oceanogr.*, *18(12)*, 1811–1854.

Robinson, A., M. Spall, L. Walstad, & W. Leslie, 1989: Data assimilation and dynamical interpolation in Gulfcasting experiments. *Dyn. Atmos. Oceans*, *13(3-4)*, 301–316.

Rodrigues, R. R., L. M. Rothstein, & M. Wimbush, 2007: Seasonal Variability of the South Equatorial Current Bifurcation in the Atlantic Ocean: A Numerical Study. *J. Phys. Oceanogr.*, *37(1)*, 16–30.

Rodríguez-Marroyo, R. & A. Viúdez, 2009: Vortex Rossby waves in mesoscale dipoles. *J. Geophys. Res.*, *114(C10009)*, 1–15.

Schmidt, A., W. Belo, & J. Lima, 2007: Modelo paramétrico analítico para a estrutura de velocidade do sistema Corrente do Brasil. *Rev. Bras. Geofis.*, *25(1)*, 75–91.

Schmidt, A. C. K., 2004: Interação margem continental, vórtices e jatos geofísicos. Tese de Doutorado, Universidade de São Paulo, São Paulo, 201 pp.

Shchepetkin, A. & J. McWillians, 2005: The Regional Ocean Modeling System (ROMS): a split-explicit, free-surface, topography following coordinates ocean model. *9(4)*, 347–404.

Signorini, S. R., 1978: On the circulation and the volume transport of the Brazil Current between the Cape of São Tomé and Guanabara Bay. *Deep-Sea Res.*, *25(5)*, 481–490.

Silveira, I. C. A., 2007: O Sistema Corrente do Brasil na Bacia de Campos, rj. Tese de Livre Docência, Instituto Oceanográfico, Universidade de São Paulo, 160 pp.

Silveira, I. C. A., L. Calado, B. M. Castro, M. Cirano, J. A. M. Lima, & A. S. Mascarenhas, 2004: On the baroclinic structure of the Brazil Current-Intermediate Western Boundary Current System. *Geophys. Res. Lett.*, *31(14)*, L14.308.

Silveira, I. C. A. & G. R. Flierl, 2002: Eddy formation in 2-1/2 layer, quasigeostrophic jets. *J. Phys. Oceanogr.*, *32(3)*, 729 – 745.

Silveira, I. C. A., G. R. Flierl, & W. S. Brown, 1999: Dynamics of separating western boundary currents. *J. Phys. Oceanogr.*, *29(2)*, 119–144.

Silveira, I. C. A., J. A. Lima, A. C. K. Schmidt, W. Ceccopieri, A. Sartori, & R. F. C. Fontes, 2008: Is the meander growth in the Brazil Current system due to baroclinic instability? *Dyn. Atmos. Oceans*, *45*, 187–207.

Silveira, I. C. A., L. B. Miranda, & W. S. Brown, 1994: On the origins of the North Brazil Current. *J. Geophys. Res.*, *99(C11)*, 22.501 – 22.512.

Silveira, I. C. A., A. C. K. Schmidt, E. J. D. Campos, S. S. Godoi, & Y. Ikeda, 2000: A Corrente do Brasil ao largo da costa leste brasileira. *R. Bras. Oceanogr.*, *48(2)*, 171–183.

Soutelino, R. G., I. C. A. Silveira, A. Gangopadhay, & J. A. Miranda, 2011: Is the Brazil Current eddy-dominated to the north of 20° S? *Geophys. Res. Lett.*, *38(L03607)*, DOI: 10.1029/2010GL046.276.

Spall, M. A. & A. R. Robinson, 1990: Regional primitive equation studies of the Gulf Stream meander and ring formation region. *J. Phys. Oceanogr.*, *20(7)*, 985–1016.

Stern, M. E., 1985: Lateral wave breaking and shingle formation in large-scale shear-flow. *J. Phys. Oceanogr.*, *15(10)*, 1274–1283.

Stern, M. E. & J. A. Whitehead, 1990: Separation of a boundary jet in a rotating fluid. *J. Fluid. Mech.*, *217*, 41–69.

Stramma, L., 1991: Geostrophic Transport of the South Equatorial Current in the Atlantic. *J. Mar. Res.*, *49(2)*, 281–294.

Stramma, L. & M. England, 1999: On the water masses and mean circulation of the South Atlantic Ocean. *J. Geophys. Res.*, *104(C9)*, 20.863–20.883.

Velhote, D., 1998: Modelagem numérica da ressurgência da quebra de plataforma induzida por vórtices ciclônicos da Corrente do Brasil na Bacia de Santos. Dissertação de Mestrado, Universidade de São Paulo, São Paulo, 134 pp.

Verron, J., P. A. Davies, & J. M. Dakin, 1991: Quasigeostrophic flow past a cape in a homogeneous fluid. *Fluid Dyn. Res.*, *7*, 1–21.

Waterman, S. & S. Jayne, 2011: Eddy-Mean Flow Interactions in the Along-Stream Development of a Western Boundary Current Jet: An Idealized Model Study. *J. Phys. Oceanogr.*, *41*, 682–707.

Xue, H. J. & G. Mellor, 1993: Instability of the Gulf Stream Front in the South Atlantic Bight. *J. Phys. Oceanogr.*, *23(11)*, 2326–2350.